Dynamics of CO oxidations on noble metal single-crystal surfaces studied by infrared chemiluminescence spectroscopy

~Vibrational energy states of product molecules and structure of activated complex~

Kenji Nakao

(Doctoral Program in Materials Science)

Submitted to the Graduate School of

Pure and Applied Sciences

in Partial Fulfillment of the Requirements

for the Degree of Doctor of Philosophy in

Engineering

at the

University of Tsukuba

学位論文要旨

本論文は，貴金属（Pd, Pt, Rh）単結晶上での定常的 CO 酸化反応における，反応速度や反応ダイナミクスについて述べたものである．酸化剤（O_2, NO, N_2O）や反応条件（分圧，表面温度）を変化させることによって，各反応系における反応速度を比較するとともに，赤外線化学発光法による，生成 CO_2 分子の振動エネルギー状態の観測から活性錯合体構造について考察し，CO_2 生成ダイナミクスについて検討した．

Pd(110), Pd(111), Pt(110), Pt(111), Rh(111)上で CO + O_2 反応を行った．反応速度は，金属種（Pd(111) > Rh(111) > Pt(111)）や表面構造（Pd(110) > Pd(111), Pt(110) > Pt(111)）に敏感であることがわかった．赤外発光測定の結果から，同じ平坦な(111)面でも金属が異なれば，生成 CO_2 分子の振動励起状態は大きく異なり，平均の振動温度（T_V^{AV}）と変角振動温度（T_V^{B}）の序列は，Pd(111) > Pt(111) > Rh(111)のようになった．これは，遷移状態におけるエネルギー準位の高さと，活性錯合体の角度（$\angle_{OCO}$）が影響しているからだと考えられる．Pd 単結晶上の高温側におけるCO_2分子の振動状態は，表面構造の影響を大きく受けることがわかった．Pd(111)上では変角振動が，Pd(110)上では逆対称伸縮振動が励起したCO_2が生成することから，Pd(111)上では曲がった活性錯合体，Pd(110)上ではより直線的な活性錯合体をとることを見出した．一方，低温側では，CO の被覆率が非常に高く，これに伴い，いずれの表面でも逆対称伸縮振動が非常に励起した CO_2 が生成することがわかった．CO 被覆率の大きさによって表面再構成が起こる Pt(110)上では，反応条件によって，励起状態が変化することを明らかにした．高温で CO 被覆率が低い条件では，傾いた(111)terrace 面を持つ Pt(110)(1 × 2)構造が安定となり，この時生成する CO_2 は，変角振動が励起していることがわかった．これに対し，低温かつ CO 被覆率の高い条件では，(1 × 1)構造へ変化するため，逆対称伸縮振動が励起するようになることを見出した．

Pd(110)および Pd(111)上における CO + NO 反応では，反応速度が表面構造に非常に敏感であることが明らかとなった．Pd(110)上における赤外発光測定結果の CO + O_2 反応との比較から，CO + NO 反応の高温側で生成する CO_2 分子は非常に振動励起しており，特に変角振動が励起していることがわかった．これらの結果から，NO の解離が律速であり，解離は step でのみしか起こらないこと，高温側における CO + NO 反応での CO_2 生成ダイナミクスが CO + O_2 反応と異なることが示唆された．また，Pd(110)上での CO + N_2O 反応では，CO + NO 反応よりもさらに小さい活性であることがわかった．赤外発光測定の結果から，生成 CO_2 分子の励起状態は CO + O_2 反応と類似しており，活性錯合体はより直線的な形をとることを見出した．

Abstract of thesis

This thesis describes the dynamics of CO oxidation by O_2, NO, and N_2O on noble metal (Pd, Pt, Rh) single-crystal surfaces, studied at pressures of *ca.* 10^{-2} Torr using infrared chemiluminescence (IR emission) of desorbed CO_2 as a probe of the structure of the transition state. The CO_2 was formed by CO oxidations using a free-jet molecular-beam method over single-crystal surfaces.

Steady-state CO + O_2 reactions were carried out over Pd(110), Pd(111), Pt(110), Pt(111), and Rh(111) surfaces. The CO_2 formation rate was sensitive to metal species (Pd(111) > Rh(111) > Pt(111)) and surface structures (Pd(110) > Pd(111) and Pt(110) > Pt(111)). Measurements and analyses of IR emission of CO_2 over each (111) surface supplied information about the vibrational energy states of CO_2 as the average vibrational temperature (T_V^{AV}), bending temperature (T_V^{B}), and antisymmetric temperature (T_V^{AS}). The order of the T_V^{AV} and T_V^{B} values was Pd(111) > Pt(111) > Rh(111). The order is considered to correspond to the potential energy of the transition state and the angle of the activated complex ($\angle_{OCO}$). On Pd(110) and Pd(111) at higher surface temperatures, the activated complex has a more bent form on Pd(111), and a less bent form on Pd(110) because CO_2 from Pd(111) is bending vibrationally excited and that from Pd(110) is antisymmetric vibrationally excited. In contrast, at lower surface temperatures, antisymmetric vibration is highly excited on both surfaces, a fact that can be related to high CO coverage. On the Pt(110) surface, the highly excited bending vibrational mode was observed at low CO coverage and also at high surface temperatures, which might be related to the activated complex of CO_2 formation in a more bent form on the inclined (111) terraces of the Pt(110)(1 × 2) structure. On the other hand, at high CO coverage or at low surface temperatures, T_V^{AS} was higher than T_V^{B}, which can be result from the reconstruction of the Pt(110)(1 × 2) surface to the (1 × 1) form with high CO coverage.

The CO + NO reaction on Pd(110) and Pd(111) showed high structure-sensitivity, meaning that the rate-determining step is NO dissociation on step sites. The IR emission spectra of CO_2 during the CO + NO reaction at high surface temperature show the bending vibration of CO_2 in the CO + NO reaction on Pd(110) to be much more excited than that in the CO + O_2 reaction, as described in terms of the difference in the dynamics of both reactions. The activity of the CO + N_2O reaction on Pd(110) was smaller than that of CO + NO reaction. Results of IR emission measurements showed that the vibrationally excited states of CO_2 in the CO + N_2O reaction resemble that in the CO + O_2 reaction, and that the structure of the activated complex is in a less bent form.

Contents

Chapter 1

General Introduction

1.1. CO oxidations on noble metal single-crystal surfaces

Steady-state catalytic reactions on single-crystal surfaces have been studied actively by only a few groups [1–6]. Numerous investigations of CO oxidations on noble metal surfaces have revealed the elemental steps of surface-catalyzed reaction [1–9]. However, few reports have elucidated steady-state reactions on single-crystal surfaces (Table 1-1(a) and 1-1(b)); especially few have described the formation rate (turnover frequency (TOF)) [3,5,6]. A brief summary of studies of steady-state CO oxidations ($CO + O_2$, $CO + NO$, and $CO + N_2O$ reactions) on noble metal (Pd, Pt, and Rh) single-crystal surfaces is given next before discussing the dynamics of CO oxidation on Pd, Pt, and Rh surfaces in section 1.2.

1.1.1. $CO + O_2$ reaction

The formation of CO_2 through catalytic oxidation of carbon monoxide (CO) by oxygen on noble metal surfaces (Pd, Pt, and Rh) has been a widely studied surface-catalyzed reaction. Recently, $CO + O_2$ reaction has attracted renewed attention because of its technological importance in the area of pollution control [10–13] and fuel cells [14,15]. Currently, the removal of CO from automobile exhaust is accomplished through oxidation of CO in catalytic converters using supported Pd, Pt, and Rh catalysts. For optimum operation of low-temperature fuel cells, it is well established that a continuous supply of CO-free hydrogen is necessary. Although, proton-exchange-membrane fuel cells can tolerate a few part-per-million (ppm) level of CO in the hydrogen stream, alkaline fuel cells require CO-free hydrogen. Conventional hydrogen production technologies such as steam reforming, partial oxidation and autothermal reforming of hydrocarbons produce large amounts of CO as a by-product [14,15]. Therefore, it is extremely important to have a $CO + O_2$ reaction catalyst that offers very high efficiency and one that can preferentially oxidize CO for production of CO-free hydrogen stream. Numerous studies of steady-state $CO + O_2$ reaction on single-crystal

surfaces [1–6,16–57] and model catalysts [7,8] have been performed in the past; because the reaction mechanism and kinetics are simple compared to those of other catalytic processes, the reaction represents the best understood catalytic reaction. However, despite numerous publications related to the kinetics of CO oxidation on noble metal surfaces (Pd, Pt, and Rh), much less is known about the dynamics of this reaction.

Ertl and co-workers studied the CO + O_2 reaction on Pd (Pd(111) and Pd(110)) [1,16–18] and Pt (Pt(111), Pt(110), and Pt(100)) [1,19–30] surfaces at ultrahigh vacuum (UHV) conditions using molecular-beam technique, photoemission electron microscopy (PEEM), and scanning tunneling microscopy (STM). They proposed the mechanism of CO + O_2 reaction on noble metal surfaces as a Langmuir-Hinshelwood mechanism for the first time, as described by the following equations.

$$CO + V \leftrightarrow CO(a) \quad (1)$$

$$½O_2 + V \rightarrow O(a) \quad (2)$$

$$CO(a) + O(a) \rightarrow CO_2 + 2V \quad (3)$$

Therein, V represents a vacant site. They studied the reaction kinetics estimating the reaction order and the activation energy of surface reaction (Eq. (3)) depending on the coverages of CO and oxygen [1,16,21,28]; they also studied the dynamics by probing a $\cos\theta$ angular distribution of CO_2 desorbing from the surface [16,28]. Furthermore, they observed various kinetic oscillations on Pd(110) [17], Pt(110) [19–25], and Pt(100) [25] caused by surface reconstruction or subsurface oxygen using PEEM, STM, and work function measurements.

Goodman and co-workers investigated the CO + O_2 reaction on Pd (Pd(110) and Pd(111)) [3,31,32], Pt(100) [31], and Rh (Rh(100) and Rh(111)) [3,33,34] surfaces at high-pressure conditions such as 16 Torr. They reported that the apparent activation energies on Pd(110) and Pd(111) were, respectively, 33.1 and 28.1 kcal/mol. In the case of the Rh surface, the reaction was structure-insensitive, as evidenced by the formation rate, activation energies, and partial pressure dependencies measured on the Rh(100) and Rh(111) surfaces. Furthermore, both surfaces deactivated at high O_2 partial pressures because of the formation of a near-surface oxide (probably Rh_2O_3).

Kunimori *et al.* used infrared chemiluminescence spectroscopy to study the steady-state CO + O_2 reaction on Pd (Pd(110), Pd(111), Pd(100), and Pd(335)) [35–43], Pt (Pt(110) and Pt(111)) [44–47], and Rh(111) [43] surfaces at the pressure condition of about 10^{-2} Torr. They reported that the kinetics and dynamics of surface catalyzed reaction (*i.e.*, transition state) were structure-sensitive because the formation rate and the vibrational state of product CO_2 molecules were greatly dependent on surface structure.

Bowker *et al.* studied CO oxidation on Rh(110) [49] and Pd(110) [50] using a thermal molecular beam. They carried out the reaction under the total flux of around 1×10^{13} molecules cm^{-2} s^{-1} (*ca.* 1×10^{-7} Torr). They reported that the reactivity of Rh crystal might be divisible into two regimes, depending on oxygen coverage. At $\theta_O > 0.6$, the reaction became much slower than at lower oxygen coverage, especially at $T > 400$ K. At low temperatures, the reaction was inhibited by the presence of CO; above $T \approx 400$ K, the steady-state coverage of CO became small and the reaction became inhibited by adsorbed oxygen [49]. For Pd(110), Bowker *et al.* determined the coverages of CO and oxygen using high-resolution X-ray photoelectron spectroscopy (XPS), thereby revealing the sticking probabilities of CO and O_2, and the activation energies of CO and O_2 desorption [50].

Schmidt *et al.* [51] measured the formation rate and coverages of CO and oxygen under the steady-state CO + O_2 reaction on an Rh(111) surface, and compared data for kinetics of experimental results and simulation based on the Langmuir-Hinshelwood model. Their reaction conditions were a wide range of CO and O_2 gas-phase compositions (CO/O_2 = 8/1–1/4) and surface temperatures (300–875 K) for pressures between 10^{-8} and 10^{-6} Torr. They reported that, below 425 K, the reaction rate increased with surface temperature with the activation energy of 20 kcal/mol, but at temperatures greater than 450 K, the rate decreased with temperature, with the activation energy of −7 kcal/mol. At low temperatures and in excess CO, the reaction rate was negative-first-order in P_{CO} and positive-first-order in P_{O_2}, but in excess O_2 and at high temperatures, the reaction rate was more than first-order (*e.g.*, +1.5) in P_{CO} and negative order (–0.5) in P_{O_2}.

Matsushima *et al.* studied the CO_2 desorption dynamics during the steady-state CO + O_2 reaction on Pd(110) [4,52,53], Pd(100) [4,54], Pt(110) [4,55–57], and Rh(110) [4,58,59] surfaces

using angle-resolved steady-state desorption (AR-SSD) measurements and low-energy electron diffraction (LEED). On Pd(110), CO_2 desorption is sharply collimated along the surface normal and is described as $\cos^6\theta$ in the lower θ_{CO} coverage region, and as a close cosine form ($\cos^{1.5}\theta$) in the higher θ_{CO} region. The velocity distribution of desorbing CO_2 was then deconvoluted into two components: the thermalized component, and a fast one with a translational temperature of 2300–2500 K. For Pt(110), two-direction CO_2 desorption was clear at the low CO coverage because of the declining (111) terrace of the reconstructed (1 × 2) surface. In contrast, at the high CO coverage, the desorption became the normally directed form, which was attributable to the (1 × 1) surface structure lifted by adsorbed CO. The Rh(110) surface readily undergoes reconstruction by oxygen adsorption and forms different superstructures depending on the coverage and surface temperature [58,59]. They reported that CO_2 productivity was enhanced in the low CO pressure range; furthermore, CO_2 desorption was split into inclined lobes nearly along the local normal of declining terraces of the missing-row structure. Simultaneously, the (1 × 2) LEED pattern attributable to the missing-row structure was confirmed, indicating that enhanced CO_2 formation on the inclined terrace. The metastable (1 × 2) missing-row structure was proposed to be responsible for this formation. In contrast, in the high CO pressure range, the CO_2 desorption was collimated sharply along the surface normal. This phenomenon was attributed to the (1 × 1) form of the Rh(110) surface, and at the same time, the (1 × 1) LEED pattern was observed.

Recently, studies of theoretical calculations related to CO oxidation have proliferated. Eichler *et al.* [60–63] studied the transition state of CO(a) + O(a) reaction over the (111) and (100) surfaces of transition metals (Pd, Pt, and Rh) using the density functional theory (DFT) calculations. They reported that, in addition to activation energies (*e.g.*, 32.3 kcal/mol on Pd(111), 17.1 kcal/mol on Pt(111), and 23.7 kcal/mol on Rh(111)) and reaction pathway, angle of the activated complex ($\angle_{OCO}$) can also derived based on transition state theory. Hu and co-workers used DFT calculations to investigate the reaction pathway and transition state in CO oxidation on Pd (Pd(100) and Pd(111)) [64,65], Pt(111) [66–69], and Rh(111) [69,70]. Hu *et al.* reported bonding energies and length, most stable sites, and reaction energies. They further suggested two crucial events in the reaction pathway: (i) the adsorbed O atom must be activated from the initial hollow chemisorption

site and (ii) the CO molecule must approach the O atom in the correct direction. Salo *et al.* [71] reported that the most stable sites of CO and oxygen are three-fold hollow sites, and proposed that both CO and oxygen are located near bridge sites next to each other at the transition state. Zhdanov *et al.* [72–74] investigated various phenomena that occur during heterogeneous catalytic reactions (*e.g.*, the energy of transition state and the oscillations of reaction rate and surface structure) using various theoretical calculations such as Monte Carlo simulations.

1.1.2. CO + NO reaction

In the early-1970s, world-wide acceptance of numerous environmental protection regulations for controlling the automobile exhaust emissions (*e.g.*, the Clean Air Act in the U.S. in 1970) has tightened restrictions on exhaust gases originating from mobile sources. Increasingly, stringent requirements for automobile emissions have cultivated intense scientific interest in the development of better catalytic conversion technologies, which has led to development of Pt/Rh (90/10) three-way catalysts (TWC) that simultaneously oxidize CO to CO_2, reduce NOx to N_2, and combust unburned hydrocarbons [10,11]. In the mid-1990s Pd-only TWCs that consist of Pd particles deposited on a high surface area metal-oxide support (typically γ-Al_2O_3) containing varying amounts of stabilizers and/or promoters such as CeO_2, SiO_2, La_2O_3, and BaO were introduced as an alternative to Pt/Rh (90/10) catalyst: Pd rapidly became the most highly consumed precious metal by the automobile industry for emission-control purposes [13].

Fundamental chemical and physical phenomena that take place on active sites of catalysts must be understood at the atomic or molecular level to design heterogeneous catalysts with higher performance. Therefore, the study of the CO + NO reaction on Pd, Pt, and Rh single-crystal surfaces is of vital importance. Many UHV studies have specifically addressed the nature of CO or NO chemisorption on single-crystal surfaces (*e.g.*, the study of CO and NO co-adsorption on Pd [75,76], Pt [77,78], and Rh [79,80]). However, only a few groups have studied the steady-state CO + NO reaction over well-defined Pd [4,5,75,81–89], Rh [99–117], and Pt [4,118] surfaces. Moreover, few reports have presented a comparison of the activity on single-crystal surfaces with different planes.

The Goodman group studied the steady-state CO + NO reaction on single-crystal surfaces (Pd – (110), (100), and (111) [5,75,81–89]; Rh – (100) and (111) [33,34]) at total pressure of several Torr (*e.g.*, 16 Torr) using infrared reflection-absorption (IRAS), temperature-programmed desorption (TPD) and reaction spectra (TPRS). They reported the activity of the CO + NO reaction on Pd surfaces at temperatures of 525–650 K as follows: Pd(111) > Pd(100) > Pd(110). This behavior was attributable to the influence of the adsorbed nitrogen species (N(a)). They reported that NO dissociates immediately on more open surfaces (Pd(110) and Pd(100)) to form atomic nitrogen (N(a)) [75,81,82]. The N(a) species are bound strongly to the surface and inhibit NO and CO adsorption. Therefore, the activity (TOF) on Pd(110) and Pd(100) was lower than that on Pd(111), and the rate-determining step is nitrogen desorption. In particular, they showed that 80% of the surface sites were covered by nitrogen species during the reaction on Pd(100), while only 20% were similarly covered by nitrogen species on Pd(111) [82]. For an Rh surface, the activity on Rh(100) was higher than that on Rh(111). They reported that the kinetics on Rh(111) were well described using a kinetic model [33,34], which predicts that the surface is covered predominantly by adsorbed nitrogen atoms and NO molecules, and that the rate is limited by the recombination of N(a) (denoted β-N_2 formation), which frees up adsorption sites on the surface for the other reactants (notably CO). The reaction on Rh(100) might be rate-limited by δ-N_2 formation (NO(a) + N(a) $\rightarrow$ N_2 + O(a)) because of the greater activation energy for β-N_2 formation on this surface.

Our group has studied steady-state reactions on Pd(110) and Pd(111) at pressures of about 10^{-2} Torr, and measured the rate of CO_2 formation and the IR emission spectra of CO_2 molecules [42,87–89]. The kinetic experimental results indicate that the activity of Pd(110) was much higher than that of Pd(111) at our pressure condition, which means that the rate-determining step is NO dissociation on step sites, and that the CO + NO reaction is highly structure-sensitive. From analyses of IR emission spectra of CO_2 on Pd(110), the average vibrational temperature (T_V^{AV}) of the CO + NO reaction was much higher than that of the CO + O_2 reaction in the high surface temperature range; furthermore, antisymmetric vibrational temperature (T_V^{AS}) was higher than the bending one (T_V^{B}) in the CO + O_2 reaction at all surface temperatures. In contrast, T_V^{B} was much higher than T_V^{AS} in the CO + NO reaction at higher surface temperatures (800 K and 850 K), which

indicates that the structure of the activated complex of CO_2 formation in the CO + NO reaction is in a more bent form than that in the CO + O_2 reaction, and that the reaction dynamics of CO_2 formation differ between the reactions at higher surface temperatures.

Matsushima and co-workers studied the angular and velocity distribution of desorbing N_2 and CO_2 molecules in the steady-state CO + NO reaction on Pd(110) [4,90–98], Rh(110) [93], and Pt(100) [118] in a wide range of reactant pressures (10^{-7}–10^{-5} Torr). They found that, on Pd(110), N_2 desorption was split into two inclined components collimating at ±40° in the plane along the [001] direction. Based on the close similarity of angular and velocity distributions in N_2O(a) decomposition on Pd(110), the inclined N_2 formation is proposed to originate from the N_2O(a) intermediate ($N_2O(a) \rightarrow N_2(g) + O(a)$). At low temperatures, the pathway through the N_2O(a) intermediate prevails, and, above 720 K, the associative nitrogen desorption starts to dominate ($2N(a) \rightarrow N_2(g)$). In contrast, N_2 desorption on Rh(110) was collimated sharply along the surface normal in a wide temperature region, indicating that N(a) is removed mostly through the associative process. On both surfaces, the translational temperature of desorbing N_2 was very high, reaching about 2500–3500 K. On the other hand, the CO_2 desorption always collimated along the surface normal on both surfaces with the translational temperatures of 1600–2000 K.

Schmidt *et al.* [99] measured the formation rate and coverage of CO, NO, nitrogen and oxygen under the steady-state CO + NO reaction on Rh(111) surface using X-ray photoemission spectroscopy (XPS). They considered the kinetics, comparing experimental results to those of simulations based on a modified Langmuir-Hinshelwood model, and determined the rate constants (pre-exponential factors and activation energies) of CO and NO desorption, NO dissociation, and surface reaction (CO(a) + O(a)). Their reaction conditions included a wide range of CO and NO gas-phase compositions (CO/NO = 1/4–64/1) and surface temperatures (300–875 K) for pressures between 10^{-8} and 10^{-5} Torr. They reported that the formation rate profiles had maxima. The major reaction step was NO dissociation followed by CO removal of the resulting adsorbed oxygen. The model exhibited that the rate limited by NO adsorption at high P_{CO}/P_{NO} ratios at temperatures greater than 500 K and the rate limited by the CO oxidation step (CO(a) + O(a)) at lower temperatures and at excess NO. The coverage of atomic nitrogen was never greater than 0.35 of

saturation and was neglected in the model.

Belton *et al.* studied the CO + NO reaction at high pressures (P_{total} = 9–48 Torr, CO/NO ratios = 1/8–8/1) on single-crystal Rh surfaces (Rh(110) [10,101], Rh(111) [100–105], and Rh(100) [101]), particularly measuring the activity and selectivity. They reported that the NO conversion rate (turnover numbers (TON)) on the Rh(110) surface was between 1.3 and 6.3 times higher than that on the Rh(111) surface in the range of surface temperatures (528–700 K); the TON for the Rh(100) surface was comparable to that measured for the Rh(110) surface. The Rh(110) surface exhibited a lower apparent energy (E_a), 27.2 kcal/mol, than the Rh(111) surface, E_a = 34.8 kcal/mol. They also found that the Rh(110) was considerably more selective for formation of N_2 *vs.* N_2O than the Rh(111) under all conditions studied. The higher selectivity towards N_2 was attributed to more facile dissociation of NO on the more open structure of the (110) surface. The nitrogen atoms yielded by NO dissociation can react with either NO or N to form N_2O or N_2, respectively. Similarly, the adsorbed oxygen generated by NO dissociation reacts with CO to form CO_2. This model was consistent with selectivities observed for both the Rh(110) and Rh(111) surfaces.

The Zaera and Gopinath groups investigated the kinetics and mechanism of the CO + NO reaction on Pd(111) [96,97] and Rh(111) [106–117] surfaces using effusive collimated molecular-beam technique: a molecular-beam doser is used, which consists of a 1.2-cm-diameter array of parallel microcapillary glass tubes (10 μm diameter, 2 mm long). They carried out the experiments under the total flux of about 0.5–1 monolayer per second (ML/s, 1 ML = 1.6×10^{15} molecules/cm^2 on Rh(111)) (our condition is about 10^{18}–10^{19} molecules/cm^2·sec), CO/NO ratios of 99/1–1/4, and surface temperatures of 350–1000 K. Their results showed that on Rh(111), because NO adsorbs more strongly on the surface than CO, a CO-rich gas mixture is necessary to optimize the reaction rate. The surface is covered mainly with atomic nitrogen under steady-state conditions. Even though most of this nitrogen is adsorbed strongly on the surface, its energy of adsorption is modified by the local surface arrangement of atoms in such a way that its reactivity is increased. They proposed that this behavior is attributable to the formation of adsorbate islands, the periphery of which reacts with incoming NO molecules to produce molecular nitrogen. They concluded that the rate-determining step is N_2 production, which occurs via the formation of the N–NO surface

intermediate. Therefore, they also studied the kinetics of nitrogen desorption on Rh(111) [119,120]. In the case of Pd(111), they reported that the N_2 formation limits the rate of the overall reaction below 525 K. However, the NO dissociation step contributes greatly toward the rate-determining step at temperatures greater than 525 K.

Almost no study has been done of the steady-state CO + NO reaction on single-crystal Pt surfaces, especially those of Pt(110) and Pt(111). Schmidt *et al.* [121] studied the kinetics of steady-state CO + NO reaction on polycrystalline Pt surface under UHV conditions, finding that the reaction on Pt is a bimolecular reaction between adsorbed CO and NO rather than unimolecular NO dissociation with CO removing of adsorbed oxygen because the kinetics fit only the former mechanism and reaction rates are up to about 10^4 times higher than those of NO dissociation. Bald and Bernasek measured the internal energy distributions for CO_2 produced in the CO + NO reaction on polycrystalline Pt gauze using a high-resolution tunable diode laser spectrometer. They found that the product CO_2 in the CO + NO reaction was vibrationally excited. Its internal energy distribution is similar to that of the product CO_2 in the CO + O_2 reaction. Bald and Bernasek [122] studied the CO + NO reaction on a polycrystalline Pt surface, comparing the CO + O_2 reaction measuring the internal energy states of product CO_2. They found a rough similarity in the vibrational excitation between CO + NO and CO + O_2 reactions on a polycrystalline Pt surface.

Most studies of the CO + NO reaction on Pt(100) at least partially address the phenomena of kinetic oscillation [123–126] and explosive reaction between adsorbed CO and NO under temperature-programmed desorption (TPD) [127,128], which is attributable to the surface reconstruction between a hexagonal form (hex) and a (1 × 1) form by the adsorption of CO. Horino and Matsushima [118] reported the angular and velocity distributions of desorbing N_2 and CO_2 in the steady-state CO + NO reaction on Pt(100). From their observation of the inclined N_2 desorption, a contribution of the intermediate N_2O decomposition pathway was first proposed on this surface. In contrast, CO_2 desorption was collimated along the surface normal.

1.1.3. CO + N_2O reaction

Nitrous oxide (N_2O) reduction that occurs on noble metal surfaces has received much

attention because N_2O is an undesirable by-product of the catalytic NO reduction in automobile gas converters [10–12]. This species is not only a harmful product that contributes considerably to the greenhouse effect; it is also the key intermediate for controlling the selectivity to N_2 because its decomposition can be shared the main pathway [4].

Several reports have described the adsorption and decomposition of N_2O on Pd [129–133], Pt [134–138], and Rh [131,139–147] surfaces. The decomposition of adsorbed N_2O(a) proceeds at around 100 K or even below it. To keep its decomposition continuous, a reducing reagent such as CO is necessary to remove the deposited surface oxygen. The steady-state reduction is inferred to be controlled by either N_2O adsorption or CO adsorption. However, few groups have studied the steady-state CO + N_2O reaction on well-defined single-crystal Pd [148–151] and Rh [152] surfaces.

Matsushima and co-workers examined the products (N_2 and CO_2) desorption dynamics in the CO + N_2O reaction on Pd(110) by angle-resolved mass spectroscopy combined with cross-correlation time-of-flight techniques. They reported that the N_2 yield in the CO + N_2O reaction was about 20% of that in the CO + NO reaction under the optimum conditions (*ca*. 10^{-6} Torr, $CO/N_2O = 1/6$) at the same N_2O and NO pressure [148]. This small yield was attributable to the small N_2O dissociation or adsorption probability. The N_2 desorption sharply collimated along about 45° off the normal toward the [001] direction; the desorbed N_2 molecules showed translational temperatures in the range of 2000–5000 K. They proposed that the decomposition proceeds in N_2O(a) oriented along the [001] direction. On the other hand, the CO_2 desorption sharply collimated along the surface normal, showing a translational temperature of about 1600 K.

Recently, we measured the IR emission of CO_2 produced by the steady-state CO + N_2O reaction (*ca.* 10^{-2} Torr) on Pd(110) surface, and studied the dynamics compared to results of the CO + O_2 and CO + NO reactions [42]. The activity of CO + N_2O reaction on Pd(110) was very small, and the order of the activity was as follows: CO + O_2 > CO + NO > CO + N_2O. Analyses of IR emission spectra of CO_2 from the three reactions showed that the antisymmetric vibrational mode of CO_2 was more excited in the case of the CO + N_2O and CO + O_2 reactions. In contrast, the bending vibrational mode was more excited in the case of the CO + NO reaction. These results suggest that the activated complex of CO_2 in the CO + NO reaction has a more bent structure than those in the

$CO + N_2O$ and $CO + O_2$ reactions.

Belton and Schmieg [152] studied the $CO + N_2O$ reaction on Rh(111) surface at pressures of 1 – 20 Torr. They measured the apparent activation energy (E_a) of 40.0 kcal/mol under 4 Torr of CO and 4 Torr of N_2O between 570 and 670 K. In addition, by varying the reactant pressures (T = 623 K), they determined that the reaction orders were +1.1 in N_2O pressure and −1.2 in CO pressure, and discussed that the rate-determining step is N_2O dissociation and the barrier for N_2O dissociation is 17.5 kcal/mol.

Table 1-1(a) Steady-state CO oxidation by O_2 on noble metal single-crystal surfaces.

Reaction	Authors	Metals and surface surfaces	Reaction conditions	References
$CO + O_2$	Ertl	Pd(111)	Molecular-beam *ca.* 10^{-7} Torr 400–700 K	1,16
		Pd(110)		1,17,18
		Pt(110)		1,19–26
		Pt(100)		27
		Pt(111)		28–30
	Goodman	Pd(110), Pd(111)	1–100 Torr 450–650 K	3,31,32
		Pt(100)		31
		Rh(111), Rh(100)		33,34
	Kunimori	Pd(110), Pd(111)	Molecular-beam (free-jet) 10^{-3}–10^{-2} Torr 450–900 K IR emission method	6,35–43
		Pd(335)		6,38
		Pd(100)		37
		Pt(110), Pt(111)		44–47
		Rh(111)		43
	Bowker	Rh(110)	Molecular-beam *ca.* 10^{-7} Torr 300–800 K	49
		Pd(110)		50
	Schmidt	Rh(111)	10^{-8}–10^{-6} Torr 425–900 K	51
	Matsushima	Pd(110)	10^{-7}–10^{-5} Torr 450–750 K Angle-resolved measurements	4,52,53
		Pd(100)		1,54
		Pt(110)		4,55–57
		Rh(110)		4,58,59

Table 1-1(b) Steady-state CO oxidation by NO and N_2O on noble metal single-crystal surfaces.

Reactions	Authors	Metal surfaces	Conditions	References
CO + NO	Goodman	Pd(100), Pd(111)	1–100 Torr 525–650 K	5,75,81–86
		Pd(110)		82
		Rh(100), Rh(111)		33,34
	Kunimori	Pd(110), Pd(111)	Molecular-beam (free-jet) 10^{-3}–10^{-2} Torr 450–900 K IR emission method	42,87–89
	Matsushima	Pd(110)	10^{-7}–10^{-4} Torr 450–800 K Angle-resolved measurements	6,90–95,98
		Rh(110)		93
		Pt(100)		118
	Zaera and Gopinath	Pd(111)	Molecular-beam (effusive beam) *ca.* 10^{-7} Torr 400–800 K	96,97
		Rh(111)		106–117
	Belton	Rh(111)	1–100 Torr 525–650 K	100–105
		Rh(110)		100,101
		Rh(100)		101
$CO + N_2O$	Matsushima	Pd(110)	10^{-7}–10^{-5} Torr 450–800 K Angle-resolved measurements	98,148–151
	Kunimori	Pd(110)	Molecular-beam (free-jet) 10^{-3}–10^{-2} Torr 450–900 K IR emission method	42
	Belton	Rh(111)	1–20 Torr 570–670 K	152

1.2. Studies of CO oxidation dynamics

1.2.1. Angular distribution and translational energy measurements

The necessity of investigating surface reaction dynamics on individual sites has been well recognized for many years because of the presence of key processes in catalyzed reactions, which are sensitive to surface structures [4]. Knowledge of surface reaction dynamics, which is growing rapidly, will be useful to elucidate catalysis of solid surfaces, and to design catalysts with new functions.

The identification of reaction sites on which reactants yield molecules is the first step to investigate such dynamics. However, no suitable methods to approach these sites are available. At present, the desorption dynamics of product molecules with high-excess transitional and internal (vibrational and rotational) energy can yield structural information related to these reaction sites. The spatial and velocity distributions of desorbing products provide the dynamics of key processes involved in the product formation event as well as information on the site, *i.e.*, its symmetry and orientation. In this method, product desorption is examined separately on each site through angle-resolved flux or velocity distribution measurements. This method was first developed using angle-resolved temperature-programmed desorption (AR-TPD) by Matsushima *et al.* [4]. It was then applied to surface reactions under steady-state conditions by Matsushima *et al.* [4]. It delivers characteristics of product desorption processes even when the overall reaction rate is controlled by reactant adsorption or when the observation of the interaction between adsorbed species is obscured in steady-state kinetics.

For thermally activated surface reactions, the angular and velocity distributions of desorbing molecules have mostly been analyzed using three different methods: modulated molecular-beams (MMB) [153], angle-resolved temperature-programmed desorption (AR-TPD) [4], and angle-resolved steady-state desorption (AR-SSD) measurements [4,57,154]. All have their advantages and are often mutually complementary. The advantage of using MMB is that they can provide the kinetic parameters (rate constant, reaction order, and activation energy) of fast constituent steps as well as the surface residence time of reactants, which can all be determined with a time resolution of microsecond order, covering the residence time of most chemisorbed species.

However, steady-state conditions cannot be established for the reaction studied by this method because of the periodical change of reactants on the surface. Particularly, AR-TPD has shown that the angular and velocity distributions of desorbing products can provide information about reaction sites as well as product desorption processes [4]. These distributions do not directly involve the reaction rate and are always related to the product desorption step whenever any step becomes rate-determining. The distributions would be informative if these could be measured under steady-state conditions. For that purpose, AR-SSD was developed, in which desorbing products are analyzed in an angle-resolved form when the reaction has established its steady-state conditions. The advantage of AR-SSD is that it can provide desorption parameters at definite steady-state conditions. The AR-SSD measurements were performed for CO + O_2 reaction on noble metals in 1998 [154]. These measurements yielded drastic changes in desorption dynamics at kinetic transition conditions under which the rate-determining step switches over.

Palmer and Smith [155] first measured the density angular distribution of CO_2 produced in a surface catalyzed reaction. On a Pt(111) surface that was grown epitaxially on a mica substrate, they found, using molecular-beam reactive scattering, that the product CO_2 desorbed with an angular distribution characterized by $\cos^d\theta$, with values of d between 4 and 6 depending on the surface roughness, the latter being determined by He scattering. Becker *et al.* [156] used angularly resolved time of flight (TOF) mass spectrometry to measure, for the first time, the flux angular distribution of CO_2 produced by the surface catalyzed oxidation of CO on a Pt foil. At temperatures of 425–650 K, the measured TOF distributions became progressively broader as the surface temperature or oxygen pressure was decreased. Becker *et al.* attributed this effect to the longer time for CO to find a reaction partner at low oxygen coverage and low surface temperature.

Campbell *et al.* [28] measured the density angular distribution of CO_2 produced on Pt(111) and also found a preference for desorption near the surface normal. Their results differed somewhat from those of Palmer and Smith [155] in that the angular distribution varied with surface temperature. Campbell *et al.* were able to show, however, that changes in the surface coverage were at least partly responsible for the change in the angular distribution. The following trends were noted: the distribution broadened as the oxygen coverage decreased, the distribution broadened as

the coverage of CO decreased, and with the coverage of oxygen fixed at its maximum value, the distribution sharpened as the surface temperature was increased. Engel and Ertl [16] probed a cos θ angular distribution of CO_2 desorbing from Pd(111) at surface temperature of 570 K under steady-state reaction conditions.

More recently, Brown and Sibener used molecular-beam reactive scattering to determine the flux angular distribution of CO_2 produced on Rh(111) [157,158]. Their results showed that the mean translational energy depended strongly on the desorption angle (being 8.5 kcal/mol in the direction of the surface normal and 4.3 kcal/mol at 60° from the normal), but appeared to be independent of surface temperature in the range of 700–1000 K [158]. Furthermore, Colonell *et al.* [159] measured the CO_2 TOF distribution under steady-state conditions by chopping the product flux after the crystal as a function of desorption angle, surface temperature, and oxygen coverage. Their results showed that the angular and velocity distributions are apparently bimodal. One component is well characterized by Maxwell-Boltzmann velocity distributions at the surface temperature and a cosine angular distribution. The second component is non-Boltzmann, with energies much greater than expected for molecules that have equilibrated with the surface, and an angular distribution sharply peaked toward normal. The average energy of the high energy peaked increases slowly with oxygen coverage. The average energy of the high-energy peak is strongly affected by the surface temperature.

Matsushima [160] measured the density angular distribution of CO_2 produced on Pt(111) and polycrystalline Pt surfaces. Unlike the other angular distribution measurements on Pt(111) [28,29,155], He used AR-TPR to determine the angular distributions as a function of adsorbate coverage. In addition, Matsushima *et al.* applied AR-TPR and LEED to measure the density angular distribution of CO_2 produced during CO(a) + O(a) reaction on Pd(111) [4,161], Pd(110) [4,162,163], Pt(110) [164,165], Rh(111) [166], and Rh(110) [167]. Most recently, Matsushima *et al.* applied AR-SSD to the studies of the CO + O_2 reaction on Pd(110) [4,52,53], Pt(110) [4,55–57], and Rh(110) [4,58,59], the CO + NO reaction on Pd(110) [4,90–94,98], Rh(110) [93], and Pt(100) [118], and the CO + N_2O reaction on Pd(110) [148–151].

1.2.2. Internal energy measurements

The measurements made, thus far, of the internal (vibrational and rotational) energy distribution of CO_2 molecules share the characteristic that IR emission has been at the foundation of each study. The applicability of the technique as a probe of the structure of the transition state is based on the assumption that the energy released by crossing the transition state remains in the reaction coordinate; therefore, vibrational and rotational modes in CO_2 that comprise the reaction coordinate become excited. With the additional assumption that the reaction coordinate leads the nascent CO_2 directly into the gas phase, the important technique of the process comes to be delaying collisions until the chemiluminescence from CO_2 occurs.

The most extensive (nearly collision-free) data recorded of the internal excitation in CO_2 molecules produced on a noble metal surface was collected by Mantell *et al.* [168–171] using FT-IR spectroscopy. The reactants were delivered to a polycrystalline Pt foil using a free-jet nozzle source, which was operated under conditions that prevented the occurrence of any hard sphere collisions among nascent CO_2 molecules or between CO_2 and incoming reactant molecules (CO and O_2) prior to detection of the emission. The vibrational spectrum produced by IR emission in the antisymmetric stretch fundamental and its associated hot bands was collected both at high (0.06 cm^{-1}) and at low (8 cm^{-1}) resolution. Although the ultimate resolution of their spectrometer was insufficient to resolve the emission detected from each excited vibrational levels completely, individual rotational lines from several vibrational levels were distinguishable to allow for curve fitting of the 0.06 cm^{-1} spectrum, thereby allowing the extraction of apparent vibrational and rotational temperatures [171]. These temperatures are shown in Table 1-2 for reaction on a Pt foil surface at surface temperatures of 730 K and 900 K. For an increase in surface temperature of 170 K, the extracted temperatures also increased by nearly 170 K (within the quoted error), except for the symmetric stretch mode, which increased by 400 K. It is noteworthy that all temperatures are markedly higher than the surface temperature. Furthermore, for reactions at both surface temperatures, the low-resolution spectra are predictable by inserting the appropriate values from Table 1-2 into a model that used mode temperatures to calculate the relative intensity of approximately 300 vibrational levels, all hot bands on the fundamental [171], which was taken as

evidence that each mode was equilibrated internally, even though a state of nonequilibrium existed between modes.

Table 1-2 Vibrational and rotational temperatures determined by Mantel *et al.* [171] for CO + O_2 reaction on Pt foil

T_S / K	T_V^{SS} / K	T_V^{B} / K	T_V^{AS} / K	T_R / K
730	1300	1600	1500	1050
900	1700	1750	1600	1200

Note: The variables T_S, T_V^{SS}, T_V^{B}, T_V^{AS}, and T_R respectively represent surface temperature, symmetric vibrational temperature, bending vibrational temperature, antisymmetric vibrational temperature, and rotational temperature. Uncertainties in the temperatures were reported to be ±75 K for vibrational temperatures and ±50 K for rotational temperatures. The rotational temperatures were derived by fitting the measured rotational distributions with a Boltzmann distribution that had equal contributions from two populations: one population at the temperature shown in the table and the other at 200 K.

Generally, increasing the surface temperature also changes the reactant surface coverages, thereby rendering interpretation of the large increase in the symmetric stretch temperature difficult. To circumvent that difficulty, Mantell *et al.* [169] performed time resolved FT-IR (30 μs time resolution) at 8 cm^{-1} resolution, which allowed the reactant coverages to vary without changes in surface temperature. A steady background of oxygen was maintained on the Pt foil surface using a nozzle source, whereas pulses of CO were directed onto the surface from a second nozzle source. At the beginning of the CO pulse, when the oxygen coverage was largest, the vibrational spectrum of CO_2 was consistent with an average vibrational temperature of 1800 K (T_S = 900 K). This result showed good agreement with the average vibrational temperature determined for steady-state reaction at the same temperature, see Table 1-2. As the oxygen coverage approached zero, an abrupt shift in the spectrum occurred that placed the centroid of the spectrum closer to the band center of the fundamental, *i.e.* the average vibrational temperature apparently decreased. However, the integrated intensity of the low oxygen coverage spectrum was too large relative to the integrated intensity of the high coverage spectrum to be consistent with a simple lowering of the overall vibrational temperature. Mantell *et al.* discussed their result in terms of a decrease in the translational energy of the CO_2 with decreasing oxygen coverage, which is consistent with the

density angular distribution measurement of Segner *et al.* [29] on a Pt(111) surface. Mantell *et al.* [169] also suggested that the energy released in the reaction was partitioned selectively into the antisymmetric fundamental. Another interpretation is that more molecules were excited to the antisymmetric fundamental at the expense of population in the ground state under low coverage conditions. However, since the experiments were performed in the emission mode, the ground state could not be probed.

Coulston and Haller [172–174] studied the dynamics of CO + O_2 reaction on polycrystalline Pd, Pt, and Rh foils under nearly collision-free conditions using high-resolution (0.012 cm^{-1}) IR emission of desorbed CO_2 as a probe of the structure of the transition state. For reaction on the Pd foil at T_S = 600 K with equal fluxes (4×10^{18} molecules cm^{-2} s^{-1}) of CO and O_2, the symmetric stretch vibrational levels were populated with an apparent temperature of 3150 K, whereas the apparent antisymmetric and bending temperatures were 2130 K and 1820 K, respectively, as shown in Table 1-3. Increasing the surface temperature by 75 K disproportionately increased the apparent temperature of each mode, *e.g.*, for Pd foil at T_S = 675 K, T_V^{SS} = 3700 K, T_V^{AS} = 2530 K, and T_V^{B} = 2050 K (Table 1-3). It is noteworthy that even though T_V^{SS} is consistently larger than T_V^{B} for CO_2 produced on Pd, more energy is partitioned into the bending modes because of the higher density of bending levels in CO_2. Table 1-4 shows that they calculated the partitioning of energy into various degrees of freedom of CO_2 based on the apparent temperatures, T_V^{B}, T_V^{SS}, T_V^{AS}, and T_R given in Table 1-3. The observed changes in the vibrational populations were likely to have been caused by changes in the reactant coverages as the surface temperature increased because similar changes in the apparent temperatures are inducible by changing only the reactant partial pressures above the Pd surface (Table 1-4). Reaction on Pt at T_S = 814 K also produced vibrationally excited CO_2, but the apparent vibrational temperatures for each mode were nearly identical, equivalent to 1580 K. Similar behavior was observed for reaction on Rh at T_S = 584 K: the average apparent vibrational temperature was equal to 1295 K. A transition state to CO_2 formation that was approximately linear and aligned along the surface normal on Pt and Rh; it was bent on Pd (although still primarily interacting with the surface through only one oxygen), and was consistent with the measured vibrational level populations.

Table 1-3 Apparent vibrational and rotational temperatures determined by Coulston *et al.* [173] for CO + O_2 reaction on Pd, Pt, and Rh foil

Surface	$CO:O_2$ (T_S / K)	T_V^{SS} / K	T_V^{B} / K	T_V^{AS} / K	T_R / K
Pd	1:1 (600)	3150	1820	2130	845
	1:1 (675)	3700	2050	2540	900
	1:2 (600)	3900	2140	2460	880
Pt	1:1 (814)	1500	1600	1550	995
Rh	1:1 (584)	1270	1300	1210	730

Table 1-4 Partitioning of energies into product CO_2 calculated by Coulston *et al.* [173] for CO + O_2 reaction on Pd, Pt, and Rh foil

	Pd			Pt	Rh
	$CO:O_2$=1:1 600 K	$CO:O_2$=1:2 600 K	$CO:O_2$=1:1 675 K	$CO:O_2$=1:1 814 K	$CO:O_2$=1:1 584 K
Vibration					
Antisymmetric	7.5	9.6	10.0	3.8	2.1
Symmetric	18.8	25.1	23.4	6.7	4.6
Bending	23.0	27.2	25.9	18.4	14.6
Rotation	4.6	4.6	5.0	5.9	3.6
Total	53.9	66.5	64.3	34.8	24.9

The amount of energy partitioned into the degree of freedom of CO_2 based on the apparent temperatures derived from the high resolution spectra. All values reported in kJ/mol. The zero of energy for CO_2 is taken as 300 K.

Bernasek and Leone [175] and then Brown and Bernasek [176] studied the CO + O_2 reaction on Pt gauze using IR emission spectroscopy under a high-pressure system (1 Torr); both investigations showed that the product CO_2 molecules were vibrationally excited after having been produced. They found that the average apparent vibrational temperature of CO_2 was 1900 K, although the apparent antisymmetric vibrational temperature was 1500 K, both for reaction on the

gauze of 1000 K. The deviation in the two temperatures was taken as evidence that the vibrational modes of CO_2 were not in equilibrium, in agreement with the results of Mantell *et al.* [171]. Brown and Bernasek also reported that the vibrational temperature increased with increasing surface temperature and decreased with increasing oxygen coverage. Bald and Brown [122,177] used a high resolution TDL spectrometer to detect internal energy distributions for CO_2 molecules produced in the oxidation of CO by O_2 [177] and NO [122] on polycrystalline Pt gauze. Absorption spectra were collected for CO_2 produced in a flow cell reactor for a wide range of temperatures and reactant ratios. Their results showed that antisymmetric stretching mode consistently exhibited a higher vibrational Boltzmann temperature than the bending or symmetric stretching modes in both CO + O_2 and CO + NO reactions. The level of vibrational excitation for all vibrational modes was sensitive to oxygen coverage, *i.e.*, as either the O atom/CO molecule ratio or the surface temperature was increased, the vibrational temperature of the product CO_2 increased considerably. Kunimori and Haller [178] used a pulsed CO beam and time-resolved IR emission spectroscopy (4 cm^{-1} resolution) to examine the dependence of the internal energy of product CO_2 on the surface oxygen coverage in the CO + O_2 reaction on polycrystalline Pt and Pd surfaces. They found that the average vibrational temperature (T_V^{AV}) decreased drastically with decreasing oxygen coverage on Pt surface. In contrast, no such drastic change in T_V^{AV} was observed on the Pd surface, but T_V^{AV} was decreased only slightly with decreasing oxygen coverage. In addition, the higher T_V^{AV} values on Pd than on Pt were consistent with results of the steady-state CO oxidation.

Kunimori and co-workers [179–181] studied the dynamics of partial oxidation of hydrocarbons (such as butane (C_4H_{10}) and ethylene (C_2H_4)) on a polycrystalline Pt surface measuring IR emission of product CO molecules. Their results indicated that the product CO was substantially vibrationally excited, but rotationally very cool. Furthermore, recently, they have succeeded, for the first time, in measuring the IR emission of CO_2 produced by the steady-state CO + O_2 reaction (*ca.* 10^{-2} Torr) on single-crystal Pd [6,35–38] and Pt [44–46] surfaces. Their results showed that the reaction is structure-sensitive both in terms of the kinetics and in the dynamics by comparing the reaction rate and the internal energy state of CO_2 molecules between those surfaces. The activated complex of CO_2 formation (the transition state of CO_2 formation from CO(a) + O(a))

had a more bent structure on Pd(111) and a straighter structure on Pd(110) at higher surface temperatures (T_S > 650 K) because CO_2 from Pd(111) was more excited vibrationally than CO_2 from Pd(110) [6,35–38]. On the other hand, in the case of Pt surfaces, CO_2 from Pt(110) was more excited than CO_2 from Pt(111) [44–46] at higher surface temperatures (T_S > 680 K), which was attributable to the reconstructed (1 × 2) form of Pt(110). Most recently, the author has studied CO oxidation by O_2, NO, and N_2O on single-crystal Pd, Pt, and Rh surfaces at pressure of about 10^{-2} Torr and surface temperatures of 400–900 K [39–43,47,87–89]. I modified the apparatus, which enable observations under severer conditions (*i.e.*, lower CO_2 formation rates at lower surface temperature) [40,41,47,89]. More detailed analyses of IR emission spectra have become possible using IR intensity [40,41,47,89], as described in Section 1.4.

1.3. Apparatus

A molecular-beam reaction system, in combination with a FT-IR spectrometer (InSb detector, Nexus670; Thermo Electron Corp.), was used to measure IR emissions of product CO_2 molecules that desorbed on metal surfaces during catalytic reactions [40,41,47,89]. A UHV chamber (base pressure < 1.0×10^{-9} Torr) was equipped with: a CaF_2 lens, which collected IR emission; an Ar^+ ion gun for sample cleaning; and a quadrupole mass spectrometer (QMS, QME200; Pfeiffer Vacuum Technology AG) with a differential pumping system (Figure 1-1). Two free-jet molecular-beam nozzles (0.1-mm-diameter orifice) supplied the reactant gases. The reactant fluxes were controlled using mass flow controllers (Figure 1-2). The CO, O_2, NO, and N_2O gases were exposed to single-crystal Pd, Pt, and Rh surfaces: Pd(110), Pd(111), Pt(110), Pt(111), Rh(110), and Rh(111). Steady-state CO oxidations (CO + O_2, CO + NO, and CO + N_2O reactions) were performed at temperatures of 400–900 K. Another UHV chamber (base pressure < 2.0×10^{-10} Torr) was used to prepare the samples and to characterize single-crystal surfaces. It was equipped with an Ar^+ ion gun, low-energy electron diffraction (LEED), and a QMS. Before the molecular-beam reaction, the single-crystal surfaces were cleaned using a standard procedure (O_2 treatment, Ar^+ bombardment, and annealing) [40,41,47,89].

1.4. Measurements and Analysis

Unless stated otherwise, the IR emission spectra of the CO_2 molecules desorbed from the surface were measured with 4 cm^{-1} resolution. At that low resolution, no individual vibration-rotation lines were resolved. Figure 1-3 shows an IR emission spectrum of CO_2 produced by the CO + O_2 reaction on Pd(111) at surface temperature (T_S) = 850 K. It was taken at 1 cm^{-1} resolution. The CO_2 emission spectrum was observed in the region of 2400−2200 cm^{-1}, whereas the emission spectrum of the non-reacted CO, which was scattered from the surface, was centered at 2143 cm^{-1}. In the spectrum with 1 cm^{-1} resolution, the rotational lines (P and R branches) of CO molecules are clearly visible; notwithstanding, those of CO_2 molecules were not resolved.

The IR emission spectra of product CO_2 were analyzed based on simulations of model spectra. They yielded an average vibrational Boltzmann temperature (T_V^{AV}: an average temperature of antisymmetric stretch, symmetric stretch and bending modes) and a rotational Boltzmann temperature (T_R) [171,178]. The value of T_V^{AV} was calculated from the degree of red-shift from the fundamental band (2349 cm^{-1}); then T_R was derived from the emission-band width (Figs. 1-4(a) and 1-4(b)). Although the IR emission observed here is in the antisymmetric stretch vibrational region – (n_{SS}, n_B^l, n_{AS}) → (n_{SS}, n_B^l, n_{AS} − 1) – the vibrational excitation levels of symmetric stretch (n_{SS}) and bending (n_B) also affect this region [6,171]. Here, n_{SS}, n_B and n_{AS} are vibrational quantum numbers of respective modes. The quantum number of vibrational angular momentum in linear molecules is denoted by l. Note that the emission intensity is normalized using the rate of CO_2 production. Consequently, the emission intensity is related to the extent of excitation in the antisymmetric stretch of CO_2, which is given as

$$f \propto e^{-x} + e^{-2x} + e^{-3x} \cdots \doteqdot e^{-x}/(1-e^{-x}), \qquad (4)$$

where f is the emission intensity normalized per unit of CO_2 yield, and x equals to $\Delta E_V/k_B T_V^{AS}$ (ΔE_V is the energy spacing, k_B is the Boltzmann constant and T_V^{AS} is the antisymmetric temperature). High-resolution steady-state results (0.06 cm^{-1}) [171] show the energy distribution in respective vibrational modes, T_V^{SS}, T_V^{B}, and T_V^{AS}, for which the superscripts respectively indicate symmetric stretch, bending, and antisymmetric stretch. Here, the steady-state CO + O_2 reaction on polycrystalline Pt foil was performed with the previous conditions as [171] (CO = O_2 = 4.1 × 10^{18}

cm^{-2} s^{-1}; Fig. 1-5). The IR emission spectra of CO_2 molecules were measured with 4 cm^{-1} resolution at the surface temperature (T_S) of 900 K (Fig. 1-6). The resultant spectrum was compared to previous results (T_V^{AS} = 1600 K) [171]. We estimated the emission intensity as T_V^{AS} = 1600 K. This emission intensity and T_V^{AS} on the polycrystalline Pt surface were used as standards for various conditions on Pd surfaces (Fig. 1-4(c)). Based on T_V^{AS} and T_V^{AV}, it is possible to deduce the bending vibrational temperature (T_V^{B}). The relation between T_V^{AV} and respective vibrational temperatures is represented as

$$T_V^{AV} = (T_V^{AS} + T_V^{SS} + 2T_V^{B}) / 4, \quad (5)$$

where $2T_V^{B}$ corresponds to the degeneration of two bending vibrational modes. Assuming that T_V^{B} is equal to T_V^{SS} because of the Fermi resonance [173,177], T_V^{B} is expected to be $(4T_V^{AV} - T_V^{AS})/3$. This assumption is plausible based on previous reports [171,177]. It must be added that T_V^{AV}, T_V^{AS}, T_V^{B}, and T_R were used here as parameters to characterize the extent of vibrational and rotational excitation of the product CO_2. A number and time of scanning necessary for measurement of IR emission spectra are described in respective experimental sections of chapters 2–6. The activity was stable during measurement. Therefore, we infer that the results reflected the CO_2 states under steady-state conditions.

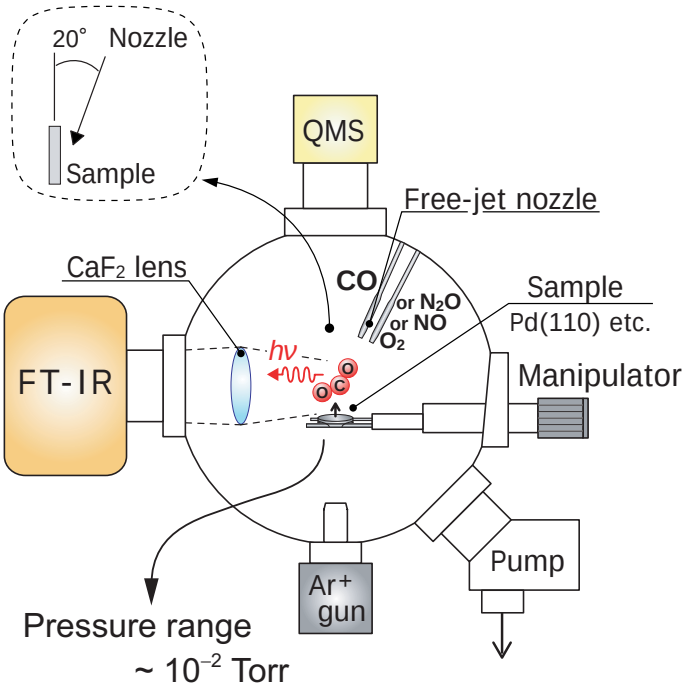

Figure 1-1 Schematic view of a free-jet molecular-beam reaction chamber equipped with an FT-IR spectrometer, QMS, and Ar^+ ion gun.

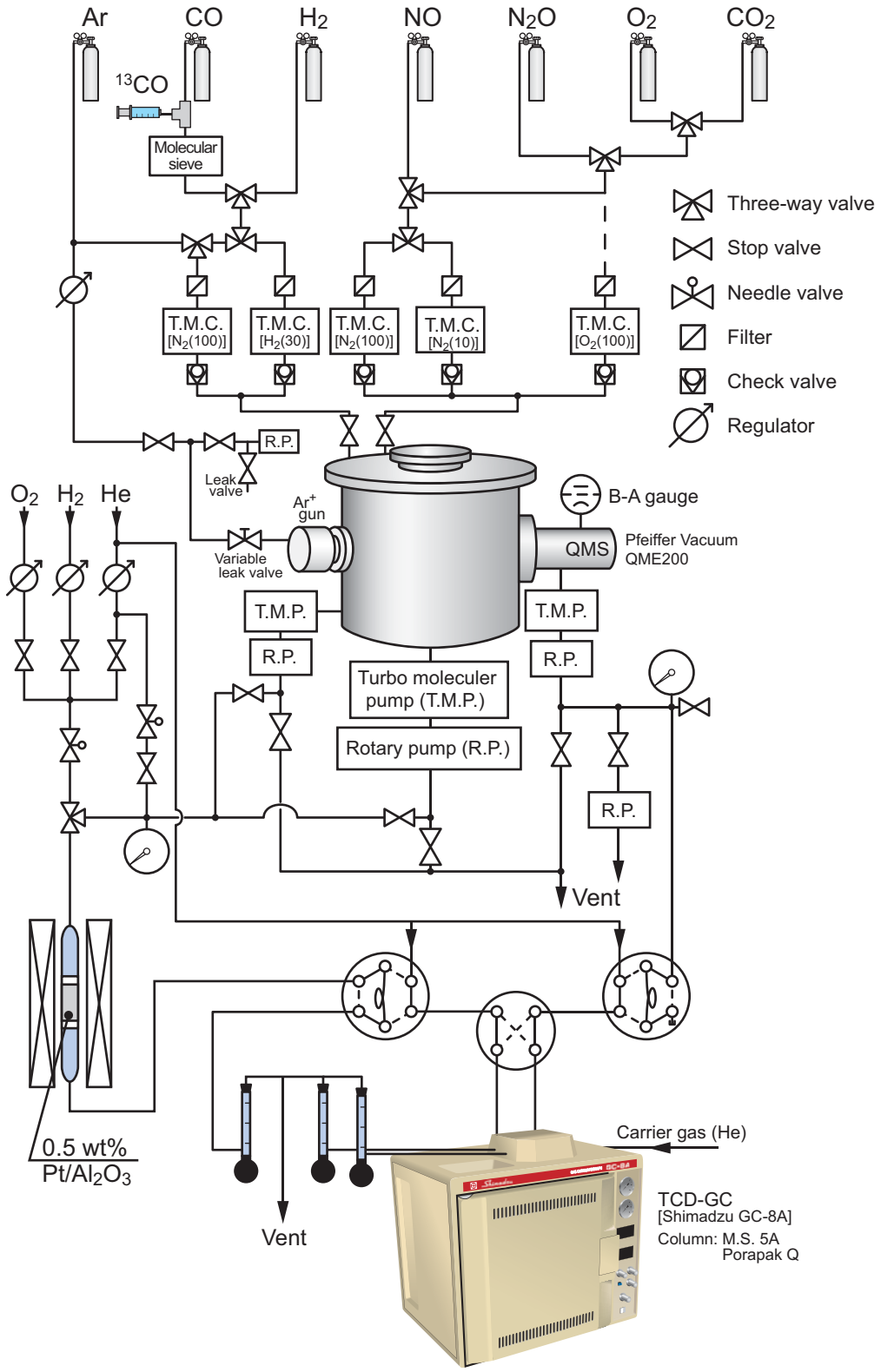

Figure 1-2 Schematic diagram of reaction system for the study of steady-state CO oxidations on single-crystal surfaces.

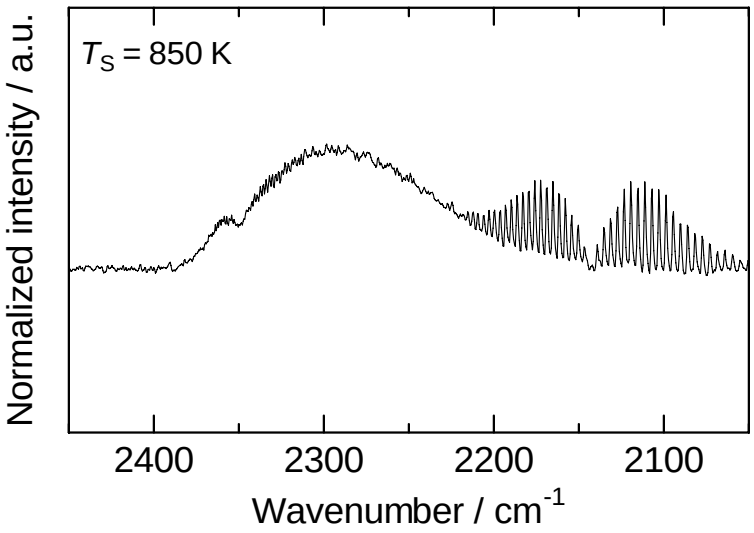

Figure 1-3 IR emission spectra of CO_2 desorbed by the CO + O_2 reaction on Pd(111). The surface temperature (T_S) was 850 K. The total flux of reactant CO and O_2 was 8.2×10^{18} molecules cm^{-2} s^{-1} at $CO/O_2 = 1$. The spectral resolution was 1 cm^{-1}.

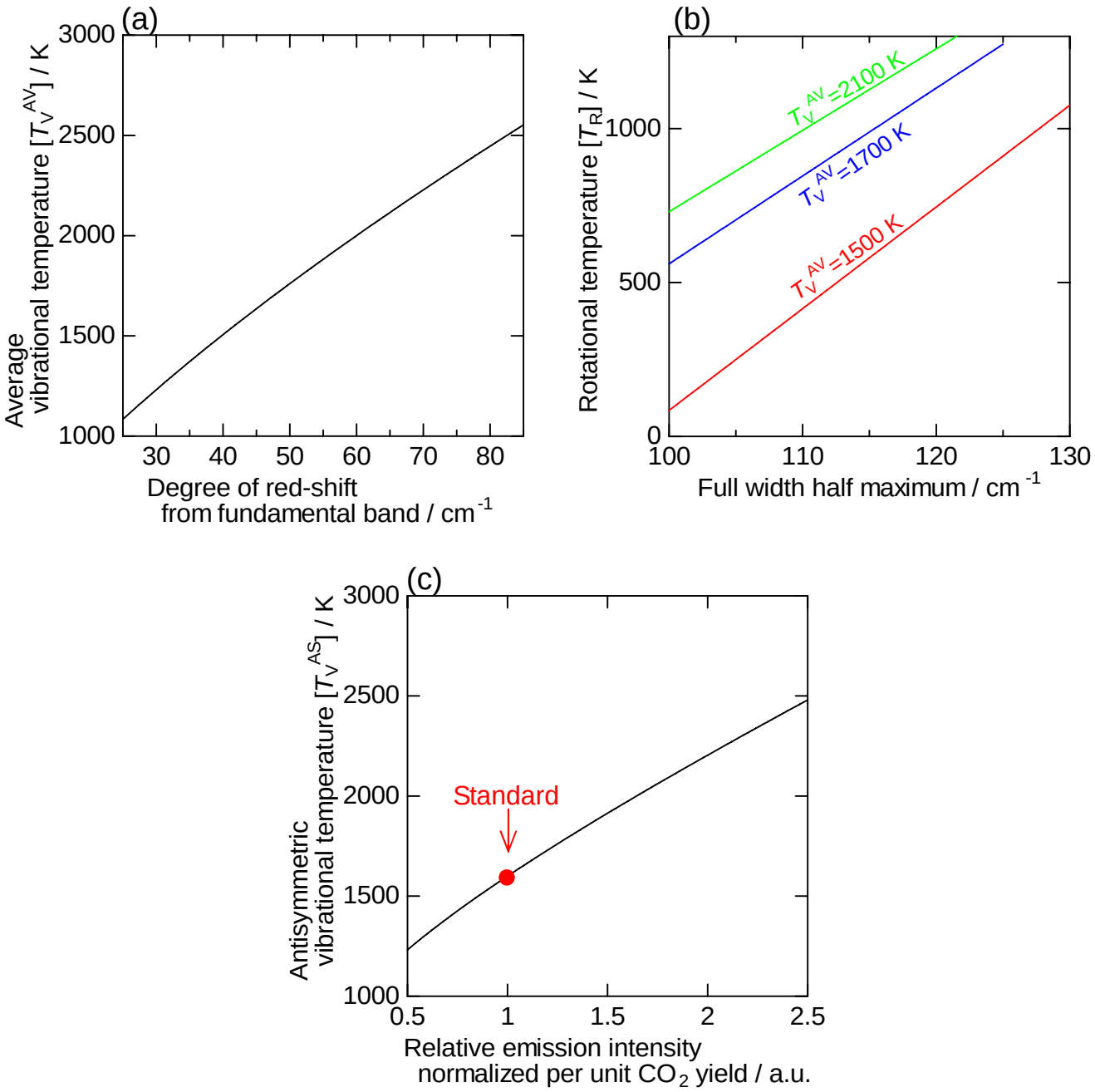

Figure 1-4 Analyses of average vibrational temperature (T_V^{AV}), rotational temperature (T_R) and antisymmetric vibrational temperature (T_V^{AS}): (a) T_V^{AV} as a function of degree of red-shift from fundamental band; (b) T_R as a function of full-width at half-maximum (T_V^{AV} = 1500, 1700 and 2100 K); (c) T_V^{AS} as a function of relative emission intensity normalized per unit of CO_2 yield.

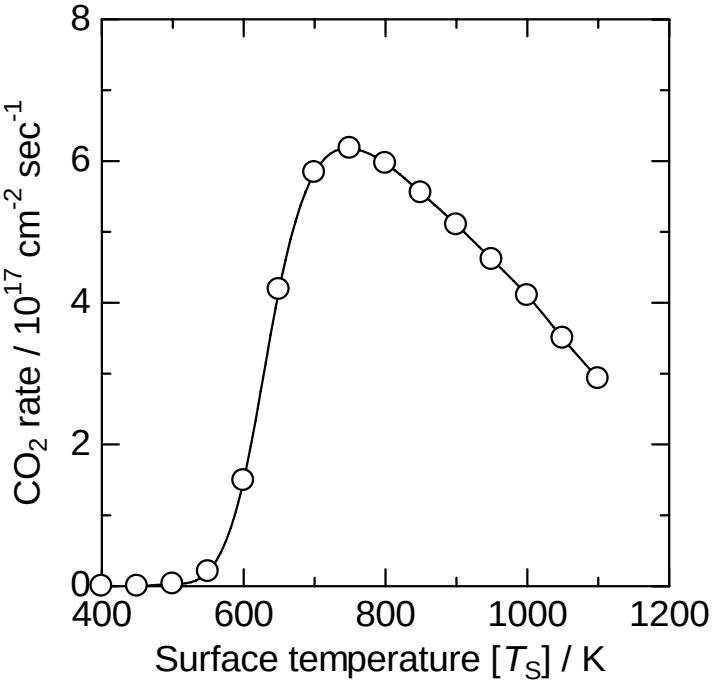

Figure 1-5 The formation rate of CO_2 during the CO + O_2 reaction (CO/O_2 = 1) on polycrystalline Pt foil as a function of surface temperature. The total flux of reactant CO and O_2 was 8.2×10^{18} molecules cm^{-2} s^{-1} at CO/O_2 = 1.

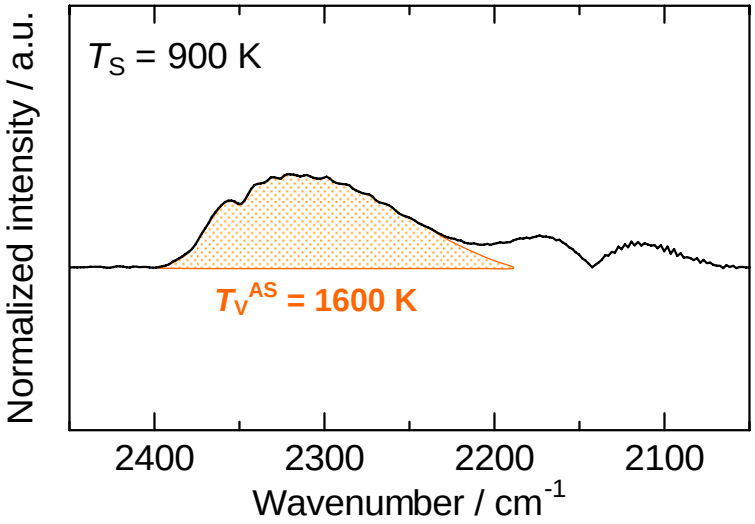

Figure 1-6 IR emission spectra of CO_2 desorbed by the CO + O_2 reaction on polycrystalline Pt foil. The surface temperature (T_S) was 900 K. The total flux of reactant CO and O_2 was 8.2×10^{18} molecules cm^{-2} s^{-1} at $CO/O_2 = 1$.

1.5. Purpose of this thesis

Elucidation of reaction mechanisms is important for catalyst design and control of reaction routes. Single-crystal surfaces are useful to elucidate reaction mechanism over heterogeneous catalysts. The reactions of CO oxidation by O_2, NO, and N_2O are important automobile exhaust control reactions catalyzed by noble metals such as Pd, Pt, and Rh. An effective method is an investigation of internal (vibrational and rotational) energy of desorbed molecules, which are the products (CO_2) of catalytic reaction, from the catalyst surface. The IR emission of the product molecules from catalytic reaction enables analysis of the vibrationally excited states, as described above. Recently, the Kunimori group [6,35-38,44-46] found that the steady-state CO + O_2 reaction on single-crystal Pd and Pt surfaces is structure-sensitive both in its kinetics and in its dynamics. From that study, however, only information about the average vibrational temperature (T_V^{AV}) at the higher surface temperature was reported.

1.5.1. Elucidation of reaction dynamics of CO + O_2 reaction on Pd, Pt, and Rh surfaces: effect of surface structure and metal species

As stated above, our group has reported the IR emission of CO_2 from steady-state CO + O_2 reaction on single-crystal Pd and Pt surfaces combined with kinetic results [6,35–38,44–46]. However, only information about the dynamics at the higher surface temperature was observed. The author modified an apparatus that has enabled observation under severe conditions (*i.e.*, with lower CO_2 formation rates at lower surface temperature). Furthermore, more detailed analyses of IR emission spectra have been possible using IR intensity. Generally, the catalytic reactions using real and practical catalysts are carried out at lower reaction temperatures. Consequently, chemiluminescence investigations at a lower temperature range are of greater practical value. This thesis specifically addresses such severe reaction conditions. The kinetics and dynamics of CO + O_2 reaction on Pd, Pt, and Rh surface were studied, and the effects of surface structure were discussed, especially those of (110) and (111), and metal species.

1.5.2. Elucidation of reaction dynamics and kinetics of CO oxidations: effect of oxidant (O_2, NO, and N_2O)

Numerous studies have been done of the steady-state CO + O_2 reaction on noble metal single-crystal surfaces. However, only a few groups have investigated the steady-state CO + NO and CO + N_2O reaction on single-crystal surface. Furthermore, almost no work has been performed to elucidate the vibrational energy state of CO_2 produced from the CO + NO and CO + N_2O reactions on single-crystal surfaces. For that reason, the author studied the steady-state CO + NO reaction on Pd(110) and Pd(111) compared to the CO + O_2 reaction; in addition, the structure-sensitivity of the kinetics of CO + NO reaction and the vibrational state of CO_2 molecules in CO + NO reaction were discussed. Moreover, the dynamics of CO + N_2O reaction on Pd(110) were investigated, comparing the results of CO + O_2 and CO + NO reactions.

1.6. Outline of this thesis

This thesis presents the results of the elucidation of activities and dynamics of CO_2 formation during steady-state CO oxidation by O_2, NO, and N_2O on well-defined noble metal (Pd, Pt, Rh) single-crystal surfaces. This thesis includes seven chapters. Each chapter of is written based on one or two different publications, and can be read independently.

Chapter 1 presents a general introduction. A review of steady-state CO oxidations on single-crystal surfaces and studies of the dynamics of surface catalyzed reactions are presented there, along with important features of the apparatus, measurements, and analysis of this research are mentioned. The purpose of this thesis is also described.

Chapter 2 describes the dynamics of CO + O_2 reaction on Pd(110) and Pd(111) surfaces combined with kinetic results. The structure of the activated complex of CO_2 formation on both surfaces at higher and at lower surface temperatures has been proposed from results of IR emission measurements.

The description included in chapter 3 is of partial reactant pressure and surface temperature dependence of the steady-state CO + NO reaction on Pd(110) and Pd(111) surfaces compared to those of the CO + O_2 reaction. The structure-sensitivity of the CO + NO reaction and the interesting

behavior of the vibrational state of CO_2 from the CO + NO reaction are discussed.

Chapter 4 includes an investigation of the vibrational state of CO_2 from CO + N_2O reaction on Pd(110); it is compared to vibrational states of CO_2 from CO + O_2 and CO + NO reactions. Detailed analyses of kinetics and dynamics of three reactions at a high surface temperature (750 K), and the interpretation in terms of the structure of the activated complex and the reaction mechanism were discussed.

Chapter 5 describes the dynamics of CO_2 formation in steady-state CO + O_2 reaction on Pt(110) and Pt(111) surfaces. A Pt(110) surface is well known to be reconstructed to a (1 × 2) missing-row structure, and the reconstruction is lifted to the (1 × 1) form by adsorbed CO. The vibrational energy states of the product CO_2 molecules, which are changed by lifting the surface structure of Pt(110), were analyzed circumstantially.

Chapter 6 specifically addresses the effect of metal species. The dynamics of CO_2 formation during the CO + O_2 reaction on single-crystal Rh(111) surface are reported: they correspond to the first presentation of the IR emission studies on a single-crystal Rh surface. The results are compared to those for Pd(111) and Pt(111), and salient tendencies were discussed through comparison of the author’s experimental results and those of reported theoretical studies on the transition state of CO oxidation.

In chapter 7, all results of this thesis are summarized.

References

[1] T. Engel, G. Ertl, *Adv. Catal.* **28** (1979) 1.

[2] B.E. Nieuwenhuys, *Adv. Catal.* **44** (1999) 259.

[3] A.K. Santra, D.W. Goodman, *Electrochim. Acta* **47** (2002) 3595.

[4] T. Matsushima, *Surf. Sci. Rep.* **52** (2003) 1.

[5] E. Ozensoy, D.W. Goodman, *Phys. Chem. Chem. Phys.* **6** (2004) 3765.

[6] H. Uetsuka, K. Watanabe, H. Kimpara, K. Kunimori, *Langmuir* **15** (1999) 5795.

[7] C.R. Henry, *Surf. Sci. Rep.* **31** (1998) 231.

[8] J. Libuda, H.-J. Freund, *Surf. Sci. Rep.* **57** (2005) 157.

[9] V.P. Zhdanov, B. Kasemo, *Surf. Sci. Rep.*, **29** (1997) 1.

[10] K.C. Taylor, *Catal. Rev. Sci. Eng.* **35** (1993) 457.

[11] R.M. Heck, R.J. Farrauto, *Catalytic Air Pollution Control: Commercial Technology, International Thomson Publishing*, New York, NY, (1995).

[12] S. Bhattacharyya, R. Das, *Int. J. Energy Res.* **23** (1999) 351.

[13] A.H. Tullo, *Chem. Eng. News* **80**(34) (2002) 17.

[14] J.N. Armor, *App. Catal. A: Gen.* **176** (1999) 159.

[15] J.R. Rostrup-Nielsen, *Catal. Rev. Sci. Eng.* **46** (2004) 197.

[16] T. Engel, G. Ertl, *J. Chem. Phys.* **69** (1978) 1267.

[17] S. Ladas, R. Imbihl, G. Ertl, *Surf. Sci.* **219** (1989) 88.

[18] S. Ladas, R. Imbihl, G. Ertl, *Surf. Sci.* **280** (1993) 14.

[19] M. Eiswirth, G. Ertl, *Surf. Sci.* **177** (1986) 90.

[20] S. Ladas, R. Imbihl, G. Ertl, *Surf. Sci.* **198** (1988) 42.

[21] K. Krischer, M. Eiswirth, G. Ertl, *J. Chem. Phys.* **96** (1992) 9161.

[22] S. Nettesheim, A. von Oertzen, H.H. Rotermund, G. Ertl, *J. Chem. Phys.* **98** (1993) 9977.

[23] A. von Oertzen, H.H. Rotermund, A.S. Mikhailov, G. Ertl, *J. Phys. Chem. B* **104** (2000) 3155.

[24] J. Wolff, A.G. Papathanasiou, I.G. Kevrekidis, H.H. Rotermund, G. Ertl, *Science* **294** (2001)

134.

[25] M. Bertram, C. Beta, M. Pollmann, A.S. Mikhailov, H.H. Rotermund, G. Ertl, *Phys. Rev. E* **67** (2003) 036208.

[26] T. Gritsch, D. Coulman, R.J. Behm, G. Ertl, *Appl. Phys. A* **49** (1989) 403.

[27] R. Imbihl, M.P. Cox, G. Ertl, *J. Chem. Phys.* **84** (1985) 3519.

[28] C.T. Campbell, G. Ertl, H. Kuipers, J. Segner, *J. Chem. Phys.* **73** (1980) 5862.

[29] J. Segner, C.T. Campbell, G. Doyen, G. Ertl, *Surf. Sci.* **138** (1984) 505.

[30] J. Wintterlin, S. Völkening, T.V.W. Janssens, T. Zambelli, G. Ertl, *Science* **278** (1997) 1931.

[31] P.J. Berlowitz, C.H.F. Peden, D.W. Goodman, *J. Phys. Chem.* **92** (1988) 5213.

[32] J. Szanyi, W.N. Kuhn, D.W. Goodman, *J. Phys. Chem.* **98** (1994) 2978.

[33] S.H. Oh, G.B. Fisher, J.E. Carpenter, D.W. Goodman, *J. Catal.* **100** (1986) 360.

[34] C.H.F. Peden, D.W. Goodman, D.S. Blair, P.J. Berlowitz, G.B. Fisher, S.H. Oh, *J. Phys. Chem.* **92** (1988) 1563.

[35] H. Uetsuka, K. Watanabe, H. Ohnuma, K. Kunimori, *Chem. Lett.* (1996) 227.

[36] H. Uetsuka, K. Watanabe, H. Ohnuma, K. Kunimori, *Surf. Sci.* **377-379** (1997) 765.

[37] H. Uetsuka, K. Watanabe, H. Ohnuma, K. Kunimori, *Surf. Rev. Lett.* **4** (1997) 1359.

[38] K. Watanabe, H. Ohnuma, H. Kimpara, H. Uetsuka, K. Kunimori, *Surf. Sci.* **402-404** (1998) 100.

[39] K. Nakao, S. Ito, K. Tomishige, K. Kunimori, *Chem. Phys. Lett.* **410** (2005) 86.

[40] K. Nakao, S. Ito, K. Tomishige, K. Kunimori, *J. Phys. Chem. B* **109** (2005) 17553.

[41] K. Nakao, S. Ito, K. Tomishige, K. Kunimori, *Catal. Today* **111** (2006) 316.

[42] K. Nakao, S. Ito, K. Tomishige, K. Kunimori, *Surf. Sci.* **600** (2006) 4221.

[43] K. Nakao, O. Watanabe, T. Sasaki, S. Ito, K. Tomishige, K. Kunimori, *Surf. Sci.* in press.

[44] H. Uetsuka, K. Watanabe, K. Kunimori, *Chem. Lett.* (1995) 633.

[45] K. Watanabe, H. Ohnuma, H. Uetsuka, K. Kunimori, *Surf. Sci.* **368** (1996) 366.

[46] K. Watanabe, H. Uetsuka, H. Ohnuma, K. Kunimori, *Catal. Lett.* **47** (1997) 17.

[47] K. Nakao, S. Ito, K. Tomishige, K. Kunimori, *J. Phys. Chem. B* **109** (2005) 24002.

[48] Q. Guo, R.W. Joyner, M. Bowker, *Surf. Sci.* **280** (1993) 50.

[49] M. Bowker, I.Z. Jones, R.A. Bennet, F. Esch, A. Baraldi, S. Lizzit, G. Comelli, *Catal. Lett.* **51** (1998) 187.

[50] I.Z. Jones, R.A. Bennet, M. Bowker, *Surf. Sci.* **439** (1999) 235.

[51] S.B. Schwartz, L.D. Schmidt, G.B. Fisher, *J. Phys. Chem.* **90** (1986) 6194.

[52] K. Kimura, Y. Ohno, T. Matsushima, *Surf. Sci.* **429** (1999) L455.

[53] Md. Golam Moula, S. Wako, G. Cao, I. Kobal, Y. Ohno, T. Matsushima, *Appl. Surf. Sci.* **169–170** (2001) 268.

[54] Md. Golam Moula, S. Wako, Y. Ohno, M.U. Kislyuk, I. Kobal, T. Matsushima, *Phys. Chem. Chem. Phys.* **2** (2000) 2773.

[55] Md.G. Moula, A.B.P. Mishra, I. Rzeźnicka, M.U. Kislyuk, S. Liu, Y. Ohno, T. Matsushima, *Chem. Phys. Lett.* **341** (2001) 225.

[56] I. Rzeźnicka, L. Morales de la Garza, T. Matsushima, *J. Vac. Sci. Technol. A* **20** (2002) 1475.

[57] I. Rzeźnicka, Md.G. Moula, L. Morales de la Garza, Y. Ohno, T. Matsushima, *J. Chem. Phys.* **119** (2003) 9829.

[58] I. Rzeźnicka, T. Matsushima, *Chem. Phys. Lett.* **377** (2003) 279.

[59] I. Rzeźnicka, T. Matsushima, *J. Phys. Chem. B* **107** (2003) 8479.

[60] K.-P. Bohnen, A. Eichler, J. Hafner, *Surf. Sci.* **368** (1996) 222.

[61] A. Eichler, J. Hafner, *Phys. Rev. B* **59** (1999) 5960.

[62] A. Eichler, J. Hafner, *Surf. Sci.* **433–435** (1999) 58.

[63] A. Eichler, *Surf. Sci.* **498** (2002) 314.

[64] C.J. Zhang, P. Hu, *J. Am. Chem. Soc.* **123** (2001) 1166.

[65] Z.-P. Liu, P. Hu, *Top. Catal.* **123** (2001) 1166.

[66] A. Alavi, P. Hu, T. Deutsch, P.L. Silvestrelli, J. Hutter, *Phys. Rev. Lett.* **80** (1998) 3650.

[67] K. Bleakley, P. Hu, *J. Am. Chem. Soc.* **121** (1999) 7644.

[68] M. Lynch, P. Hu, *Surf. Sci.* **458** (2000) 1.

[69] A.-P. Liu, P. Hu, *J. Chem. Phys.* **115** (2001) 4977.

[70] C.J. Zhang, P. Hu, *J. Am. Chem. Soc.* **122** (2000) 2134.

[71] P. Salo, K. Honkala, M. Alatalo, K. Laasonen, *Surf. Sci.* **516** (2002) 247.

[72] V.P. Zhdanov, B. Kasemo, *Surf. Sci. Rep.* **20** (1994) 111.

[73] V.P. Zhdanov, *Surf. Sci. Rep.* **45** (2002) 231.

[74] V.P. Zhdanov, *Surf. Sci. Rep.* **55** (2004) 1.

[75] X. Xu, P. Chen, D.W. Goodman, *J. Phys. Chem.* **98** (1994) 9242.

[76] K. Honkala, P. Pirila, K. Laasonen, *Surf. Sci.* **489** (2001) 72.

[77] C. Tang, S. Zou, M.J. Weaver, *Surf. Sci.* **412/413** (1998) 344.

[78] C. Tang, S. Zou, S.-C. Chang, M.J. Weaver, *J. Electroanal. Chem.* **467** (1999) 92.

[79] L.H. Dubois, P.K. Hansma, G.A. Somorjai, *J. Catal.* **65** (1980) 318.

[80] T.W. Root, G.B. Fisher, L.D. Schmidt, J. Chem. Phys. 85 (1986) 4687.

[81] S.M. Vesecky, P. Chen, X. Xu, D.W. Goodman, *J. Vac. Sci. Technol. A* **13** (1995) 1539.

[82] S.M. Vesecky, D.R. Rainer, D.W. Goodman, *J. Vac. Sci. Technol. A* **14** (1996) 1457.

[83] D.R. Rainer, S.M. Vesecky, M. Koranne, W.S. Oh, D.W. Goodman, *J. Catal.* **167** (1997) 234.

[84] E. Ozensoy, C. Hess. D.W. Goodman, *J. Am. Chem. Soc.* **124** (2002) 8524.

[85] C. Hess, E. Ozensoy, D.W. Goodman, *J. Phys. Chem. B* **107** (2003) 2759.

[86] E. Ozensoy, C. Hess, D.W. Goodman, *Top. Catal.* **28** (2004) 1.

[87] K. Nakao, H. Hayashi, H. Uetsuka, S. Ito, H. Onishi, K. Tomishige, K. Kunimori, *Catal. Lett.* **85** (2003) 213.

[88] K. Nakao, S. Ito, K. Tomishige, K. Kunimori, *Catal. Lett.* **103** (2005) 179.

[89] K. Nakao, S. Ito, K. Tomishige, K. Kunimori, *J. Phys. Chem. B* **109** (2005) 17579.

[90] I. Kobal, K. Kimura, Y. Ohno, T. Matsushima, *Surf. Sci.* **445** (2000) 472.

[91] T. Matsushima, *Catal. Surv. Japan* **5** (2002) 71.

[92] Y. Ma, I. Rzeźnicka, T. Matsushima, *Chem. Phys. Lett.* **388** (2004) 201.

[93] I. Rzeźnicka, Y. Ma, G. Gengyu, T. Matsushima, *J. Phys. Chem. B* **108** (2004) 14232.

[94] T. Matsushima, I. Rzeźnicka, Y. Ma, *Chem. Rec.* **5** (2005) 81.

[95] Y. Ma, I. Rzeźnicka, T. Matsushima, *App. Surf. Sci.* **244** (2005) 558.

[96] K. Thirunavukkarasu, K Thirumoorthy, J. Libuda, C.S. Gopinath, *J. Phys. Chem. B* **109** (2005) 13272.

[97] K. Thirunavukkarasu, K Thirumoorthy, J. Libuda, C.S. Gopinath, *J. Phys. Chem. B* **109** (2005) 13283.

[98] Y. Ma, T. Matsushima, K. Shobatake, A. Kokolj, *J. Chem. Phys.* **124** (2006) 144711.

[99] S.B. Schwartz, G.B. Fisher, L.D. Schmidt, *J. Phys. Chem.* **92** (1988) 389.

[100] C.H.F. Peden, D.N. Belton, S.J. Schmieg, *J. Catal.* **155** (1995) 204.

[101] G.S. Herman, C.H.F. Peden, S.J. Schmieg, D.N. Belton, *Catal. Lett.* **62** (1999) 131.

[102] D.N. Belton, S.J. Schmieg, *J. Catal.* **144** (1993) 9.

[103] H. Permana, K.Y.S. Ng, C.H.F. Peden, S.J. Schmieg, D.N. Belton, *J. Phys. Chem.* **99** (1995) 16344.

[104] H. Permana, K.Y.S. Ng, C.H.F. Peden, S.J. Schmieg, D.K. Lambert, D.N. Belton, *J. Catal.* **164** (1996) 194.

[105] H. Permana, K.Y.S. Ng, C.H.F. Peden, S.J. Schmieg, D.K. Lambert, D.N. Belton, *Catal. Lett.* **47** (1997) 5.

[106] M. Aryafar, F. Zaera, *J. Catal.* **175** (1998) 316.

[107] C.S. Gopinath, F. Zaera, *J. Catal.* **186** (1999) 387.

[108] F. Zaera, C.S. Gopinath, *J. Chem. Phys.* **111** (1999) 8088.

[109] F. Zaera, C.S. Gopinath, *Chem. Phys. Lett.* **332** (2000) 209.

[110] C.S. Gopinath, F. Zaera, *J. Phys. Chem. B* **104** (2000) 3194.

[111] F. Zaera, C.S. Gopinath, *J. Mol. Catal. A: Chem.* **167** (2001) 23.

[112] V. Bustos, C.S. Gopinath, R. Uñac, F. Zaera, G. Zgrablich, *J. Chem. Phys.* **114** (2001) 10927.

[113] C.S. Gopinath, F. Zaera, *J. Catal.* **200** (2001) 270.

[114] F. Zaera, C.S. Gopinath, *Phys. Chem. Chem. Phys.* **5** (2003) 646.

[115] V. Bustos, R. Uñac, F. Zaera, G. Zgrablich, *J. Chem. Phys.* **118** (2003) 9372.

[116] L.A. Avalos, V. Bustos, R. Uñac, F. Zaera, G. Zgrablich, *J. Mol. Catal. A: Chem.* **228** (2005) 89.

[117] L.A. Avalos, V. Bustos, R. Uñac, F. Zaera, G. Zgrablich, *J. Phys. Chem. B* **110** (2006) 24964.

[118] H. Horino, T. Matsushima, *J. Phys. Chem. B* **109** (2005) 675.

[119] F. Zaera, S. Wehner, C.S. Gopinath, J.L. Sales, V. Gargiulo, G. Zgrablich, *J. Phys. Chem. B*

105 (2001) 7771.

[120] F. Zaera, C.S. Gopinath, *J. Chem. Phys.* **116** (2002) 1128.

[121] R.L. Klein, S. Schwartz, L.D. Schmidt, *J. Phys. Chem.* **89** (1985) 4908.

[122] D.J. Bald, S.L. Bernasek, *J. Chem. Phys.* **109** (1998) 746.

[123] Th. Fink, K. Krischer, R. Imbihl, *J. Vac. Sci. Technol. A* 10 (1992) 2440.

[124] N.P. Magtoto, H.H. Richardson, *Surf. Sci.* **417** (1998) 189.

[125] E.D.L. Rienks, J.W. Bakker, A. Baraldi, S.A.C. Carabineiro, S. Lizzit, C.J. Weststrate, B.E. Nieuwenhuys, *J. Chem. Phys.* **119** (2003) 6245.

[126] V.P. Zhdanov, *J. Chem. Phys.* **110** (1999) 8748.

[127] M.W. Lesley, L.D. Schmidt, *Chem. Phys. Lett.* **102** (1983) 459.

[128] Y. Ohno, P. Sarawut, H. Horino, I. Kobal, A. Hiratsuka, T. Matsushima, *Chem. Phys. Lett.* **373** (2003) 161.

[129] Y. Ohno, K. Kimura, M. Bi, T. Matsushima, *J. Chem. Phys.* **110** (1999) 8221.

[130] Y. Ohno, I. Kobal, I. Rzeźnicka, T. Matsushima, *App. Surf. Sci.* **169–170** (2001) 273.

[131] H. Horino, I. Rzeźnicka, A. Kokalj, I. Kobal, Y. Ohno, A. Hiratsuka, T. Matsushima, *J. Vac. Sci. Technol. A* **20** (2002) 1592.

[132] T. Matsushima, *Catal. Surv. Japan* **5** (2002) 71.

[133] S. Haq, A. Hodgson, *Surf. Sci.* **463** (2000) 1.

[134] C.G. Takoudis, L.D. Schmidt, *J. Catal.* **80** (1983) 274.

[135] N.R. Avery, *Surf. Sci.* **131** (1983) 501.

[136] K. Sawabe, Y. Matsumoto, *Chem. Phys. Lett.* **194** (1992) 45.

[137] H. Uetsuka, N. Mizutani, H. Hayashi, H. Onishi, K. Kunimori, *Catal. Lett.* **69** (2000) 165.

[138] V.A. Kondratenko, M. Baerns, *J. Catal.* **225** (2004) 37.

[139] Y. Li, M. Bowker, *Surf. Sci.* **348** (1996) 67.

[140] K. Imamura, T. Matsushima, *Catal. Lett.* **97** (2004) 197.

[141] K. Imamura, H. Horino, I. Rzeźnicka, I. Kobal, A. Kokalj, Y. Ohno, B.E. Nieuwenhuys, A. Hiratsuka, T. Matsushima, *Surf. Sci.* **566–568** (2004) 1076.

[142] A. Kokalj, T. Matsushima, *J. Chem. Phys.* **122** (2005) 034708.

[143] T. Matsushima, K. Imamura, H. Horino, A. Hiratsuka, Y.-S. Ma, I. Rzeźnicka, O. Nakagoe, *App. Surf. Sci.* **244** (2005) 141.

[144] V.P. Zhdanov, T. Matsushima, *Surf. Sci.* **583** (2005) 253.

[145] J.-F. Paul, J. Pérez-Ramírez, F. Ample, J.M. Ricart, *J. Phys. Chem. B* **108** (2004) 17921.

[146] S. Wehner, M.T. Paffett, F. Zaera, *J. Phys. Chem. B* **108** (2004) 18683.

[147] R.O. Uńac, V. Bustos, J. Wilson, G. Zgrablich, F. Zaera, *J. Chem. Phys.* **125** (2006) 074705.

[148] Y. Ma, I. Kobal, T. Matsushima, *J. Phys. Chem. B* **109** (2005) 689.

[149] V.P. Zhdanov, Y. Ma, T. Matsushima, *Surf. Sci.* **583** (2005) 36.

[150] Y. Ma, S. Han, T. Matsushima, *Langmuir* **21** (2005) 9529.

[151] Y. Ma, A. Kokalj, T. Matsushima, *Phys. Chem. Chem. Phys.* **7** (2005) 3716.

[152] D.N. Belton, S.J. Schmieg, *J. Catal.* **138** (1992) 70.

[153] C.R. Arumainayagam, R.J. Madix, *Prog. Surf. Sci.* **38** (1991) 1.

[154] G. Cao, Y. Seimiya, T. Matsushima, *J. Mol. Catal. A* **141** (1999) 63.

[155] R.L. Palmer, J.N. Smith, *J. Chem. Phys.* **60** (1974) 1453.

[156] C.A. Becker, J.P. Cowin, L. Wharton, D.J. Auerbach, *J. Chem. Phys.* **67** (1977) 3394.

[157] L.S. Brown, S.J. Sibener, *J. Chem. Phys.* **89** (1988) 1163.

[158] L.S. Brown, S.J. Sibener, *J. Chem. Phys.* **90** (1989) 2807.

[159] J.I. Colonell, K.D. Gobson, S.J. Sibener, *J. Chem. Phys.* **103** (1995) 6677.

[160] T. Matsushima, *Surf. Sci.* **127** (1983) 403.

[161] T. Matsushima, H. Asada, *J. Chem. Phys.* **85** (1986) 1658.

[162] T. Matsushima, *J. Chem. Phys.* **91** (1989) 5722.

[163] T. Matsushima, K. Shobatake, Y. Ohno, K. Tabayashi, *J. Chem. Phys.* **97** (1992) 2783.

[164] T. Matsushima, Y. Ohno, *Chem. Phys. Lett.* **169** (1990) 569.

[165] Y. Ohno, T. Matsushima, H. Uetsuka, *J. Chem. Phys.* **101** (1994) 5319.

[166] T. Matsushima, T. Matsui, M. Hashimoto, *J. Chem. Phys.* **81** (1984) 5151.

[167] T. Matsushima, Y. Ohno, *Catal. Lett.* **23** (1994) 313.

[168] D.A. Mantell, S.B. Ryali, B.L. Halpern, G.L. Haller, J.B. Fenn, *Chem. Phys. Lett.* **81** (1981) 185.

[169] D.A. Mantell, S.B. Ryali, G.L. Haller, *Chem. Phys. Lett.* **102** (1983) 37.

[170] D.A. Mantell, K. Kunimori, S.B. Ryali, G.L. Haller, J.B. Fenn, *J. Vac. Sci. Technol. A* **3** (1985) 1663.

[171] D.A. Mantell, K. Kunimori, S.B. Ryali, G.L. Haller, J.B. Fenn, *Surf. Sci.* **172** (1986) 281.

[172] S.W. Coulston, G.L. Haller, *J. Chem. Phys.* **92** (1990) 5752.

[173] S.W. Coulston, G.L. Haller, *J. Chem. Phys.* **95** (1991) 6932.

[174] S.W. Coulston, G.L. Haller, *ACS Symp. Ser.* **482** (1992) 58.

[175] S.L. Bernasek, S.R. Leone, *Chem. Phys. Lett.* **84** (1981) 401.

[176] L.S. Brown, S.L. Bernasek, *J. Chem. Phys.* **82** (1985) 2110.

[177] D.J. Bald, R. Kunkel, S.L. Bernasek, *J. Chem. Phys.* **104** (1996) 7719.

[178] K. Kunimori, G.L. Haller, *Bull. Chem. Soc. Jpn.* **65** (1992) 2450.

[179] K. Kunimori, K. Uetsuka, T. Iwade, T. Watanabe, S. Ito, *Surf. Sci.* **283** (1993) 58.

[180] K. Kunimori, T. Iwade, K. Uetsuka, *J. Electron Spectrosc. Relat. Phenom.* **64/65** (1993) 451.

[181] H. Uetsuka, K. Watanabe, T. Iwade, K. Kunimori, *J. Chem. Soc. Faraday Trans.* **91** (1995) 1801.

Chapter 2

Reaction mechanism and activated complex of CO_2 formation in $CO + O_2$ reaction on Pd(110) and Pd(111) surfaces

2.1. Introduction

Elucidation of reaction mechanisms is important for catalyst design and control of reaction routes. Single-crystal surfaces can be used to elucidate reaction mechanisms over heterogeneous catalysts [1,2]. An effective method is spectroscopic observation of reaction intermediates, which are surface species in a metastable state, to obtain information about reaction mechanisms. Another method is investigation of internal (vibrational and rotational) energy and translational energy of desorbed molecules, which are the products of catalytic reaction, from the catalyst surface [3–19]. The energy states of desorbed molecules can reflect the catalytic reaction dynamics, which can correspond to a transition state [3–19]. Numerous investigations of CO oxidation on Pt and Pd surfaces have revealed the elemental steps of surface catalyzed reactions [1–25]. Furthermore, CO oxidation is a prototype reaction for the study of dynamics; measurements of internal energy states of the produced CO_2 molecules have been performed using infrared chemiluminescence (IR emission) method under steady-state catalytic reactions using molecular-beam technique [3–15]. Analyses of vibrational and rotational states can yield information about the structure of the activated CO_2 complex (i.e., the dynamics of CO oxidation) from which the gas phase molecules desorbed. Furthermore, the vibrational energy state of product CO_2 depends on its surface structure [8–16]. Consequently, information about the active sites is obtainable from the IR emission spectra of CO_2 under a steady-state catalytic reaction.

Our group has reported IR chemiluminescence of CO_2 from the steady-state $CO + O_2$ reaction on Single-crystal Pd surfaces combined with kinetic results [11–15]. The activated complex of CO_2 formation (the transition state of CO_2 formation from CO(a) + O(a)) has a more bent structure on Pd(111) and a straighter structure on Pd(110) at higher surface temperatures (T_S > 650 K) because CO_2 from Pd(111) is more excited vibrationally than CO_2 from Pd(110) [14,15]. Results

of kinetic investigations show that the CO_2 formation rate in the CO + O_2 reaction increases with increasing surface temperature in the low-temperature range. The temperature at which the catalytic activity of CO_2 formation is maximal is denoted herein and in previous studies by our group as T_S^{max} [14,15]. We have specifically examined higher temperature conditions than T_S^{max} and find that as the catalytic activity in the CO + O_2 reaction is greatly dependent on the CO coverage in this range, it decreases with increasing surface temperature. However, catalytic reactions using real and practical catalysts are usually carried out at lower reaction temperatures. For that reason, chemiluminescence investigation at a lower temperature range is of greater practical value. This study specifically examines such reaction conditions.

2.2. Experimental

A molecular-beam reaction system, in combination with a FT-IR spectrometer (InSb detector Nexus670; Thermo Electron Corp.), was used to measure IR emissions of product CO_2 molecules that desorbed on metal surfaces during catalytic reactions [14–16]. A UHV chamber (base pressure < 1.0×10^{-9} Torr) was equipped with: a CaF_2 lens, which collected IR emission; an Ar^+ ion gun for sample cleaning; and a quadrupole mass spectrometer (QMS, QME200; Pfeiffer Vacuum Technology AG) with a differential pumping system. Two free-jet molecular-beam nozzles (0.1-mm-diameter orifice) supplied the reactant gases. The reactant fluxes were controlled using mass flow controllers. The CO and O_2 gases (total flux of $2.1–20 \times 10^{18}$ cm^{-2} s^{-1}; CO/O_2 = 0.3–7) were exposed to single-crystal Pd surfaces (Pd(110) and Pd(111)). Steady-state CO + O_2 reactions were performed at temperatures of 400–900 K. Another UHV chamber (base pressure < 2.0×10^{-10} Torr) was used to prepare the samples and to characterize Pd(110) and Pd(111) surfaces. It was equipped with an identical molecular-beam reaction system, an Ar^+ ion gun, low energy electron diffraction (LEED), and a QMS. Before the molecular-beam reaction, the Pd(110) and Pd(111) were cleaned using a standard procedure (O_2 treatment, Ar^+ bombardment, and annealing) [14–16].

The IR emission spectra of the CO_2 molecules desorbed from the surface were measured with 4 cm^{-1} resolution unless stated otherwise. At that low resolution, no individual vibration-rotation lines were resolved. The IR emission spectra of product CO_2 were analyzed based

on simulations of model spectra. They yielded an average vibrational Boltzmann temperature (T_V^{AV}: an average temperature of antisymmetric stretch, symmetric stretch and bending modes) and a rotational Boltzmann temperature (T_R) [4,6]. T_V^{AV} was calculated from the degree of red-shift from the fundamental band (2349 cm^{-1}), and then T_R was derived from the emission-band width. Although the IR emission observed here is in the antisymmetric stretch vibrational region – (n_{SS}, n_B^l, n_{AS}) → (n_{SS}, n_B^l, n_{AS} − 1) – the vibrational excitation levels of symmetric stretch (n_{SS}) and bending (n_B) also affect this region [4,15]. Here, n_{SS}, n_B and n_{AS} are the vibrational quantum numbers of respective modes. The quantum number of vibrational angular momentum in linear molecules is denoted by l. Note that the emission intensity is normalized using the rate of CO_2 production. Consequently, the emission intensity is related to the extent of excitation in the antisymmetric stretch of CO_2, which is given by the following equation:

$$f \propto e^{-x} + e^{-2x} + e^{-3x} \cdots \fallingdotseq e^{-x}/(1-e^{-x}), \qquad (1)$$

where f is the emission intensity normalized per unit of CO_2 yield, and x equals to $\Delta E_V/k_B T_V^{AS}$ (ΔE_V is the energy spacing, k_B is the Boltzmann constant and T_V^{AS} is the antisymmetric temperature). High-resolution steady-state results (0.06 cm^{-1}) [4] show the energy distribution in respective vibrational modes (T_V^{SS}, T_V^B, T_V^{AS}), where the superscripts respectively indicate symmetric stretch, bending, and antisymmetric stretch. Here, the steady-state CO + O_2 reaction on polycrystalline Pt foil was performed with the previous conditions as [4] (CO = O_2 = 4.1 × 10^{18} cm^{-2} s^{-1}). The IR emission spectra of CO_2 molecules were measured with 4 cm^{-1} resolution at the surface temperature (T_S) of 900 K. The obtained spectrum was compared with previous results (T_V^{AS} = 1600 K) [4]. We estimated the emission intensity at T_V^{AS} = 1600 K. This emission intensity and T_V^{AS} on the polycrystalline Pt surface were used as standards for various conditions on Pd surfaces. Based on T_V^{AS} and T_V^{AV}, it is possible to deduce the bending vibrational temperature (T_V^B). The relation between T_V^{AV} and respective vibrational temperatures is represented as

$$T_V^{AV} = (T_V^{AS} + T_V^{SS} + 2T_V^B) / 4, \qquad (2)$$

where $2T_V^B$ corresponds to the degeneration of two bending vibrational modes. Assuming that T_V^B is equal to T_V^{SS} because of the Fermi resonance [5,23], T_V^B is expected to be $(4T_V^{AV} - T_V^{AS})/3$. This assumption is plausible on the basis of previous reports [4,23]. It should be added that T_V^{AV}, T_V^{AS},

T_V^B and T_R were used here as parameters to characterize the extent of the vibrational and rotational excitation of the product CO_2. About 900–1800 s were required to measure the IR spectra with 1000–2000 scans. The activity was stable during measurement. Therefore, we infer that the results reflected the CO_2 states under steady-state conditions.

2.3. Results and Discussion

Figure 2-1 shows the rate of CO_2 formation in the steady-state CO + O_2 reaction on Pd(110) as a function of surface temperature (T_S) for various total fluxes of reactants (CO/O_2 = 1). The CO oxidation proceeded at temperatures greater than 500 K. The formation rate profiles showed maxima on the Pd(110) surface. The temperature at which the highest activity was obtained is denoted as T_S^{max}. It is shifted to a higher temperature and the formation rate of CO_2 increases with the increasing total flux of reactants. These behaviors agree well with the general Langmuir-Hinshelwood (LH) kinetics of CO oxidation on Pd surfaces [1,2]. Though it will be also discussed later in Figure 2-7, at temperatures lower than T_S^{max}, the surface coverage of CO is known to be high. The rate-determining step is O_2 adsorption on the vacant site, which is formed by the desorption of CO(a). At temperatures greater than T_S^{max}, the formation rate of CO_2 decreases gradually with increasing surface temperature. This behavior is attributable to the decreased CO coverage. Generally, in the CO + O_2 reaction on Pd surfaces at lower surface temperatures, the reaction order of CO is negative-first-order; that of O_2 is positive-first-order [2]. Consequently, the formation rate of CO_2 is zero-order with respect to total pressure. Goodman et al. reported that the reaction rate of CO oxidation on Pd(110) at temperatures T_S= 450–600 and at total pressure of 16 Torr is zero-order with respect to total pressure [22]. On the other hand, at higher surface temperatures, the CO coverage (θ_{CO}) can be minute ($\theta_{CO} \ll 0.01$) and oxygen coverage (θ_O) approaches the saturation level ($\theta_O \approx 0.5$) [26]. Therefore, the reaction orders of CO and O_2 are respectively inferred to be positive-first-order and zero-order. The total formation rate of CO_2 included the reaction order of total pressure as positive-first-order with a constant CO/O_2 ratio. These explanations are true for our cases, in which the gas pressure range is lower than those reported previously [22].

Figure 2-2 shows IR emission spectra of CO_2 molecules produced by CO + O_2 reaction on Pd(110) at T_S = 650 K for the various total fluxes (CO/O_2 = 1). The CO_2 emission spectra observed in the region of 2400–2200 cm^{-1} are considerably red-shifted from 2349 cm^{-1} (fundamental band of antisymmetric stretch), whereas the emission spectra of the non-reacted CO, which was scattered from the surface, was centered at 2143 cm^{-1}. The degree of red-shift from the fundamental band, which reflects the vibrational state of excited molecules, is nearly equal for all total flux conditions. On the other hand, the emission intensity increases with increasing total flux, indicating changes in the antisymmetric vibrational excited state (T_V^{AS}), as explained later.

Figure 2-3(a) shows the vibrational temperature (T_V^{AV}) and the rotational temperature (T_R) derived from IR emission spectra of CO_2 at T_S = 650 K as a function of the total flux. Each T_V^{AV} value is shown as much higher than T_S, indicating that the product CO_2 is vibrationally excited. However, it is almost constant under all flux conditions. The T_R value is also shown as higher than T_S, indicating that the product CO_2 is rotationally excited. The T_R value is shown as nearly constant between 2.1–8.2 × 10^{18} cm^{-2} s^{-1}. However, the value decreases gradually beyond the total flux = 1.0 × 10^{19} cm^{-2} s^{-1}. The decrease of T_R value is attributable to rotational relaxation by the gas phase collision between departing (CO_2) and arriving (CO + O_2) molecules [7]. Therefore, we measured the IR emission spectra of CO_2 molecules with no rotational relaxation condition where the total flux of reactants is 8.2 × 10^{18} cm^{-2} s^{-1}. Figure 2-7(b) shows the antisymmetric vibrational temperature (T_V^{AS}) and the bending vibrational temperature (T_V^{B}) derived from IR emission intensity of CO_2 as a function of the total flux. The T_V^{AS} value increases gradually with increasing total flux.

Figure 2-4 shows the CO_2 formation rate in the steady-state CO + O_2 reaction on Pd(110) as a function of surface temperature (T_S) for various CO/O_2 ratios. The total flux of reactants is shown as constant at 8.2 × 10^{18} cm^{-2} s^{-1}. The temperature dependence of the curves shows the maximum value: the observed behavior resembles that shown in Fig. 2-1. In Fig. 2-4, T_S^{max} is shown to increase considerably with the increasing CO/O_2 ratio. At surface temperatures lower than T_S^{max} (e.g. 525 K) under all pressure conditions, the CO_2 formation rate decreases sharply with the increasing CO/O_2 ratio, which is explainable by the reaction orders with respect to CO and O_2, as depicted in

Fig. 2-1. In stark contrast, at surface temperatures higher than T_S^{max} (e.g. 700 K) for CO/O_2 ratios of 0.3–2.1, the CO_2 formation rate increases with increasing CO/O_2 ratio. This behavior is implied by the reaction orders. Furthermore, the CO_2 formation rate at T_S^{max} under each CO/O_2 ratio increases concomitant with the increasing CO/O_2 ratio of 0.3–2.1, but decreases for ratios of 3.0–7.0. Especially at very high CO/O_2 ratios, the oxygen coverage decreases, thereby lowering the CO_2 formation rate. This study measured the IR emission spectra at T_S = 600 K because this temperature is lower than T_S^{max} under CO/O_2 = 1.4–7.0. It is higher than T_S^{max} under CO/O_2 = 0.3–1.0. Observation at this temperature reveals the relation between the vibrational state of CO_2 and T_S^{max}.

Figure 2-5 depicts the IR emission spectra of CO_2 molecules produced by CO + O_2 reaction on Pd(110) at T_S = 600 K for various CO/O_2 ratios. The red-shift from the fundamental band is shown to be almost equal for various CO/O_2 ratios. However, the emission intensity increases concomitant with the increasing CO/O_2 ratio. Figure 2-6(a) shows T_V^{AV} and T_R, obtained from IR emission spectra of CO_2, as a function of the CO/O_2 ratio. The T_R value is almost identical (1000 K), indicating that the rotationally excited state is independent of the CO/O_2 ratio. The T_V^{AV} value increases slightly with the increasing CO/O_2 ratio, whereas the value remains nearly unchanged at a low value of CO/O_2 ($CO/O_2 < 0.6$). Figure 2-6(b) shows T_V^{AS} and T_V^{B} obtained from IR emission intensity of CO_2 as a function of CO/O_2. In the low CO/O_2 region, the T_V^{AS} value is nearly constant, but the T_V^{AS} increases sharply in the higher CO/O_2 region. This result indicates that the antisymmetric vibrational mode of the product CO_2 is much more excited with higher CO/O_2. Particularly, much higher T_V^{AS} is apparent at CO/O_2 = 7.0, where $T_S < T_S^{max}$. These results suggest that the vibrational state of CO_2 at T_S lower than T_S^{max} differs from that at T_S higher than T_S^{max}.

Figure 2-7 shows the rate of CO_2 formation in the steady-state CO + O_2 reaction on Pd(110) and Pd(111) as a function of surface temperature. At temperatures greater than 500 K, the CO oxidation proceeds and the temperature dependence of the formation rate is maximal on both Pd surfaces. Descriptions similar to those of Figs. 2-1 and 2-4 are applicable to these behaviors. The T_S^{max} and the formation rate of CO_2 also differed for each surface. Comparison of the two surfaces revealed that the CO oxidation on Pd surfaces is structure-sensitive under the steady-state reaction condition with the total pressure of ca. 10^{-3}–10^{-2} Torr.

As is known well, the mechanism of the CO + O_2 reaction on Pd surfaces is as follows [2,20]:

$$CO(g) + V \leftrightarrow CO(a), \quad (3)$$

$$O_2(g) + 2V \rightarrow 2O(a), \quad (4)$$

$$CO(a) + O(a) \rightarrow CO_2(g) + 2V, \quad (5)$$

where V represents a vacant site. It is possible to make the equations regarding the coverage of each intermediate as shown below [12,25].

$$d\theta_{CO} / dt = f_{CO} s_{CO} (1 - \theta_{CO} - \theta_O) - k_{CO}^{des} \theta_{CO} - r_{CO_2}, \quad (6)$$

$$d\theta_O / dt = 2 f_{O_2} s_{O_2} (1 - \theta_{CO} - \theta_O)^2 - r_{CO_2}. \quad (7)$$

Here, the rate of O_2 desorption is small enough to be neglected [2,12,25]. The CO_2 formation rate, r_{CO_2}, was obtained from the experimental results shown in Fig. 2-7. The initial sticking coefficients of CO and O_2 and the kinetic parameters used are listed in Table 2-1. The results of the coverage calculation in CO + O_2 reaction on Pd(110) are also shown in Fig. 2-7. As mentioned in Fig. 2-1, it is known that at temperatures lower than T_S^{max}, the surface coverage of CO (θ_{CO}) is high, and the rate-determining step is O_2 adsorption on the vacant site, which is formed by the desorption of CO(a). At temperatures higher than T_S^{max}, the formation rate of CO_2 decreased gradually with increasing surface temperature, and this behavior is due to the drastic decrease of θ_{CO}. Generally, in CO + O_2 reaction on Pd surfaces at lower surface temperatures, reaction order of CO is negative-first-order, and that of O_2 is positive-first-order [2]. On the other hand, at higher temperatures, θ_{CO} can be very small (θ_{CO} « 0.01) and oxygen coverage (θ_O) approaches almost saturation level (θ_O ~ 0.5) [26]. Therefore, the reaction orders of CO and O_2 are respectively inferred to be positive-first-order and zero-order. The CO_2 formation rate can be plotted as a function of inverse surface temperature in Arrhenius form, as in Fig. 2-7. From the temperature range T_S = 475–600 K of this plot, the apparent activation energies of Pd(111) and Pd(110) are estimated respectively as 27.8 kcal/mol and 34.3 kcal/mol. These values agree with the value of 28.1 kcal/mol on Pd(111) [21] and that of 33.1 kcal/mol on Pd(110) [20], which were obtained by Goodman et al. in high-pressure conditions, or that of 25 kcal/mol on Pd(111), which was obtained by Engel and Ertl [1] in UHV studies. The agreement of activation energies of CO oxidation over

Pd surfaces suggests that the surface structure was maintained during catalytic and steady-state reactions. Generally speaking, the planar surface prepared by treatments such as annealing can be changed to a rough surface during reactions. However, Pd(110) and Pd(111) have considerably stable surface structures even under reaction conditions. Based on this inference, we can estimate the Turnover frequency (TOF) of CO_2 formation over Pd(110) and Pd(111). At T_S = 575 K, TOFs over Pd(110) and Pd(111) are calculated respectively as 440 s^{-1} and 74 s^{-1}.

Figures 2-8(a) and 2-8(b) show IR emission spectra of CO_2 molecules produced by CO + O_2 reaction on Pd(110) and Pd(111) surfaces (CO/O_2 = 1) for various surface temperatures. The peaks centered at 2143 cm^{-1} are IR emissions from the non-reacted CO molecules, which are fully accommodated to the surface. The higher the surface temperature, the greater the red-shift from the antisymmetric stretch fundamental (2349 cm^{-1}) was observed in the CO_2 emission spectra. In contrast, at low surface temperatures (T_S = 550–600 K), the degree of red-shift from 2349 cm^{-1} is almost constant, even though the emission intensity is extremely high in this temperature range.

Figures 2-9(a) and 2-9(c) show the average vibrational temperature (T_V^{AV}) and the rotational temperature (T_R) on Pd(110) and Pd(111) surfaces derived from IR emission spectra of CO_2 as a function of T_S. The T_V^{AV} and T_R values are much greater than that of T_S, which also indicates that the product CO_2 is excited both vibrationally and rotationally. The T_R value is almost constant, thereby indicating that the rotationally excited state is independent of the surface temperature. The T_V^{AV} value increases with increasing T_S at temperatures greater than 600 K. In particular, the T_V^{AV} values on Pd(111) are much higher than those of Pd(110), whereas it was almost constant at low surface temperatures (T_S < 600 K) on both surfaces. Figures 2-9(b) and 2-9(d) show T_V^{AS} and T_V^{B} derived from IR emission intensity of CO_2 as a function of T_S. For surface temperatures above 600 K, the T_V^{AS} value increases gradually with increasing T_S. In contrast, the T_V^{AS} value increases drastically with decreasing T_S at low temperatures of 550–600 K, indicating that the vibrational states of desorbed CO_2 change at about 600 K on both surfaces. The T_V^{AS} values of Pd(111) are similar to those of Pd(110) in Figs. 2-9(b) and 2-9(d) at the higher surface temperatures. However, the T_V^{B} values of Pd(111) are much higher than those of Pd(110), meaning that the bending vibrational mode is more highly excited than the antisymmetric vibrational mode on Pd(111) at the

higher T_S. This fact is reflected in the structure of the activated complex of CO_2 formation. Particularly in the bending vibrational mode, CO_2 on Pd(111) is excited. For that reason, the structure of the activated complex is more bent. In contrast, CO_2 on Pd(110) is a slightly more excited in the antisymmetric stretching vibration than in the bending one. Therefore, the activated complex has a straighter form.

Based on those behaviors, Figs. 2-10(a) and 2-10(b) present the structure of the activated complex at 850 K, higher than T_S^{max}. Along with them, an appropriate model is presented and described. At higher temperatures, adsorbed oxygen and CO are diffused on the surface. However, it is known that a three-fold hollow site is more stable as an adsorption site of oxygen on Pd(111) [30–32] and Pd(110) [33,34]. A stable adsorption site of CO is a three-fold hollow site on Pd(111) [2,31,32,35] and a bridge site on Pd(110) [2,34,36]. Therefore, the model describes that CO_2 is formed by the reaction between two adsorbed species at each stable site. For Pd(111), adsorbed oxygen and carbon atoms in CO are located at a similar distance from the surface. The activated complex of CO_2 formation can be bent. On the other hand, in the case of Pd(110) because the adsorbed oxygen is located at the lower level, it is expected that the activated complex has a straighter structure than that on Pd(111). In contrast to the profile at higher temperatures, a different tendency is apparent on both surfaces at lower temperatures, e.g. 550 K (Figs. 2-10(c) and 2-10(d)). Under such conditions, it is characteristic that T_V^{AS} is much higher than T_V^{B}. This result indicates that desorbed CO_2 is highly excited in the antisymmetric vibrational mode and that the excitation level of the bending vibrational mode is low, which is explainable by the linear structure of the activated complex. At low temperatures such as 550 K, the adsorbed CO has some mobility, but the adsorbed oxygen's mobility is much lower because its adsorption energy is much higher than that of CO [2]. Therefore, we infer that CO, mounted on adsorbed oxygen, can form a linear activated complex. The coverage of adsorbed CO is high at lower surface temperatures. Therefore, the structure of the activated complex can be influenced by the CO coverage.

According to the report by Hu et al. [31] on coadsorption system of CO and oxygen on Pd(111) by means of the density functional theory (DFT) calculations, the most stable adsorption states of adsorbed CO and oxygen are a three-fold hollow site, and CO oxidation process can be

divided into three distinguished periods. First, CO(a) moves freely from its initial position (three-fold hollow site), while O(a) vibrates around the three-fold hollow position. The energy change in this period is very small. Second, O(a) becomes activated and moves toward a bridge site. If CO(a) moves toward O(a) in the correct direction, then transition state can be achieved. In this period, the energy increases dramatically. Third, O(a) and CO(a) move toward each other, to form a CO_2. In addition, Salo et al. [32] have also reported that the most stable sites of CO and oxygen are a three-fold hollow site, however, they have proposed that at the transition state both CO and oxygen are located near the bridge sites next to each other. Anyway, the transition state is much more unstable than stable adsorption site. This can be related to CO_2 desorption with high vibrational excitation. On the other hand, only a few groups have studied the coadsorption of CO and oxygen system on Pd(110) surface [34]. It has been reported that a three-fold hollow site between the first and second layer is more stable as the adsorption site of oxygen, and that of CO is a bridge site in the first layer on Pd(110) [34]. We illustrate the model structures of CO + O_2 reaction in T_S range above T_S^{max} in Figs. 2-10(a),(b).

In the lower surface temperature range, the coverage of CO is much higher and that of oxygen is much lower compared to high surface temperature conditions. Under high CO coverage condition, bridge or on-top sites can appear on Pd(111) [35] and on-top sites can appear on Pd(110) [31]. In addition, Salo et al. have shown that the reaction barrier of CO adsorbed on-top and oxygen on three-fold hollow site is lower than that of CO adsorbed on a three-fold hollow site and oxygen on a hollow site. Iwasawa et al. [34] have investigated adsorption and oxidation of CO on Pd(110)-c(2×4)–O, and they have considered that at high CO coverage CO is linearly bound to the first layer Pd, which is directly coordinated by oxygen atoms, and that the linear CO mainly reacts to form CO_2 with oxygen below 250 K. Therefore in our case, considering the CO pressure in the gas phase is much higher than UHV conditions, CO can be adsorbed on more unstable site, e.g. on-top site rather than three-fold hollow and bridge sites on both surfaces in high CO coverage range. In addition, at the lower T_S, the antisymmetric vibrational mode was much more excited than bending vibrational mode. Especially, T_V^{AS} on Pd(110) at the low T_S (e.g., 550 K) was higher than T_V^{AS} on Pd(110) at the high T_S (e.g., 850 K). This result suggests that the activated complex of CO_2

formation in this low temperature range has more linear structure than that on Pd(110) in high temperature range. Therefore, it is thought that the linear activated complex can be formed by CO mounting on adsorbed oxygen (Figs. 2-10(c),(d)). Considering that the coverage of adsorbed CO is rather high at the temperatures lower than T_S^{max}, the structure of the activated complex can be influenced by the CO coverage. Since the activated complex can be bound with the surface through one oxygen atom, its structure is not so influenced by the surface structure.

Regarding angular and velocity distribution measurements for CO_2 molecules produced in CO oxidation on Pd(110), Matsushima et al. [18] showed that the translational energy of CO_2 increases with increasing CO pressure, and increases with decreasing surface temperature (T_S < 500 K). They concluded that these phenomena are closely related to CO coverage because the amount of CO(a) increases at low surface temperature and at high CO pressure. Our study showed that the T_V^{AS} value increases at the low surface temperature and at the high CO/O_2 flux ratio in a high CO coverage region. High CO coverage can render the activated complex of CO_2 formation as linear.

2.4. Conclusions

(1) We measured the steady-state activity of CO oxidation over Pd(110) and Pd(111) surfaces in the temperature range 400–900 K under various reactant pressure conditions. The CO_2 formation rate profile with regard to the surface temperature was maximal. This surface temperature was denoted as T_S^{max}.

(2) Measurements and analyses of IR chemiluminescence of CO_2 formed during the steady-state CO oxidation obtained the vibrational and rotational energy states of CO_2, as the average vibrational temperature (T_V^{AV}), antisymmetric vibrational temperature (T_V^{AS}), bending vibrational temperature (T_V^{B}), and rotational temperature (T_R). Results showed that T_V^{AV}, T_V^{AS}, T_V^{B} and T_R values were much higher than surface temperature (T_S) under all conditions, indicating that the product CO_2 was excited both vibrationally and rotationally.

(3) At surface temperatures higher than T_S^{max}, T_V^{B} was higher than T_V^{AS} on Pd(111) and T_V^{AS} was higher than T_V^{B} on Pd(110). This fact suggests that the activated CO_2 complex is more bent on Pd(111), and straighter on Pd(110) at the higher surface temperature, where the CO coverage

was rather low.

(4) The T_V^{AV} values of CO_2 formed in CO oxidation were similar on Pd(110) and Pd(111) surfaces when the surface temperature was less than T_S^{max}. Furthermore, the T_V^{AS} value of CO_2 increased drastically with decreasing T_S ($< T_S^{max}$), thereby indicating that antisymmetric vibration is much more highly excited than other vibrational modes. In turn, that high excitation suggests that the structure of the activated complex of CO_2 formation is straighter.

(5) The high T_V^{AS} value was always observed at T_S lower than T_S^{max}, a fact that can be related to high CO coverage. The structure of an activated complex of CO_2 formation with the interaction of the surrounding CO(a) molecules is in a more linear form.

(6) From the comparison of T_V^{AS} and T_V^{B}, the model of the activated complex of CO_2 formation in CO + O_2 reaction over Pd(111) and Pd(110) is proposed, and the transition state of reaction is discussed.

References

[1] T. Engel, G. Ertl, *J. Chem. Phys.* **69** (1978) 1267.

[2] T. Engel, G. Ertl, *Adv. Catal.* **28** (1979) 1.

[3] D.A. Mantell, PhD Thesis, Department of Physics, Yale Univ. (1983).

[4] D.A. Mantell, K. Kunimori, S.B. Ryali, G.L. Haller, J.B. Fenn, *Surf. Sci.* **172** (1986) 281.

[5] S.W. Coulston, G.L. Haller, *J. Chem. Phys.* **95** (1991) 6932.

[6] K. Kunimori, G.L. Haller, *Bull. Chem. Soc. Jpn.* **65** (1992) 2450.

[7] K. Kunimori, K. Uetsuka, T. Iwade, T. Watanabe, S. Ito, *Surf. Sci.* **283** (1993) 58.

[8] H. Uetsuka, K. Watanabe, K. Kunimori, *Chem. Lett.* (1995) 633.

[9] H. Uetsuka, K. Watanabe, K. Kunimori, *Surf. Sci.* **363** (1996) 73.

[10] K. Watanabe, H. Ohnuma, H. Uetsuka, K. Kunimori, *Surf. Sci.* **368** (1996) 366.

[11] H. Uetsuka, K. Watanabe, H. Ohnuma, K. Kunimori, *Chem. Lett.* (1996) 227.

[12] K. Watanabe, H. Uetsuka, H. Ohnuma, K. Kunimori, *Catal. Lett.* **47** (1997) 17.

[13] H. Uetsuka, K. Watanabe, H. Ohnuma, K. Kunimori, *Surf. Sci.* **377-379**, (1997) 765.

[14] K. Watanabe, H. Ohnuma, H. Kimpara, H. Uetsuka, K. Kunimori, *Surf. Sci.* **402-404**, (1998) 100.

[15] H. Uetsuka, K. Watanabe, H. Kimpara, K. Kunimori, *Langmuir* **15** (1999) 5795.

[16] K. Nakao, H. Hayashi, H. Uetsuka, S. Ito, H. Onishi, K. Tomishige, K. Kunimori, *Catal. Lett.* **85** (2003) 213.

[17] T. Matsushima, K. Shobatake, Y. Ohno, K. Tabayashi, *J. Chem. Phys.* **97** (1992) 2783.

[18] K. Kimura, Y. Ohno, T. Matsushima, *Surf. Sci.* **429** (1999) L455.

[19] Md. Golam Moula, S. Wako, G. Cao, I. Kobal, Y. Ohno, T. Matsushima, *Appl. Surf. Sci.* **169-170** (2001) 268.

[20] P.J. Berlowitz, C.H.F. Peden, D.W. Goodman, *J. Phys. Chem.* **92** (1988) 5213.

[21] J. Szanyi, W.N. Kuhn, D.W. Goodman, *J. Phys. Chem.* **98** (1994) 2978.

[22] A.K. Santra, D.W. Goodman, *Electrochim. Acta* **47** (2002) 3595.

[23] D.J. Bald, R. Kunkel, S.L. Bernasek, *J. Chem. Phys.* **104** (1996) 7719.

[24] B.E. Nieuwenhuys, *Adv. Catal.* **44** (1999) 259

[25] K. Krischer, M. Eiswirth, G. Ertl, *J. Chem. Phys.* **96** (1992) 9161.

[26] J. Goschnick, M. Wolf, M. Grunze, W.N. Unertl, J.H. Block, J. Loboda-Cackovic, *Surf. Sci.* **178** (1986) 831.

[27] R.J. Behm, K. Christmann, G. Ertl, M.A. Van Hove, *J. Chem. Phys.* **73** (1980) 2984.

[28] X. Guo, J.T. Yates Jr, *J. Chem. Phys.* **90** (1989) 6761.

[29] M. Hirsimäki, M. Valden, *J. Chem. Phys.* **114** (2001) 2345.

[30] H. Conrad, G. Ertl, J. Küppers, E.E. Latta, *Surf. Sci.* **65** (1977) 245.

[31] C.J. Zhang, P. Hu, *J. Am. Chem. Soc.* **123** (2001) 1166.

[32] P. Salo, K. Honkala, M. Alatalo, K. Laasonen, *Surf. Sci.* **516** (2002) 247.

[33] N. Takagi, Y. Yasui, M. Sawada, A. Atli, T. Aruga, M. Nishijima, *Chem. Phys. Lett.* **232** (1995) 531.

[34] K. Fukui, H. Miyauchi, Y. Iwasawa, *J. Phys. Chem.* **100** (1996) 18795.

[35] D. Loffreda, D. Simon, P. Sutet, *Surf. Sci.* **425** (1999) 68.

[36] H. Kato, J. Yoshinobu, M. Kawai, *Surf. Sci.* **427-428** (1999) 69.

Table 2-1 Kinetic parameters for the CO + O_2 reaction on Pd(110)

Reaction equation	Rate constant / s^{-1}	ν / s^{-1}	E_a / kcal mol^{-1}	Ref.
(3)	k_{CO}^{des}	1×10^{17}	35.5	[27,28]
	initial sticking coefficient			
(3)	$s_{CO} = 0.93$			[29]
(4)	$s_{O_2} = 0.86$			[26]

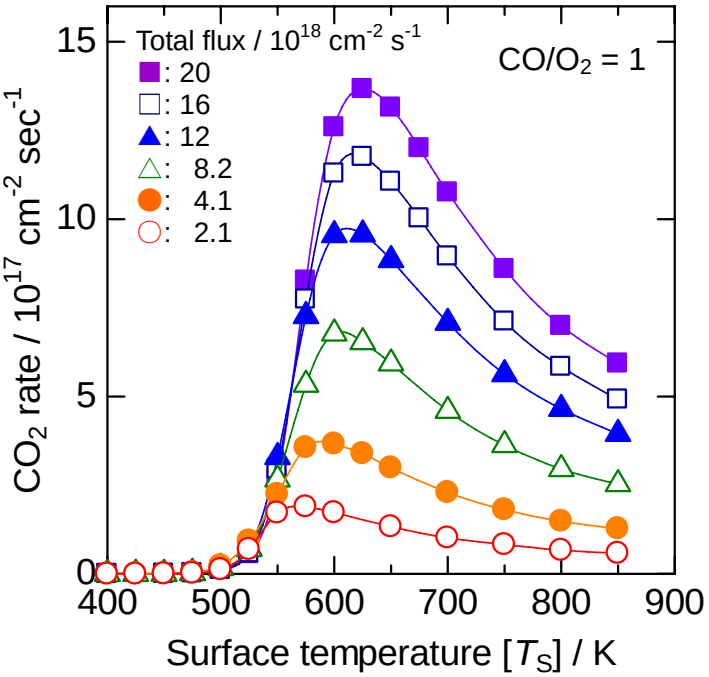

Figure 2-1 The formation rate of CO_2 during the CO + O_2 reaction (CO/O_2 = 1) on Pd(110). The total flux of reactants (CO + O_2) was 2.1−20 × 10^{18} molecules cm^{-2} s^{-1}.

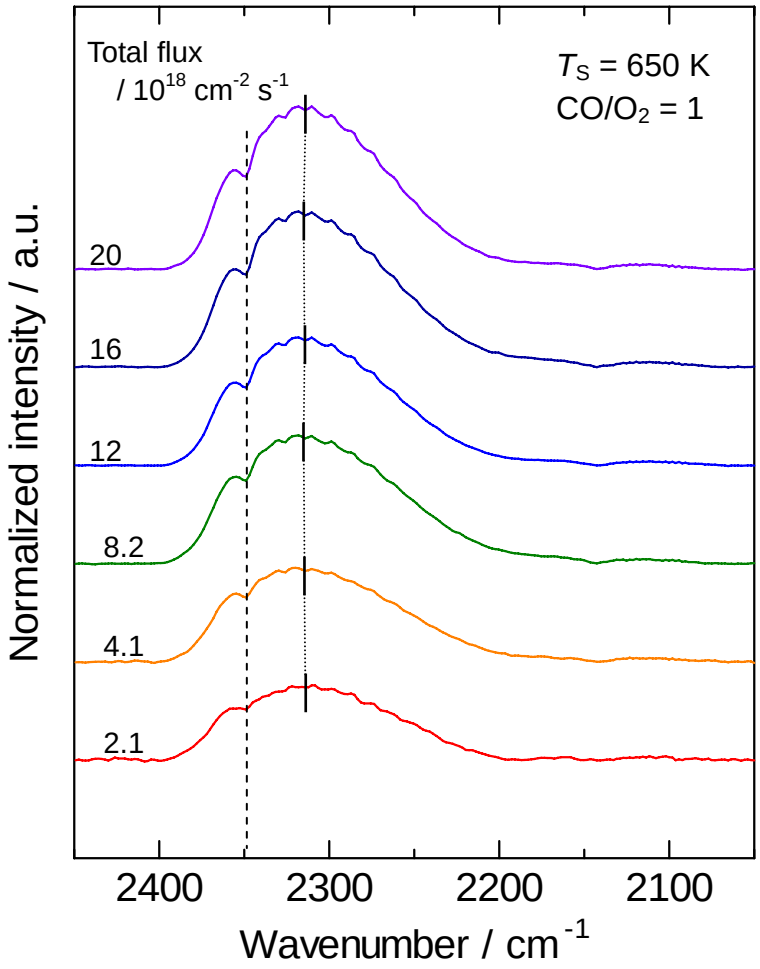

Figure 2-2 IR emission spectra of CO_2 desorbed by the CO + O_2 reaction on Pd(110). The surface temperature (T_S) was 650 K. The total flux of reactants was 2.1−20 × 10^{18} molecules cm^{-2} s^{-1} at CO/O_2 = 1. The emission intensity was normalized per unit of CO_2 yield.

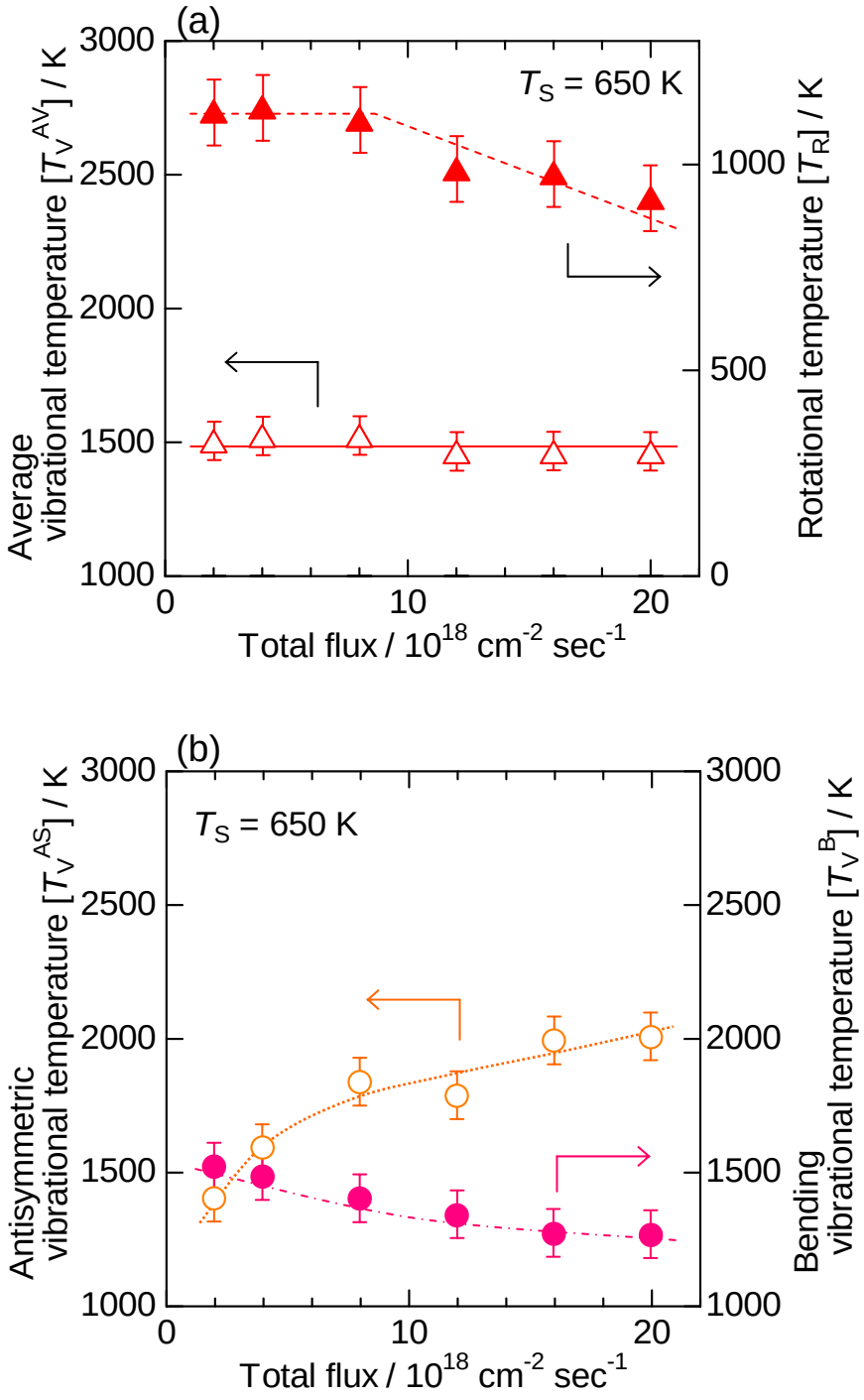

Figure 2-3 (a) Total flux dependence of average vibrational temperature (T_V^{AV}) and rotational temperature (T_R) of CO_2 formed in CO + O_2 reaction on Pd(110). (b) Total flux dependence of antisymmetric vibrational temperature (T_V^{AS}) and bending vibrational temperature (T_V^{B}). The surface temperature (T_S) was 650 K. The total flux of reactants was 2.1−20 × 10^{18} molecules cm^{-2} s^{-1} at CO/O_2 = 1.

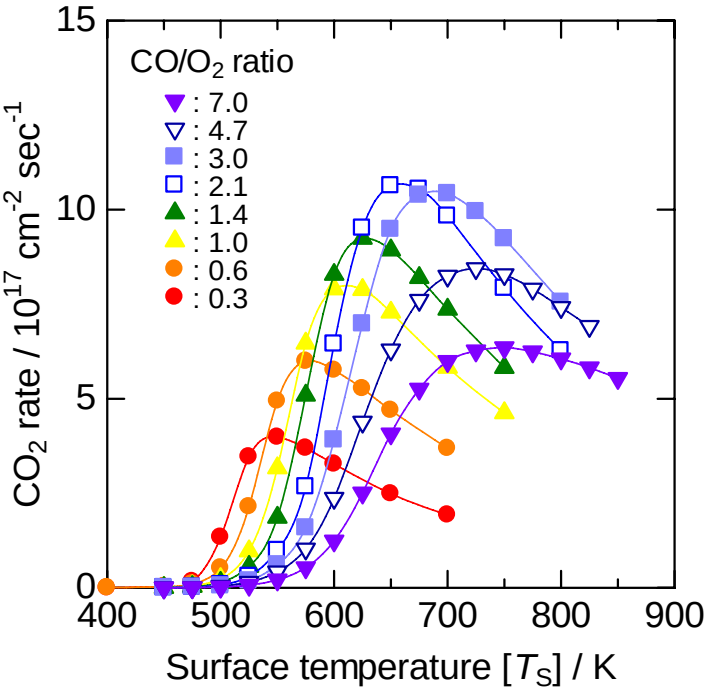

Figure 2-4 The formation rate of CO_2 during the CO + O_2 reaction (CO/O_2 = 0.3−7.0) on Pd(110). The total flux of reactants (CO + O_2) was 8.2×10^{18} molecules cm^{-2} s^{-1}.

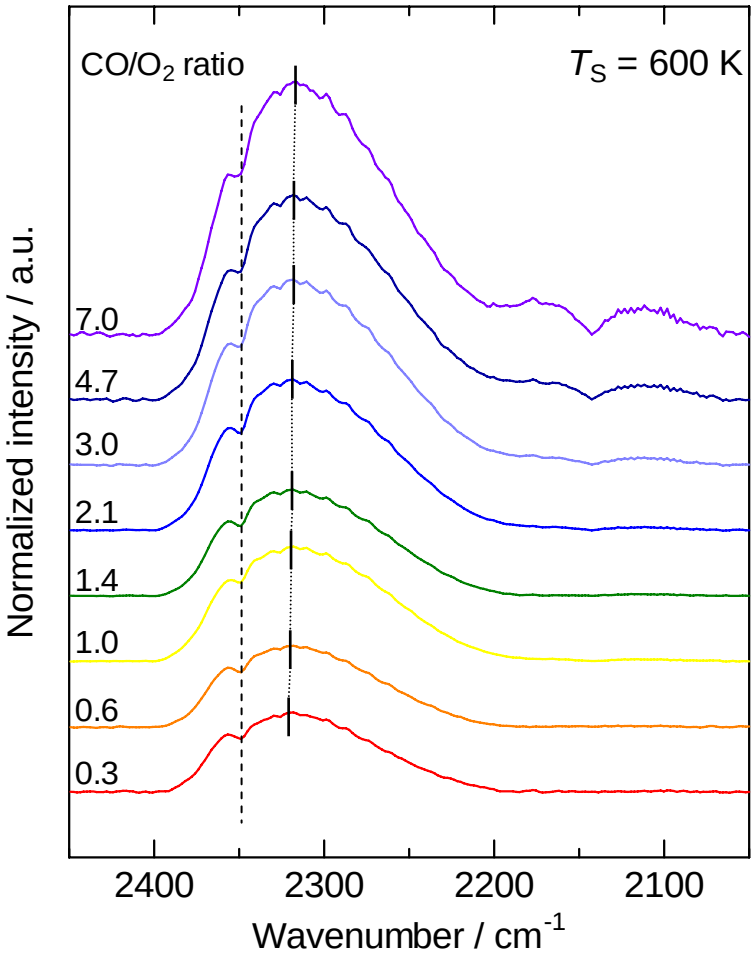

Figure 2-5 IR emission spectra of CO_2 desorbed by the CO + O_2 reaction on Pd(110). The surface temperature (T_S) was 600 K. The total flux of reactants was 8.2×10^{18} molecules cm^{-2} s^{-1} at CO/O_2 = 0.3−7.0. The emission intensity was normalized per unit of CO_2 yield.

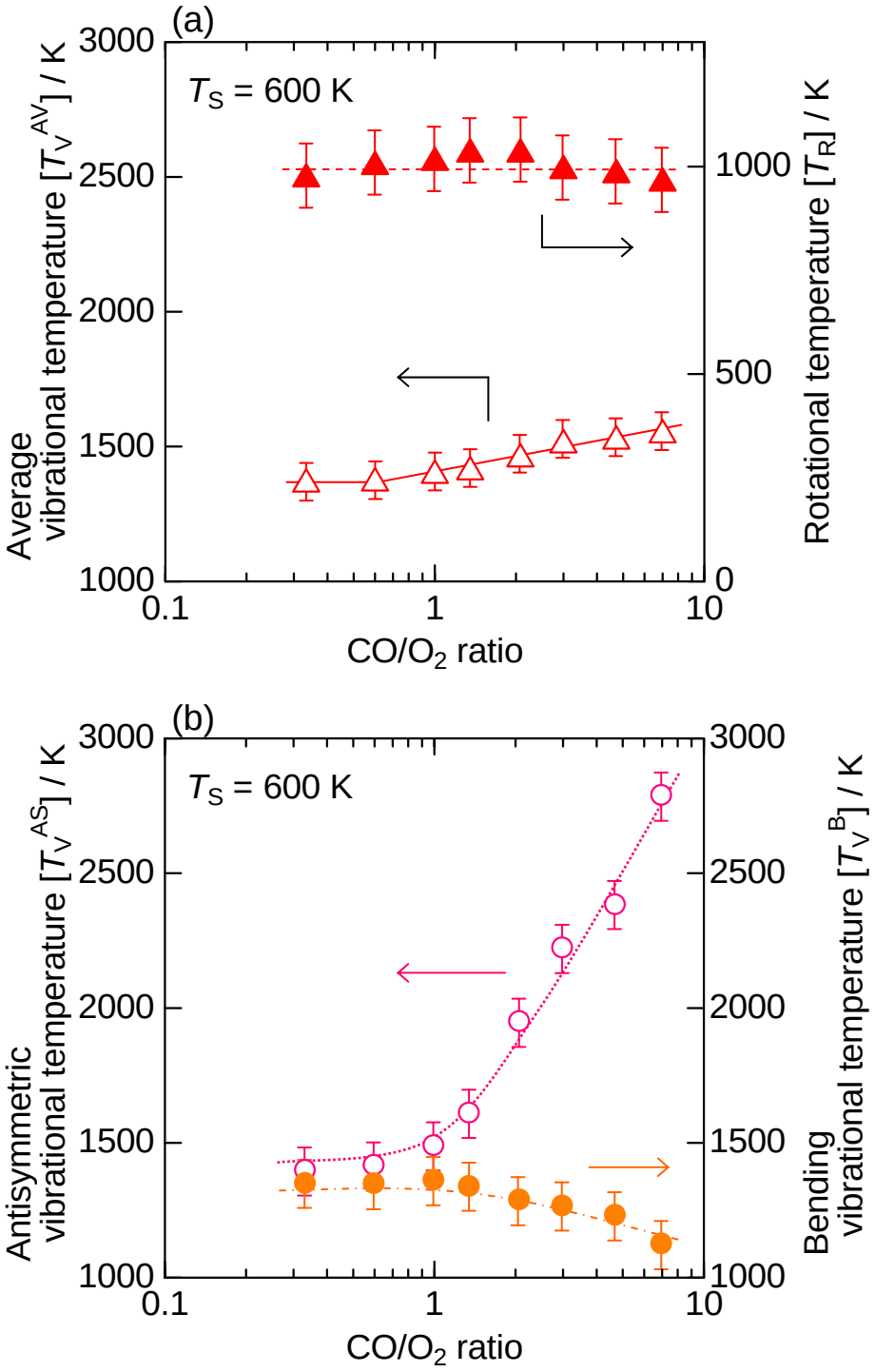

Figure 2-6 (a) CO/O_2 ratio dependence of average vibrational temperature (T_V^{AV}) and rotational temperature (T_R) of CO_2 formed in CO + O_2 reaction on Pd(110). (b) CO/O_2 ratio dependence of antisymmetric vibrational temperature (T_V^{AS}) and bending vibrational temperature (T_V^{B}). The total flux of reactants was 8.2×10^{18} molecules cm^{-2} s^{-1} at CO/O_2 = 0.3−7.0.

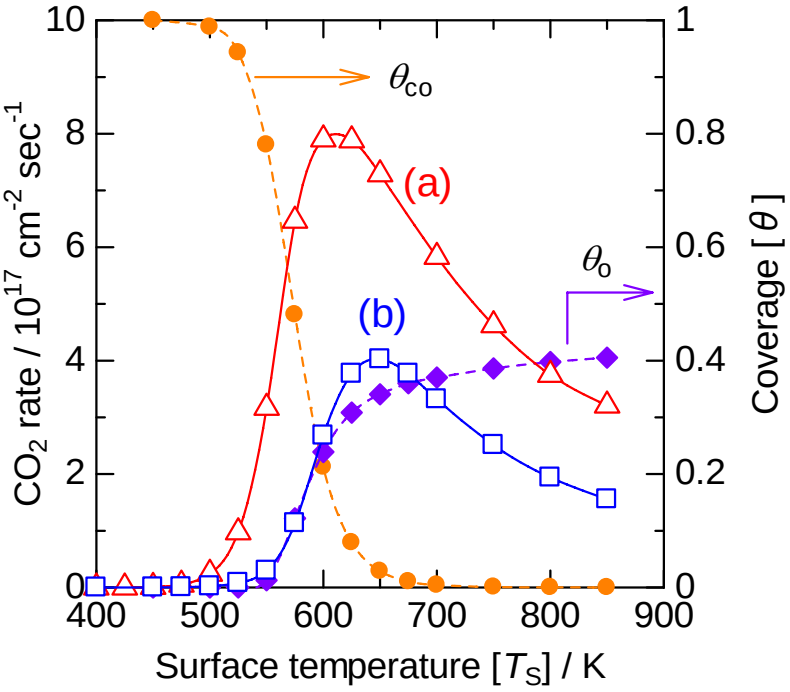

Figure 2-7 The CO_2 formation rate during the CO + O_2 reaction (CO/O_2 = 1) on (a) Pd(110) and (b) on Pd(111), and the coverage of CO and oxygen on Pd(110) as a function of surface temperature (T_S). The total flux of reactants (CO + O_2) was 8.2×10^{18} molecules cm^{-2} s^{-1}.

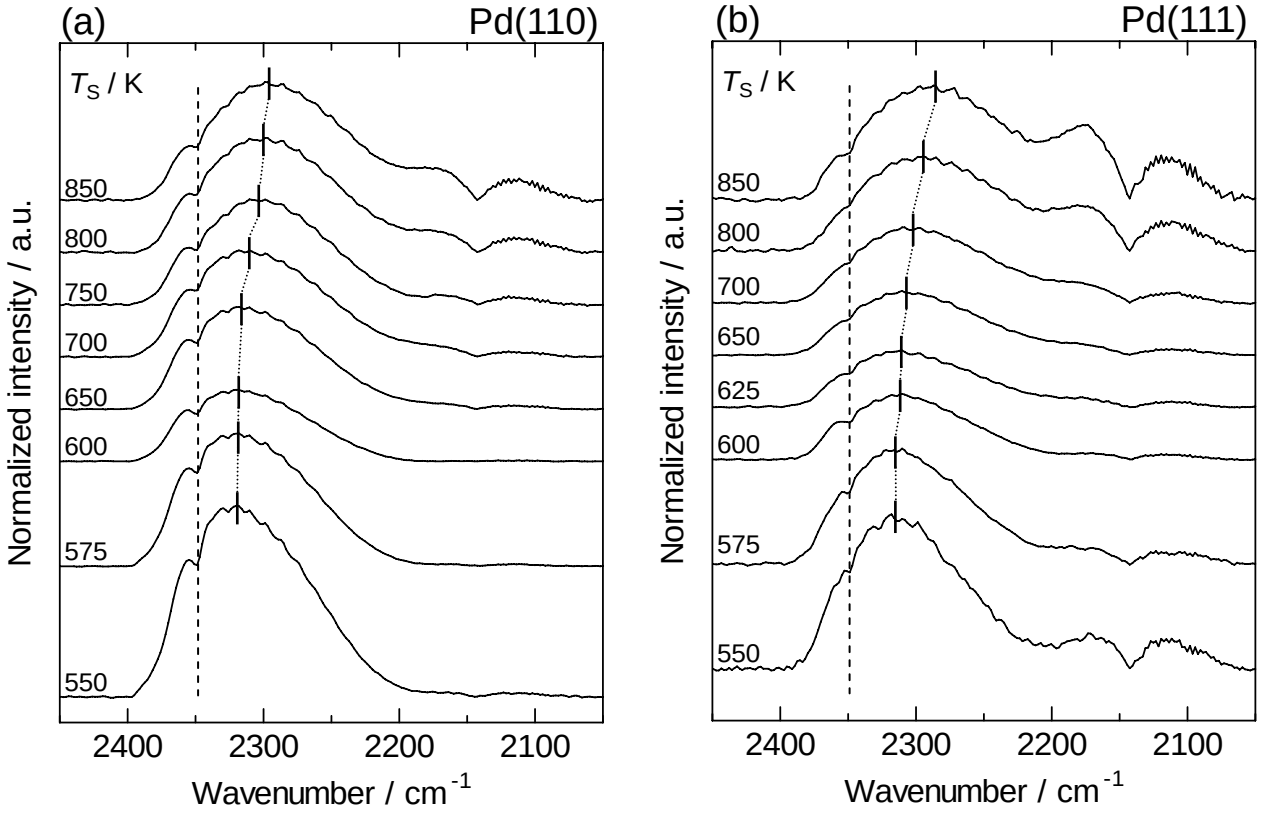

Figure 2-8 IR emission spectra of CO_2 desorbed by the CO + O_2 reaction on (a) Pd(110) and (b) Pd(111). The surface temperature (T_S) was 550–850 K. The total flux of reactants was 8.2×10^{18} molecules cm^{-2} s^{-1} at $CO/O_2 = 1$. The emission intensity was normalized per unit of CO_2 yield.

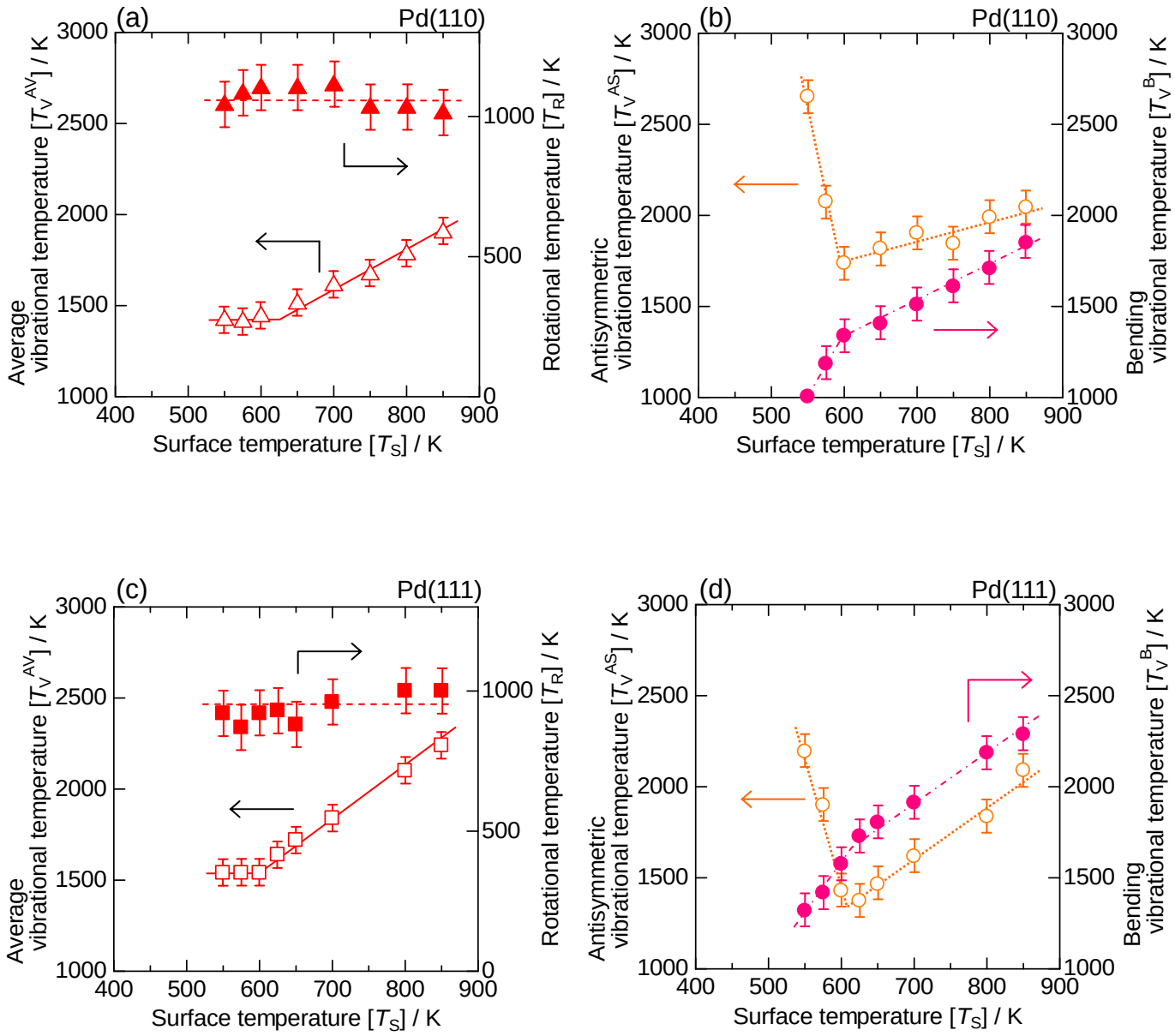

Figure 2-9 (a), (c) Surface temperature dependence of average vibrational temperature (T_V^{AV}) and rotational temperature (T_R) of CO_2 formed in CO + O_2 reaction on (a) Pd(110) and (c) Pd(111). (b), (d) Surface temperature dependence of antisymmetric vibrational temperature (T_V^{AS}) and bending vibrational temperature (T_V^{B}) on (b) Pd(110) and (d) Pd(111). The total flux of reactants was 8.2 × 10^{18} molecules cm^{-2} s^{-1} at CO/O_2 = 1.

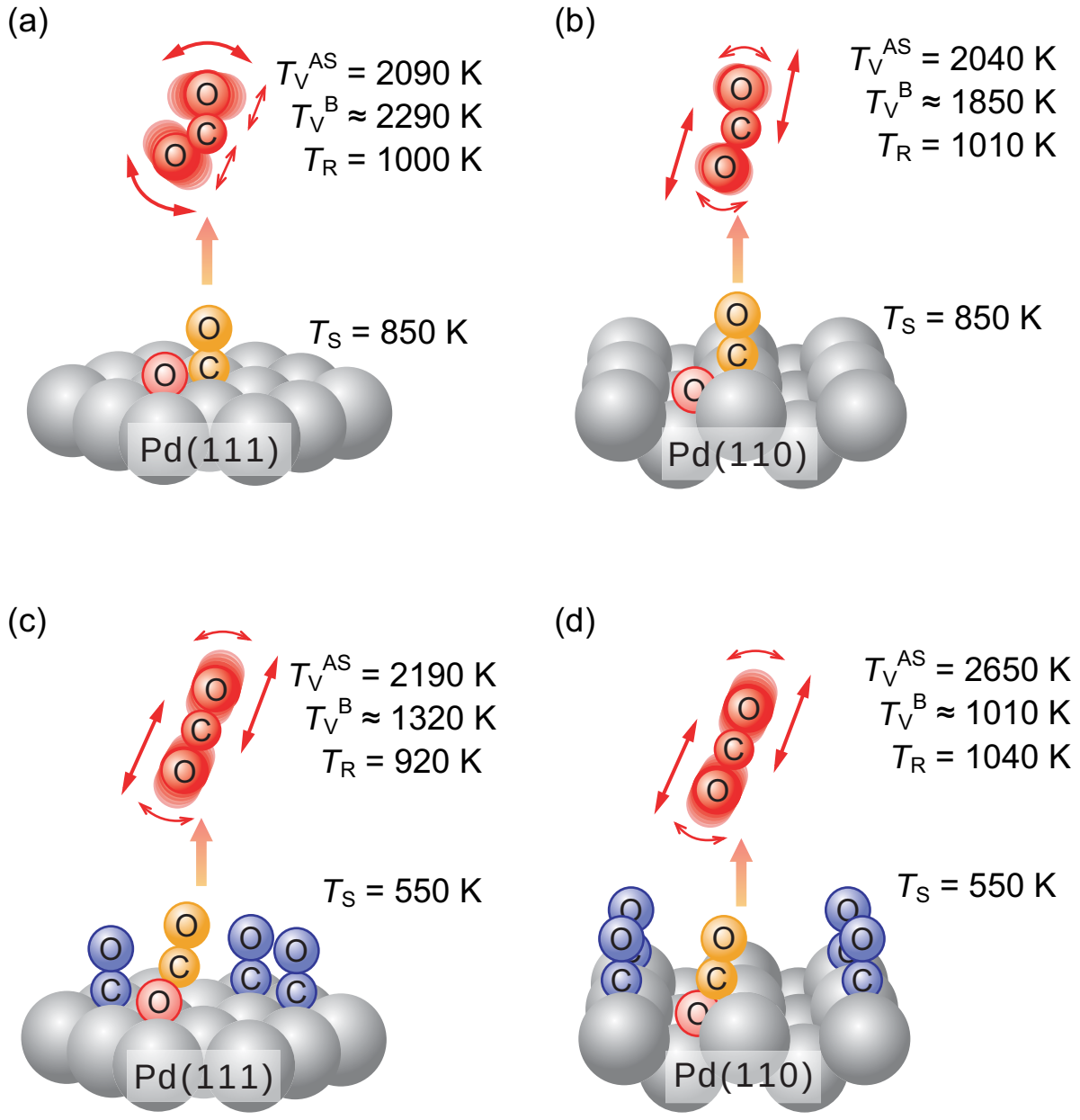

Figure 2-10 Structure of the activated complex of CO_2 formation and vibrationally excited state of desorbed CO_2 molecules: (a) Pd(111) at the higher temperature region; (b) Pd(110) at the higher temperature region; (c) Pd(111) at the lower temperature region, and (d) Pd(110) at the lower temperature region. The temperatures described in each model are based on the reaction under the total flux of reactants was 8.2×10^{18} molecules cm^{-2} s^{-1} at $CO/O_2 = 1$.

Chapter 3

CO_2 formation in CO + NO reaction on Pd(110) and Pd(111) surfaces

3.1. Introduction

The reaction of CO and NO to form CO_2 and N_2 is one of the most important automobile exhaust control reactions catalyzed by noble metals such as Pd, Rh, and Pt. Recently, there has been considerable interest in using Pd-only catalysts for three-way exhaust gas conversion [1]. Hence, a fundamental understanding of the reaction mechanism of the CO + NO reaction on Pd surfaces is of vital importance. Many ultra high vacuum (UHV) studies have focused on the nature of CO and NO chemisorption on single-crystal Pd surfaces [2–5], however, only a few groups have studied the steady-state CO + NO reaction over well-defined surfaces [6–13]. The utilization of single-crystal surfaces can be useful for the elucidation of the reaction mechanism over heterogeneous catalysts. To obtain the information on the reaction mechanism, an effective method is spectroscopic observations of reaction intermediates [8]. Another method is an investigation of internal (vibrational and rotational) energy and translational energy of product molecules desorbed from the catalyst surface [9–26]. This is because the energy states of the desorbed molecules can reflect the dynamics of catalytic reaction, which can correspond to a transition state (i.e., structure of activated complex). The infrared chemiluminescence (IR emission) of the product molecules from catalytic reaction enables one to analyze the vibrationally excited states [18–25]. Analysis of the vibrational states can give information on the structure of the activated CO_2 complex (i.e., the dynamics of CO oxidation) from which the gas-phase molecules were desorbed [16,18–25]. Furthermore, the vibrational energy state of the product CO_2 has been found to depend on the surface structure [13–16]. So, information about the active sites can be obtained in situ from the IR emission spectra of CO_2 under steady-state catalytic reaction.

Our group has reported IR chemiluminescence of CO_2 from the steady-state CO + O_2 and CO + NO reactions on single-crystal Pd surfaces combined with kinetic results [13–16]. It has been

suggested that the activated complex of CO_2 formation (i.e., the transition state of CO_2 formation from CO(a) + O(a)) had a more bent structure on Pd(111) and a relatively linear structure on Pd(110) because CO_2 from Pd(111) was more vibrationally excited than CO_2 from Pd(110) [13–16]. The results indicated that the IR chemiluminescence method can provide direct energetic evidence of the reaction mechanism and the activated complex of CO_2 formation. Almost no work on the vibrational energy of CO_2 produced from the CO + NO reaction on Pt and Pd surfaces has been performed, although Bald and Bernasek [17] found a rough similarity in the vibrational excitation between CO + NO and CO + O_2 reactions on a polycrystalline Pt surface.

In this work, we have studied dynamics and kinetics of CO_2 formation during the CO + NO reaction over single-crystal Pd(110) and Pd(111) surfaces. Almost no study has been done on the comparison of the CO + NO activity on Single-crystal Pd surfaces with different planes. Goodman et al. [6–8] have reported that Pd(111) is more active than Pd(100) and Pd(110) at the reactant pressure of 2–17 Torr. First, we elucidate the kinetics of the CO + NO reaction on Pd(110) compared with Pd(111). Secondly, we elucidate partial pressure (P_{CO}, P_{NO}) and surface temperature (T_S) dependence on the dynamics of the reaction, and the results are compared with those of CO + O_2 reaction on Pd(110) and Pd(111).

3.2. Experimental

A molecular-beam reaction system in combination with a FT-IR spectrometer (Thermo Electron, Nexus670; an InSb detector) was used to measure IR emission of product CO_2 molecules just desorbed during catalytic reaction on the metal surfaces [13–16]. A UHV chamber (base pressure < 1.0×10^{-9} Torr) was equipped with an Ar^+ ion gun for sample cleaning and a quadrupole mass spectrometer (QMS, Pfeiffer Vacuum, QME200). Two free-jet molecular-beam nozzles (0.1 mm diameter orifice) were used for the supply of reactant gases. The fluxes of the reactants were controlled by mass flow controllers. The CO and NO gases (total flux was 6.1×10^{18}–1.2×10^{19} cm^{-2} s^{-1}, CO/NO = 0.33−3) or the CO and O_2 gases (total flux was 8.2×10^{18} cm^{-2} s^{-1}, CO/O_2 = 1) were exposed to single-crystal Pd surfaces (Pd(110) and Pd(111)). Steady-state CO + NO and CO + O_2 reactions (the pressure range at the flux conditions = 10^{-2}–10^{-1} Torr) were performed in the

temperature range of 500–900 K. Another UHV chamber (base pressure < 2.0 × 10^{-10} Torr) equipped with the same molecular-beam reaction system, an Ar^+ ion gun, low energy electron diffraction (LEED) and a QMS was used to prepare the samples and to characterize Pd(110) and Pd(111) surfaces. Before the molecular-beam reaction, Pd(110) and Pd(111) were cleaned by a standard procedure (O_2 treatment, Ar^+ bombardment, and annealing) [13–16]. After cleaning, the sharp (1 × 1) LEED pattern was observed, and the reaction occurs on the (1 × 1) structure under steady-state condition [12].

The IR emission spectra of the CO_2 molecules desorbed from the surface were measured with 4 cm^{-1} resolution. Because of the low resolution (4 cm^{-1} resolution), no individual vibration-rotation lines were resolved. The IR emission spectra were analyzed on the basis of simulation of model spectra, yielding an average vibrational Boltzmann temperature (T_V^{AV}, i.e., an average temperature of the antisymmetric stretch, symmetric stretch, and bending modes), which could be estimated from analysis of the degree of the red-shift from the fundamental band (2349 cm^{-1}) [18,19]. Although the IR emission observed here is the antisymmetric stretch (AS) vibrational region, i.e., (n_{SS}, n_B^l, n_{AS}) → (n_{SS}, n_B^l, n_{AS} − 1), vibrational excitation levels of symmetric stretch (n_{SS}) and bending (n_B) also affect this region [16,18]. Here, n_{SS}, n_B and n_{AS} are the vibrational quantum number of each mode, and l is the quantum number of vibrational angular momentum in linear molecules. Note that the emission intensity is normalized by the rate of CO_2 production. Thus, the emission intensity is related to extent of excitation in the antisymmetric stretch of CO_2, which is given by the following equation:

$$f \propto e^{-x} + e^{-2x} + e^{-3x} \cdots \fallingdotseq e^{-x}/(1-e^{-x}), \qquad (1)$$

where f is the emission intensity normalized per unit CO_2 yield, and x equals to $\Delta E_V/k_B T_V^{AS}$ (ΔE_V is the energy spacing, k_B is the Boltzmann constant, and T_V^{AS} is the antisymmetric vibrational temperature). From the steady-state results at high resolution (0.06 cm^{-1}) [18], it was possible to deduce the energy distribution in each vibrational mode (T_V^{SS}, T_V^{B}, T_V^{AS}), where the superscripts, respectively, indicate symmetric stretch, bending and antisymmetric stretch. Here, steady-state CO + O_2 reaction on polycrystalline Pt foil was performed under the same conditions as reported previously [18] (CO = O_2 = 4.1 × 10^{18} cm^{-2} s^{-1}), and the IR emission spectra of CO_2 molecules were

measured with 4 cm^{-1} resolution at surface temperature (T_S) of 900 K. This obtained spectrum was compared with the previous results (T_V^{AS} = 1600 K) [18], and the emission intensity normalized by the rate of CO_2 production was defined as T_V^{AS} = 1600 K. This emission intensity and T_V^{AS} were used as a standard for various conditions on Pd surfaces. Based on T_V^{AS} and T_V^{AV}, it is possible to deduce the bending vibrational temperature (T_V^B). The relation between T_V^{AV} and each vibrational temperature is represented as the equation below.

$$T_V^{AV} = (T_V^{AS} + T_V^{SS} + 2T_V^B) / 4. \quad (2)$$

In this equation, $2T_V^B$ corresponds to the two degenerate bending vibrational modes. Assuming that T_V^B is equal to T_V^{SS} because of the Fermi resonance [17,20], T_V^B can be expected to be ($4T_V^{AV} - T_V^{AS}$)/3. This assumption is plausible on the basis of the previous reports [18,20]. It should be added that T_V^{AV}, T_V^{AS} and T_V^B were used here as parameters characterizing the extent of the vibrational excitation of the product CO_2. It took about 30–90 min to measure the IR spectra with 2000–6000 scans. During the measurement, the activity was stable, and therefore, the results reflected the CO_2 states under steady-state conditions. The production rate of CO_2 was determined using a QMS, and the amount of N_2O formation (by-product) was checked by a gas chromatograph. In our case, the selectivity of N_2O formation (N_2O / (N_2O + N_2)) was usually below a few percent (8% at most [13]).

3.3. Results and Discussion

3.3.1. Kinetics of the CO + NO reaction on Pd(110)

Figure 3-1 shows the rate of CO_2 formation in steady-state CO + NO reaction on Pd(110) as a function of surface temperature under various partial pressure conditions. In particular, Figures 3-1(a) and (b) exhibit the dependence of the reaction rate on NO pressure under the fixed CO flux and on CO pressure under the fixed NO flux, respectively. Under all the partial pressure conditions, the formation rate of CO_2 increased with increasing the surface temperature (T_S) in the lower temperature range, exhibited a maximum, and then decreased with further increasing T_S. The same behavior has also been observed in the CO + O_2 reaction [16,27]. Here, we call the temperature, where the highest CO_2 rate is observed, as T_S^{max}. From these results, it is found that the reaction

order with respect to NO and CO is about zero at surface temperatures (such as 600 K) lower than T_S^{max} under all conditions. On the other hand, at surface temperatures (such as 800 K) higher than T_S^{max}, the reaction order of NO and CO is determined to be approximately 0.5.

To understand the kinetics of the CO + NO reaction on the Pd surface under steady-state conditions, we calculated the coverages of adsorbate species on the basis of a reaction model. One of the most probable model mechanisms of the CO + NO reaction on Pd surface [28,29] is as follows (for a review of other possible mechanisms, see Ref. [30]):

$$CO(g) + V \leftrightarrow CO(a), \quad (3)$$

$$NO(g) + V \leftrightarrow NO(a), \quad (4)$$

$$NO(a) + V \rightarrow N(a) + O(a), \quad (5)$$

$$2N(a) \rightarrow N_2(g) + 2V, \quad (6)$$

$$CO(a) + O(a) \rightarrow CO_2(g) + 2V, \quad (7)$$

where V is a vacant site. In this model, it is assumed that the rate-determining step is NO dissociation (Eq.(5)), and this is based on the previous report [31]. Furthermore, the elementary steps (3) and (4) are considered to be more rapid than the reaction rate, and the adsorption of CO and NO reaches equilibrium. Using the steady-state method, we can derive the following equations for adsorbate coverages.

$$d\theta_{CO}/dt = f_{CO}\, s_{CO}\, \theta_V - k_{CO}^{des}\, \theta_{CO}, \quad (8)$$

$$d\theta_{NO}/dt = f_{NO}\, s_{NO}\, \theta_V - k_{NO}^{des}\, \theta_{NO}, \quad (9)$$

$$d\theta_N/dt = k_{NO}^{dis}\, \theta_{NO}\, \theta_V - k_{N_2}^{des}\, \theta_N^2, \quad (10)$$

$$d\theta_O/dt = k_{NO}^{dis}\, \theta_{NO}\, \theta_V - k_r\, \theta_{CO}\, \theta_O, \quad (11)$$

where f and s are the flux of reactants to the surface and the initial sticking coefficients, respectively. The k^{des}, k^{dis}, and k_r are the rate constants for CO, NO and N_2 desorption, NO dissociation and the reaction of CO with the oxygen atom to form CO_2, respectively. The fraction of vacant sites is denoted as $\theta_V = (1 - \theta_{CO} - \theta_{NO} - \theta_N - \theta_O)$. Here, we adopted the reported rate constants for k_{CO}^{des}, k_{NO}^{des}, and $k_{N_2}^{des}$ (Table 3-1). In addition, the rate constant k_r can be determined on the basis of a similar calculation for the CO + O_2 reaction on Pd(110), as will be shown in section 3.3.2. The initial sticking coefficients of CO and NO are also listed in Table 3-1. Based on the above equations

and the steady-state method ($d\theta_{CO}/dt = d\theta_{NO}/dt = d\theta_N/dt = d\theta_O/dt = 0$), the coverage of each adsorbed species during the reaction can be calculated as follows.

At lower surface temperature range;

$$\theta_{CO} = \frac{f_{CO}s_{CO}k_{NO}^{des}(1-\theta_N)}{f_{CO}s_{CO}k_{NO}^{des} + f_{NO}s_{NO}k_{CO}^{des} + k_{CO}^{des}k_{NO}^{des}}, \quad (12)$$

$$\theta_{NO} = \frac{f_{NO}s_{NO}k_{CO}^{des}(1-\theta_N)}{f_{CO}s_{CO}k_{NO}^{des} + f_{NO}s_{NO}k_{CO}^{des} + k_{CO}^{des}k_{NO}^{des}}, \quad (13)$$

$$\theta_N = \sqrt{r_{CO_2}/k_{N_2}^{des}}, \quad (14)$$

$$\theta_O = \frac{r_{CO_2}}{k_r\theta_{CO}}. \quad (15)$$

At higher surface temperature range;

$$\theta_{CO} = \frac{f_{CO}s_{CO}k_r + \sqrt{(f_{CO}s_{CO}k_r)^2 - 4f_{CO}s_{CO}k_{CO}^{des}k_r r_{CO_2}}}{2k_{CO}^{des}k_r}, \quad (16)$$

$$\theta_{NO} = \frac{f_{CO}s_{CO}f_{NO}s_{NO}k_r + f_{NO}s_{NO}\sqrt{(f_{CO}s_{CO}k_r)^2 - 4f_{CO}s_{CO}k_{CO}^{des}k_r r_{CO_2}}}{2f_{NO}s_{NO}k_{NO}^{des}k_r}, \quad (17)$$

$$\theta_N = \sqrt{r_{CO_2}/k_{N_2}^{des}}, \quad (18)$$

$$\theta_O = \frac{r_{CO_2}}{k_r\theta_{CO}}. \quad (19)$$

Here, r_{CO_2} is introduced to the above equations based on $r_{CO_2} = k_r\theta_{CO}\theta_O$, which is the formation rate of CO_2 in CO + NO reaction, and the values as a function of T_S are given from the experimental results shown in Fig. 3-1. In the calculation using θ_V, we have considered the fact that θ_O is negligible in the CO + NO reaction at lower surface temperatures because the O atoms are removed by CO(a) from the surface immediately after the NO dissociation [29]. On the other hand, we have considered the fact that θ_{CO}, θ_{NO} and θ_N are negligible at higher surface temperatures, because the desorption rate is much higher than the reaction rate [33].

The calculation results of the coverages of adsorbates under various CO/NO fluxes at T_S = 600, 675, and 800 K are shown in Figure 3-2. At T_S = 600 K, the coverage of NO and CO adsorption is strongly influenced by the flux. When the NO flux increases, θ_{NO} and θ_O increase, on the other hand, θ_{CO} decreases and θ_N is almost constant (Fig. 3-2(a)). In the case of the CO flux dependence at 600 K (Fig. 3-2(d)), the behavior is similar. When the CO flux decreases, θ_{CO}

decreases, and θ_{NO} and θ_O increase. In contrast, in the NO flux dependence at 800 K (Fig. 3-2(c)), θ_O is much higher than θ_{NO}, θ_{CO} and θ_N. When the NO flux increases, θ_O and θ_{NO} increase significantly. In contrast, when the CO flux increases, θ_{CO} increases linearly and θ_O decreases gradually (Fig. 3-2(f)). At T_S = 800 K, the positive order with respect to NO can be explained by the gradual increase of θ_O, and that with respect to CO can also be explained by the proportional increase of θ_{CO} and gradual decrease of θ_O. At T_S = 675 K, the coverage of adsorbed species can be located between T_S = 600 and 800 K. Furthermore, from the calculation at each reaction temperature, the temperature dependence of the rate constant for NO dissociation can be determined using equation (20).

$$k_{NO}^{dis} = \frac{r_{CO_2}}{\theta_{NO}\theta_V} \qquad (20)$$

This gives the pre-exponential factor $\nu = 2.7 \times 10^{14}$ s^{-1} and activation energy E_a = 34.2 kcal/mol, as listed in Table 3-1. This activation energy is close to the reported value E_a = 31.5 kcal/mol [35].

3.3.2. Comparison with kinetics of the CO + O_2 reaction on Pd(110)

The mechanism of the CO + O_2 reaction on Pd surface is well known to be as follows [27]:

$$CO(g) + V \leftrightarrow CO(a), \qquad (21)$$

$$O_2(g) + 2V \rightarrow 2O(a), \qquad (22)$$

$$CO(a) + O(a) \rightarrow CO_2(g) + 2V. \qquad (23)$$

It is possible to write equations regarding the coverage of each intermediate as shown below [38,39].

$$d\theta_{CO}/dt = f_{CO}\, s_{CO}\, (1 - \theta_{CO} - \theta_O) - k_{CO}^{des}\, \theta_{CO} - r_{CO_2}, \qquad (24)$$

$$d\theta_O/dt = 2\, f_{O_2}\, s_{O_2}\, (1 - \theta_{CO} - \theta_O)^2 - r_{CO_2}, \qquad (25)$$

where the rate of O_2 desorption is small enough to be neglected [27,38,39]. The CO_2 formation rate, r_{CO_2}, was obtained from the experimental results shown in Figure 3-3. The initial sticking coefficients of CO and O_2 and the kinetic parameters used are also listed in Table 3-1. The results of the coverage calculation in the CO + O_2 reaction on Pd(110) are shown in Fig. 3-3. It is known that, at temperatures lower than T_S^{max}, the surface coverage of CO (θ_{CO}) is high, and the rate-determining

step is O_2 adsorption on the vacant site, which is formed by the desorption of CO(a). At temperatures higher than T_S^{max}, the formation rate of CO_2 decreased gradually with increasing surface temperature, and this behavior is due to the drastic decrease of θ_{CO}. Generally, in the CO + O_2 reaction on the Pd surface at lower surface temperature, the reaction order is –1 with respect to CO and +1 with respect to O_2 [27]. On the other hand, at higher temperatures, θ_{CO} can be very small (θ_{CO} « 0.01) and oxygen coverage (θ_O) approaches the saturation level ($\theta_O \sim 0.5$) [34]. Therefore, it is thought that the reaction order is +1 and 0 with respect to CO and O_2, respectively. The formation rate of CO_2 can be plotted as a function of inverse surface temperature in Arrhenius form originated from Fig. 3-3. From the temperature range T_S = 500–625 K, the pre-exponential factor, ν, and apparent activation energy (E_a) of Eq.(23) are estimated to be 7.1×10^{15} s^{-1} and 33.6 kcal/mol, respectively, as listed in Table 3-1. The rate constant for CO(a) + O(a) reaction in the CO + O_2 reaction can be applied to that in the CO + NO reaction (Eq. (7)). Furthermore, the important point is that the CO_2 formation rate for the CO + NO reaction was much lower than that of the CO + O_2 reaction (Figs. 3-1 and 3-3). Because the CO coverage in both reactions is similar, the difference in reaction rates can be due to that in the oxygen coverage.

3.3.3. Infrared (IR) emission spectra of CO_2 desorbed by the CO + NO reaction under different partial pressures

The IR emission spectra of CO_2 formed by the CO + NO reaction were measured at T_S = 675 K (below T_S^{max}) and T_S = 800 K (above T_S^{max}) (Fig. 3-1). Figure 3-4 shows IR emission spectra of CO_2 molecules produced by the CO + NO reaction on Pd(110) for various NO fluxes at a fixed CO flux. The CO_2 emission spectra were observed in the region of 2400–2200 cm^{-1}, while the emission spectrum centered at 2143 cm^{-1} is due to the IR emission of the unreacted CO, which was scattered from the surface. At T_S = 675 K, the degree of the red-shift from the fundamental band (2349 cm^{-1}) was almost the same under the various NO fluxes, however, the emission intensity became larger with increasing NO flux. On the other hand, at T_S = 800 K, when the NO flux was decreased in the range of $2.0–8.2 \times 10^{18}$ cm^{-2} s^{-1}, more red-shift from 2349 cm^{-1} was observed in the emission spectra of CO_2. This degree of red-shift was almost constant for the higher NO flux (above

8.2×10^{18} cm^{-2} s^{-1}). The emission intensity increased monotonically with increasing NO flux. Figures 3-5(a) and (b) show IR emission spectra of the CO flux dependence in the CO + NO reaction on Pd(110) at T_S = 675 and 800 K. At both reaction temperatures, the degree of the red-shift from the fundamental band was almost constant under the various CO fluxes. The emission intensity became larger with increasing CO flux. From the analysis of the CO_2 emission spectra, information on the vibrational states of desorbed CO_2 can be obtained as shown below.

At first, the average vibrational temperature (T_V^{AV}) obtained from the red-shift in IR emission spectra of CO_2 at T_S = 675 K and 800 K as a function of (a) NO flux and (b) CO flux is shown in Figure 3-6. Each T_V^{AV} value was much higher than T_S, which indicates that the CO_2 formed is vibrationally excited. The T_V^{AV} value was not so changed under various flux conditions and surface temperatures. Next, T_V^{AS} and T_V^{B} obtained from the IR emission intensity of CO_2 as a function of NO flux at (a) T_S = 675 K and (b) T_S = 800 K are shown in Figure 3-7. At both surface temperatures, as the NO flux increased, T_V^{AS} increased and T_V^{B} decreased. T_V^{AS} at T_S = 675 K was higher than that at T_S = 800 K, on the other hand, T_V^{B} at T_S = 675 K was lower than that at T_S = 800 K. Although the average vibrational temperature was rather similar, it is found that the vibrational states of desorbed CO_2 were very dependent on the NO flux conditions. At T_S = 675 K, T_V^{AS} is higher than T_V^{B}, which means that the internal energy is distributed mainly in the antisymmetric vibrational mode. On the other hand, at T_S = 800 K, T_V^{AS} was lower than T_V^{B}, suggesting that the energy is distributed mainly to the bending vibrational modes.

Figures 3-8(a) and (b) show T_V^{AS} and T_V^{B} obtained from IR emission intensity of CO_2 as a function of CO flux at (a) T_S = 675 K and (b) T_S = 800 K. At T_S = 675 K, the CO flux dependence of T_V^{AS} and T_V^{B} was similar to the NO flux dependence. However, at T_S = 800 K, T_V^{AS} and T_V^{B} were almost constant under various flux conditions, although the tendency that T_V^{B} was higher than T_V^{AS} was common in both NO and CO flux dependences at T_S = 800 K. This common phenomenon at T_S = 800 K can be reflected by the coverage of adsorbed oxygen because the coverages of other adsorbed species were much lower than that of oxygen (Figs. 3-2(c) and (f)). On the other hand, at T_S = 675 K, the coverages of NO, CO, and nitrogen atom were not low (Figs. 3-2(b) and (e)), and this can make the excitation of the vibrational modes more complex. Zhdanov [36] has shown that

the change in the energy distribution of the reaction products with increasing coverage can be related to lateral adsorbate-adsorbate interactions in the activated state for reaction.

3.3.4. Structure-sensitivity of the CO + NO reaction on Pd(110) and Pd(111)

Figure 3-9 shows the rate of CO_2 formed in the steady-state CO + NO reaction on Pd(110) and Pd(111) surfaces as a function of T_S. The CO + NO reaction proceeded above 550 K and the temperature dependence of the formation rate had maxima on both Pd surfaces, and the observed behavior on the T_S dependence was similar to that of Fig. 3-1. It is found that Pd(110) exhibited much higher activity than Pd(111). This indicates that the CO + NO reaction on Pd surfaces is structure-sensitive under the steady-state reaction condition with the total pressure of 10^{-2} Torr. Generally, the NO dissociation proceeds on step sites, and it is difficult to proceed on the sites on the terrace plane surface, such as on Pd(111) [5,37]. Therefore, the result in Fig. 3-9 reflects the activity for NO dissociation. The turnover frequency (TOF) of CO_2 formation rate at 625 K was determined to be 18 s^{-1} and 2.8 s^{-1} on Pd(110) and Pd(111), respectively. Furthermore, the activation energy of the CO + NO reaction in the temperature range T_S = 550–650 K was determined to be 45.6 kcal/mol and 24.8 kcal/mol on Pd(110) and Pd(111), respectively. Goodman et al. [6–8] have reported the results of CO + NO reaction on Pd surfaces, and TOF on Pd(110) and Pd(111) at 625 K was determined to be 5 s^{-1} and 20 s^{-1}, respectively. In addition, the activation energy on Pd(110) and Pd(111) was estimated to be 17.0 kcal/mol and 16.2 kcal/mol, respectively. The difference from our results is due to the difference in the reactant pressure. In our case, it was of the order of 10^{-2} Torr, and in Goodman's study, it was in the range of 2–17 Torr [6–8]. They have reported that NO dissociates immediately on more open surfaces (Pd(110) and Pd(100)) to form atomic nitrogen (N(a)) [6–8]. The N(a) species are bound strongly to the surface and inhibit the adsorption of NO and CO. Therefore, the activity (TOF) on Pd(110) and Pd(100) was lower than that on Pd(111), and the rate-determining step is the nitrogen desorption. In particular, they have shown that 80% of the surface sites were covered by nitrogen species during the reaction on Pd(100), while only 20% on Pd(111) [6]. In our case, the coverage of nitrogen was very low (θ_N « 0.1) at higher temperatures (800 K), and the rate-determining step is the NO dissociation, which means that the oxygen atom

supplied from the NO dissociation can react with CO immediately.

3.3.5. Dynamics of CO + NO and CO + O_2 reactions on Pd(110) and Pd(111): surface temperature (T_S) dependence

Figure 3-10 shows the IR emission spectra for CO_2 molecules produced by the CO + NO reaction on Pd(110) and Pd(111) surfaces as a function of T_S. The higher the surface temperature, the more the red-shift from the antisymmetric stretch fundamental band (2349 cm^{-1}) was observed in the emission spectra of CO_2. Especially, more red-shift was observed at T_S > 750 K ($T_S > T_S^{max}$) on Pd(110). Figure 3-11 shows the IR emission spectra of CO_2 molecules produced by the CO + O_2 reaction on Pd(110) and Pd(111) surfaces at various surface temperatures. The higher the surface temperature, the more the red-shift from 2349 cm^{-1} was observed in the emission spectra of CO_2. The emission of the unreacted CO in the CO + O_2 reaction was much lower than that in the CO + NO reaction, and this is influenced by the difference of CO_2 formation rate. Because the formation rate of the CO + O_2 reaction was much higher than that of the CO + NO reaction as described above, the intensity of the emission spectra of CO normalized by the CO_2 formation rate can be much smaller in the case of the CO + O_2 reaction. The average vibrational temperature (T_V^{AV}) from the analysis of CO_2 emission spectra in Figs. 3-10 and 3-11 is plotted as a function of T_S in Figure 3-12. T_V^{AV} increased with increasing T_S for both reactions on Pd(110) and Pd(111). T_V^{AV} on Pd(111) in both reactions is higher than that on Pd(110), which is in good agreement with the previous results [13–16]. Especially, in the T_S range of 600–725 K, T_V^{AV} was dependent on the surface structure, and it was not dependent on the CO + NO and CO + O_2 reactions. However, in the higher temperature range above 750 K on Pd(110), T_V^{AV} of the CO + NO reaction was higher than that of the CO + O_2 reaction.

Figures 3-13 and 3-14 show T_V^{AS} and T_V^{B} derived from IR emission intensity of CO_2 as a function of T_S in CO + O_2 and CO + NO reactions, respectively. T_V^{AS} was always higher than T_V^{B} under all the surface temperatures in the CO + O_2 reaction on Pd(110) (Fig. 3-13(a)). Overall, T_V^{B} was higher than T_V^{AS} in the CO + O_2 reaction on Pd(111) at all surface temperatures (Fig. 3-13(b)). This suggests that the structure of the activated complex for CO_2 formation in the CO + O_2 reaction

on Pd(111) is more bent than that on Pd(110) as reported previously [14–16]. This can be reflected by the surface plane structure of Pd(111). As also shown in Fig. 3-13, both T_V^{AS} and T_V^{B} increased gradually with increasing T_S on Pd(110) and Pd(111), which is a general trend in the case of the CO + O_2 reaction [16,18,20]. So far, almost no discussion on surface temperature dependence of the product vibrational energy was made [40]. Experimental results on the CO + O_2 reaction on Pt and Pd showed that the increase in vibrational temperature was higher than that of surface temperature [16,18,20]. Theoretical works will be needed on the temperature dependence of the internal energy.

The T_S dependences in the CO + NO reaction are more complex than those in CO + O_2 reaction. T_V^{AS} decreased and T_V^{B} increased significantly with increasing T_S in the CO + NO reaction on Pd(110) (Fig. 3-14(a)). At lower surface temperatures, T_V^{AS} was higher than T_V^{B}. Above 700 K, T_V^{B} became higher than T_V^{AS}, which means that the more excited mode changed from the antisymmetric to the bending vibrational modes. This temperature (700 K) corresponds to T_S^{max} (Fig. 3-9). This behavior was also observed in the CO + NO reaction on Pd(111) (Fig. 3-14(b)). These results indicate that the structure of the activated complex for CO_2 formation can be very dependent on T_S. At temperatures lower than T_S^{max}, the structure of the activated complex is less bent. Furthermore, it should be noted that the bending vibration is highly excited at higher T_S. It is characteristic that the T_V^{B} in the CO + NO reaction over Pd(110) above 800 K is much higher than other cases. Although the T_V^{B} in the CO + NO reaction over Pd(111) at high temperature can not be obtained because of the low CO_2 formation rate and low IR emission, the bending vibration can be highly excited, which is suggested from the data obtained.

3.3.6. Effect of oxygen coverage on the vibrational excitation of CO_2

The effect of coverages on T_V^{AS} and T_V^{B} seems to be more complex at lower temperatures, because the coverages of the adsorbed species are rather high (Fig. 3-2). At higher temperature (800 K), however, the oxygen coverage becomes higher, and the other coverages are very low (Figs. 3-2(c) and (f)). The data at 800 K in Fig. 3-7(b) suggest that T_V^{B} decreases with increasing θ_O (judging from the result in Fig. 3-2(c)), while T_V^{AS} increased with increasing θ_O. However, the results seem to be different from those of Bald and Bernasek [17], who reported that both T_V^{B} and

T_V^{AS} increased with increasing NO/CO ratio for the CO + NO reaction over a polycrystalline Pt surface. Their results indicate that the vibrational excitation became higher with increasing θ_O [17]. On the other hand, the data at 800 K in Fig. 3-8(b) show that both T_V^B and T_V^{AS} are almost constant, although θ_O decreases with increasing CO flux (Fig. 3-2(f)). Therefore, no clear conclusion on the θ_O effect in the CO + NO reaction on Pd(110) can be done in this work.

At T_S = 800, 850 K on Pd(110), T_V^B in the CO + NO reaction (Fig. 3-14(a)) is much higher than that in the CO + O_2 reaction (Fig. 3-13(a)). As suggested in Figs. 3-2 and 3-3, at T_S = 800 K θ_O was 0.39 and 0.10 for CO + O_2 and CO + NO reactions, respectively. The coverages of other species are negligible. Such a large difference in the oxygen coverage can be observed between the different reactions. In the CO + NO reaction, θ_O can be small because the rate-determining step is the NO dissociation. One possible explanation is that the large difference in θ_O affects the dynamics of CO_2 formation. According to the reports on surface diffusion of oxygen, the activation energy for surface diffusion of oxygen atoms over Rh(111) and Pt(111) is very dependent on the coverage of oxygen. At θ_O = 0.25 and 0.5 on Rh(111), the activation energies are calculated to be E_a = 10.8 and 13.1 kcal/mol, respectively [41]. At θ_O = 0.03 and 0.25 on Pt(111), E_a is calculated to be 11.3 and 25 kcal/mol, respectively [42,43]. This suggests that the oxygen atom has a higher mobility under lower oxygen coverage. When the energy of surface diffusion can be added to the formation of the activated CO_2 complex, it is expected that its vibrational mode becomes more excited. Furthermore, in this case, since the energy of surface diffusion is along the surface, this can be distributed to the bending vibrational modes in the activated CO_2 complex rather than the asymmetric stretching vibrational mode. Although this is one explanation, it should be pointed out that this view is not reconciled with the results of the previous reports [19,20], where the vibrational excitation became higher with increasing θ_O in CO + O_2 reaction on polycrystalline Pt and Pd surfaces.

3.3.7. Structure of the activated complex and the vibrational states of CO_2 on Pd(110) surface

The analyses of CO_2 emission spectra in the CO + NO reaction on Pd(110) surface at higher surface temperatures indicated that bending vibrational mode was more excited than antisymmetric vibrational mode (Figs. 3-7(b), 3-8(b), and 3-14). This means that the activated complex of CO_2

formation in the CO + NO reaction has more bent form than that in the CO + O_2 reaction. The structure of activated complex can be strongly influenced by the adsorption sites of CO and O. The adsorption site of CO on Pd(110) at higher temperature is thought to be bridge site of the row in the first layer [27]. In contrast, the most stable adsorption site for atomic oxygen is three-fold hollow site [44] as shown in Figure 3-15. Since the angle of O–C–O ($\angle_{OCO}$) is much higher than 90°, it is expected that the activated complex formed from the reaction between the adsorbed CO and O can have a less bent structure (Fig. 3-15(a)). Judging from very high bending vibrational temperature of the CO + NO reaction, the activated complex should have a more bent structure. One possible interpretation is the activated complex formed from the reaction of the adsorbed CO with oxygen atom located on the first layer on Pd(110) (Fig. 3-15(b)). On the basis of the report on the adsorption energy of oxygen atom on the various sites over Pd(110) [44], bridged oxygen atom on the first layer has 1.1 eV higher energy than that on three-fold hollow site described in Fig. 3-15. This means that the energy state of adsorbed CO and O in CO+NO reaction is higher than that in the CO + O_2 reaction, which can be related to the result that T_V^{AV} of the CO + NO was higher than that of the CO + O_2 at the high surface temperatures.

Another possible explanation is that the dynamics of CO_2 formation can be different between the CO + NO and CO + O_2 reactions, although the same kinetic equation ((7) and (23)) is used to describe the CO_2 formation. In fact, the T_V^B and T_V^{AS} values were different at the high temperatures (800 K and 850 K) on Pd(110) (Figs. 3-13(a) and 3-14(a)). In the CO + O_2 reaction, adsorbed oxygen is accommodated to the surface, while the surface residence time of CO(a) is very short at higher surface temperatures [16]. However, the oxygen atom from NO dissociation, which reacts with CO immediately after the formation, may not be accommodated to the surface, and such a hot O atom can affect the extent of the vibrational excitation. Such dynamic roles of nascent hot oxygen have also been observed in other reaction systems [45–48]. In this case, the rate constant k_r in the CO + NO reaction (Eq. (7)) may be larger than that in the CO + O_2 reaction (Eq. (23)), which results in lower θ_O values in Figs. 3-2(c) and (f). Further investigation is necessary for the elucidation of the mechanism for the excitation of the vibrational modes of the activated complex.

3.4. Conclusions

(1) Rates of CO_2 formation during steady-state CO + NO reaction were measured over Pd(110) and Pd(111) in the pressure range of 10^{-2}–10^{-1} Torr. The activity of Pd(110) was much higher than that of Pd(111) in the low pressure condition, which means that the rate-determining step is NO dissociation on step sites.

(2) On the basis of kinetic experimental results on the partial pressure dependence of NO and CO, and the reported rate constants using the reaction model, the coverages of NO, CO, N, and O were calculated under various flux conditions, and the results are compared with those of the CO + O_2 reaction.

(3) In the IR emission spectra of CO_2 during the CO + O_2 reaction on Pd(110) and Pd(111) in the entire T_S range, the antisymmetric vibrational temperature (T_V^{AS}) was higher than the bending vibrational one (T_V^{B}) on Pd(110). In contrast, T_V^{B} was higher than T_V^{AS} on Pd(111). These behaviors suggest that the activated complex for CO_2 formation is more bent on Pd(111) than that on Pd(110), which is reflected by the surface smoothness. Both T_V^{B} and T_V^{AS} increased gradually with increasing surface temperature (T_S).

(4) From the IR emission spectra of CO_2 during the CO + NO reaction over both Pd surfaces, T_V^{AS} decreased and T_V^{B} increased significantly with increasing T_S. T_V^{B} was higher than T_V^{AS} at higher temperatures (above 700 K). T_V^{B} in CO + NO reaction on Pd(110) at 800 and 850 K was much higher than that in CO + O_2 reaction, which was discussed in terms of the large difference in the oxygen coverage and the difference in the dynamics of both reactions.

References

[1] K.C. Taylor, *Catal. Rev. Sci. Eng.* **35** (1993) 457.

[2] R.J. Behm, K. Christmann, G. Ertl, M.A. Van Hove, *J. Chem. Phys.* **73** (1980) 2984.

[3] X. Guo, J.T. Yates, Jr. *J. Chem. Phys.* **90** (1989) 6761.

[4] M. Hirsimäki, M. Valden, *J. Chem. Phys.* **114** (2001) 2345.

[5] R.D. Ramsier, Q. Gao, H.N. Waltenburg, K.-W. Lee, O.W. Nooij, L. Lefferts, J.T. Yates, Jr. *Surf. Sci.* **320** (1994) 209.

[6] S.M. Vesecky, D.R. Rainer, D.W. Goodman, *J. Vac. Sci. Technol. A* **14** (1996) 1457.

[7] D.R. Rainer, S.M. Vesecky, M. Koranne, W.S. Oh, D.W. Goodman, *J. Catal.* **167** (1997) 234.

[8] E. Ozensoy, D.W. Goodman, *Phys. Chem. Chem. Phys.* **6** (2004) 3765.

[9] I. Kobal, K. Kimura, Y. Ohno, T. Matsushima, *Surf. Sci.* **445** (2000) 472.

[10] Y. Ma, I. Rzeźnicka, T. Matsushima, *Chem. Phys. Lett.* **388** (2004) 201.

[11] I. Rzeźnicka, Y. Ma, G. Cao, T. Matsushima, *J. Phys. Chem. B* **108** (2004) 14232.

[12] T. Matsushima, *Surf. Sci. Rep.* **52** (2003) 1.

[13] K. Nakao, H. Hayashi, H. Uetsuka, S. Ito, H. Onishi, K. Tomishige, K. Kunimori, *Catal. Lett.* **85** (2003) 213.

[14] H. Uetsuka, K. Watanabe, H. Ohnuma, K. Kunimori, *Chem. Lett.* (1996) 227.

[15] K. Watanabe, H. Ohnuma, H. Kimpara, H. Uetsuka, K. Kunimori, *Surf. Sci.* **402-404** (1998) 100.

[16] H. Uetsuka, K. Watanabe, H. Kimpara, K. Kunimori, *Langmuir* **15** (1999) 5795.

[17] D.J. Bald, S.L. Bernasek, *J. Chem. Phys.* **109** (1998) 746.

[18] D.A. Mantell, K. Kunimori, S.B. Ryali, G.L. Haller, J.B. Fenn, *Surf. Sci.* **172** (1986) 281.

[19] K. Kunimori, G.L. Haller, *Bull. Chem. Soc. Jpn.* **65** (1992) 2450.

[20] S.W. Coulston, G.L. Haller, *J. Chem. Phys.* **95** (1991) 6932.

[21] D.A. Mantell, S.B. Ryali, B.L. Halpern, G.L. Haller, J.B. Fenn, *Chem. Phys. Lett.* **81** (1981) 185.

[22] S.L. Bernasek, S.R. Leone, *Chem. Phys. Lett.* **84** (1981) 401.

[23] D.A. Mantell, S.B. Ryali, G.L. Haller, *Chem. Phys. Lett.* **102** (1983) 37.

[24] M. Kori, B.L. Halpern, *Chem. Phys. Lett.* **110** (1984) 223.

[25] L.S. Brown, S.L. Bernasek, *J. Chem. Phys.* **82** (1985) 2110.

[26] D.J. Bald, R. Kunkel, S.L. Bernasek, *J. Chem. Phys.* **104** (1996) 7719.

[27] T. Engel, G. Ertl, *Adv. Catal.* **28** (1979) 1.

[28] B. Hammer, *J. Catal.* **199** (2001) 171.

[29] L. Olsson, V.P. Zhdanov, B. Kasemo, *Surf. Sci.* **529** (2003) 338.

[30] V.P. Zhdanov, B. Kasemo, *Surf. Sci. Rep.* **29** (1997) 31.

[31] F. Garin, *Appl. Catal. A* **222** (2001) 183.

[32] H. Sellers, J. Anderson, *Surf. Sci.* **475** (2001) 11.

[33] S.L. Lombardo, A.T. Bell, *Surf. Sci. Rep.* **13** (1991) 1.

[34] J. Goschnick, M. Wolf, M. Grunze, W.N. Unertl, J.H. Block, J. Loboda-Cackovic, *Surf. Sci.* **178** (1986) 831.

[35] R.G. Shrape, M. Bowker, Surf. Sci. **360** (1996) 21.

[36] V.P. Zhdanov, *Surf. Sci.* **165** (1986) L31.

[37] D. Loffreda, D. Simon, P. Sautet, *J. Catal.* **213** (2003) 211.

[38] K. Krischer, M. Eiswirth, G. Ertl, *J. Chem. Phys.* **96** (1992) 9161.

[39] K. Watanabe, H. Uetsuka, H. Ohnuma, K. Kunimori, *Catal. Lett.* **47** (1997) 17.

[40] D.A. Mantell, K. Kunimori, S.B. Ryali, G.L. Haller, J.B. Fenn, *J. Vac. Sci. Technol. A* **3** (1985) 1663.

[41] O.R. Inderwildi, D. Lebiedz, O. Deutschmann, J. Warnatz, *J. Chem. Phys.* **122** (2005) 034710.

[42] L.K. Verheij, M.B. Hugenschmidt, *Surf. Sci.* **416** (1998) 37.

[43] V.P. Zhdanov, B. Kasemo, *J. Catal.* **170** (1997) 377.

[44] Z.X. Wang, X.F. Jia, F.H. Tian, S.G. Chen, *Chinese J. Chem.* **22** (2004) 152.

[45] A.F. Carley, P.R. Davies, M.W. Roberts, *Catal. Lett.* **80** (2002) 25 (and references therein).

[46] S. Tanaka, K. Yuzaki, S. Ito, S. Kameoka, K. Kunimori, *J. Catal.* **200** (2001) 203.

[47] S. Kameoka, T. Nobukawa, S. Tanaka, S. Ito, K. Tomishige, K. Kunimori, *Phys. Chem. Chem. Phys.* **5** (2003) 3328.

[48] T. Nobukawa, M. Yoshida, S. Kameoka, S. Ito, K. Tomishige, K. Kunimori, *Catal. Today* **93** (2004) 791.

Table 3-1 Kinetic parameters for the CO + NO and CO + O_2 reactions on Pd(110)

reaction equation	rate constant /s^{-1}	ν /s^{-1}	E_a /kcal mol^{-1}	ref
(3), (21)	k_{CO}^{des}	1×10^{17}	35.5	[2,3]
(4)	k_{NO}^{des}	1×10^{17}	36.0	[5]
(5)	k_{NO}^{dis}	2.7×10^{14}	34.2	this work
(6)	$k_{N_2}^{des}$	6.5×10^{13}	29.0	[29,32]
(7), (23)	k_r	7.1×10^{15}	33.6	this work

reaction equation	initial sticking coefficient	ref
(3), (21)	$s_{CO} = 0.93$	[4]
(4)	$s_{NO} = 0.9$	[4]
(22)	$s_{O_2} = 0.86$	[34]

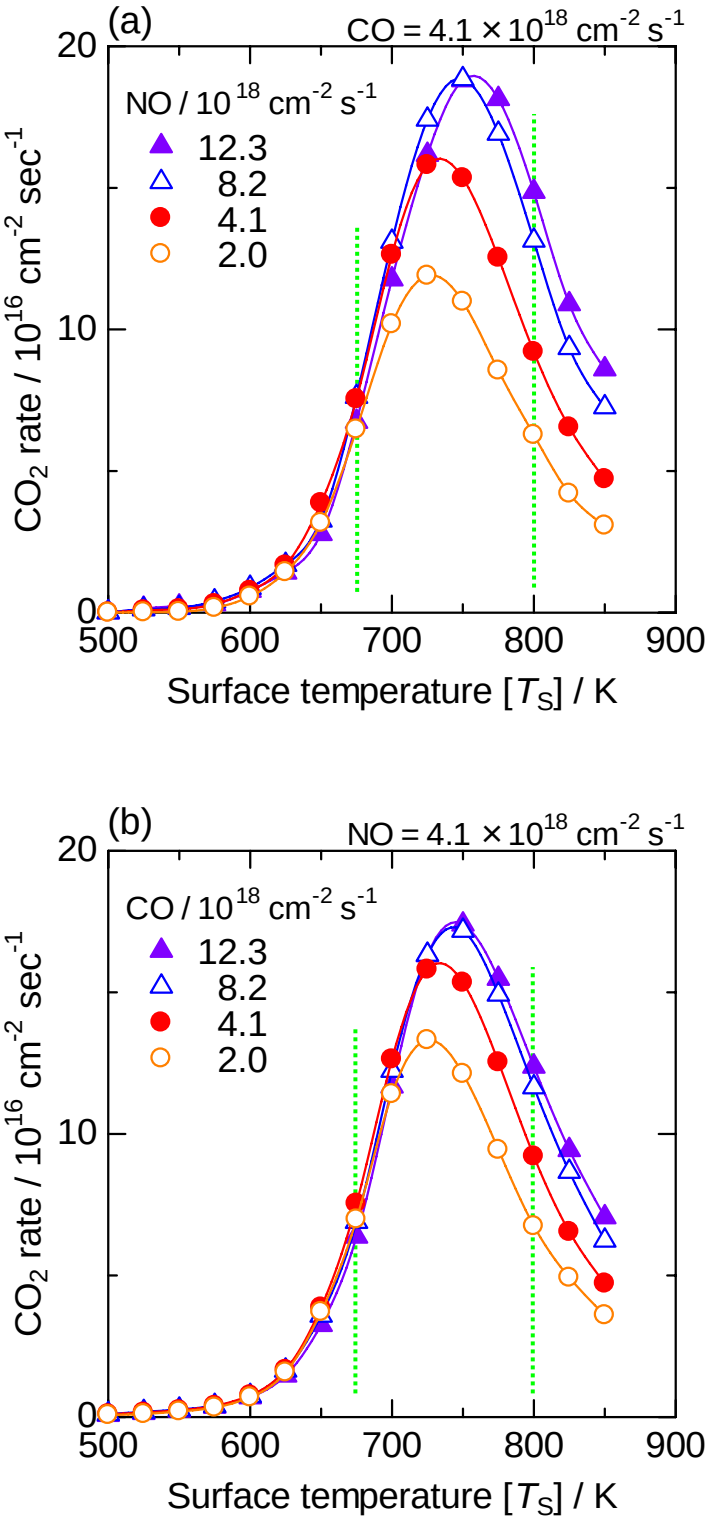

Figure 3-1 The formation rate of CO_2 during the CO + NO reaction on Pd(110) (a) CO/NO ratio = 0.25–2.0 at the fixed CO flux and (b) CO/NO ratio = 0.5–3.0 at the fixed NO flux.

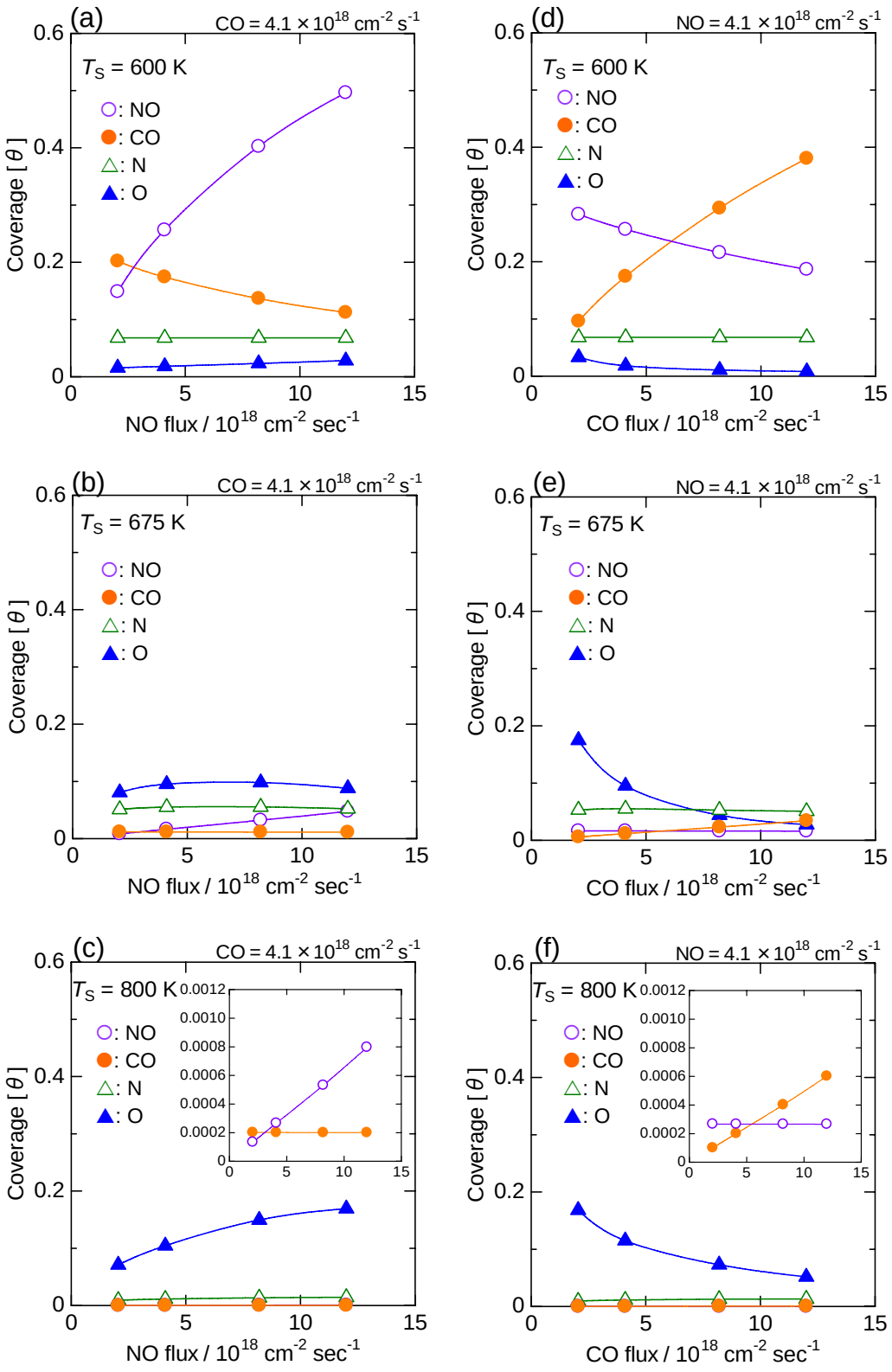

Figure 3-2 Kinetics of CO + NO reaction on Pd(110) under various CO/NO fluxes. The adsorbate coverages as a function of NO flux at (a) T_S = 600 K, (b) T_S = 675 K and (c) T_S = 800 K and as a function of CO flux at (d) T_S = 600 K, (e) T_S = 675 K and (f) T_S = 800 K.

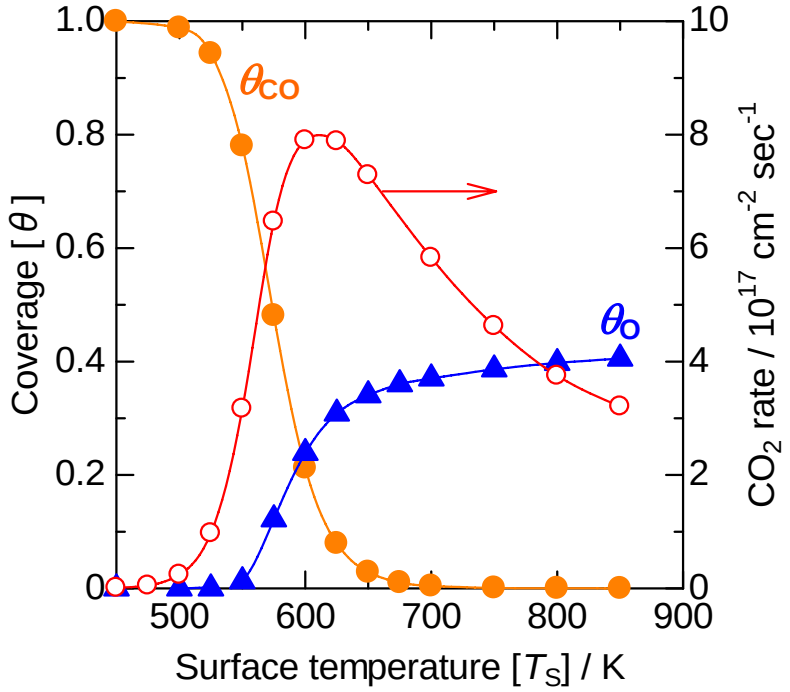

Figure 3-3 Kinetics of CO + O_2 reaction on Pd(110). The total flux of reactants was 8.2×10^{18} molecules cm^{-2} s^{-1} at the CO/O_2 ratio = 1.

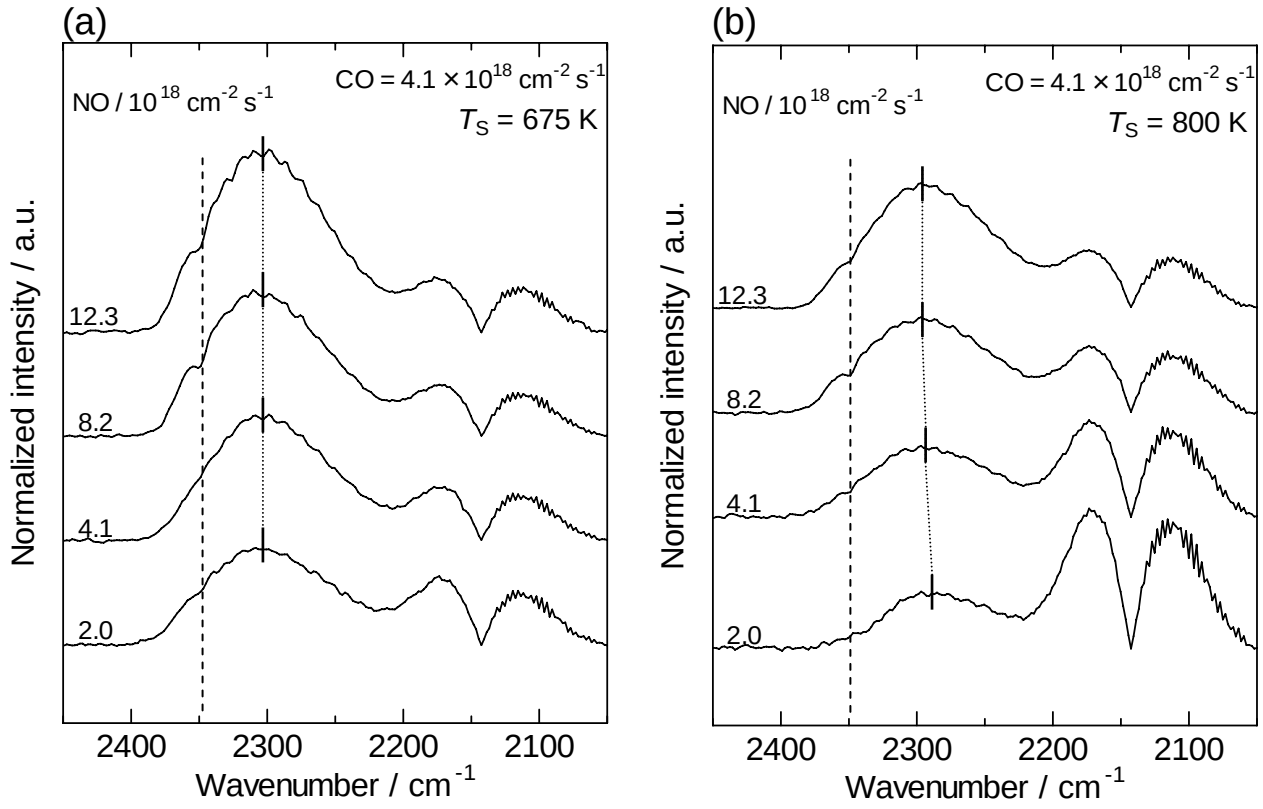

Figure 3-4 IR emission spectra of CO_2 desorbed by the CO + NO reaction on Pd(110). The surface temperature (T_S) was (a) 675 K and (b) 800 K. The NO flux was 2.0–12.3 × 10^{18} molecules cm^{-2} s^{-1} at the fixed CO flux (4.1 × 10^{18} molecules cm^{-2} s^{-1}). The emission intensity was normalized per unit of CO_2 yield.

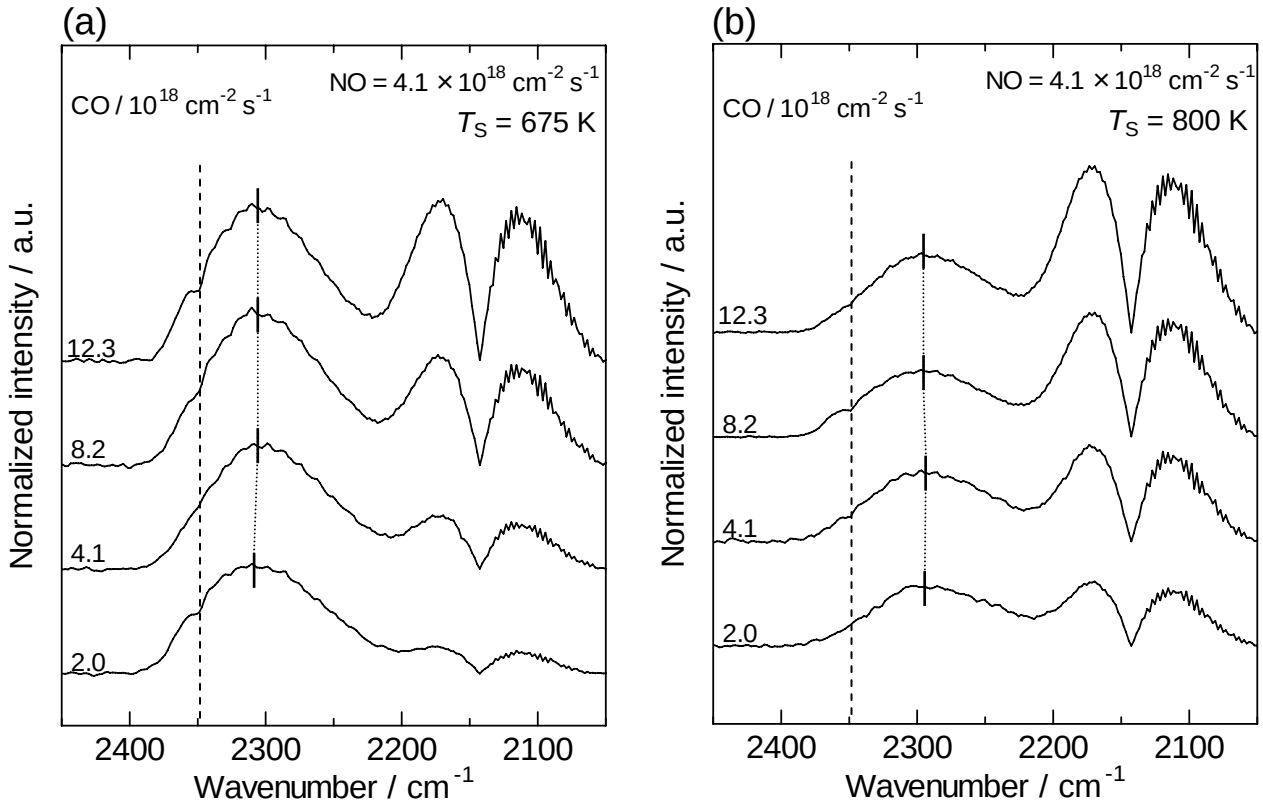

Figure 3-5 IR emission spectra of CO_2 desorbed by the CO + NO reaction on Pd(110). The surface temperature (T_S) was (a) 675 K and (b) 800 K. The CO flux was 2.0–12.3 × 10^{18} molecules cm^{-2} s^{-1} at the fixed NO flux (4.1 × 10^{18} molecules cm^{-2} s^{-1}). The emission intensity was normalized per unit of CO_2 yield.

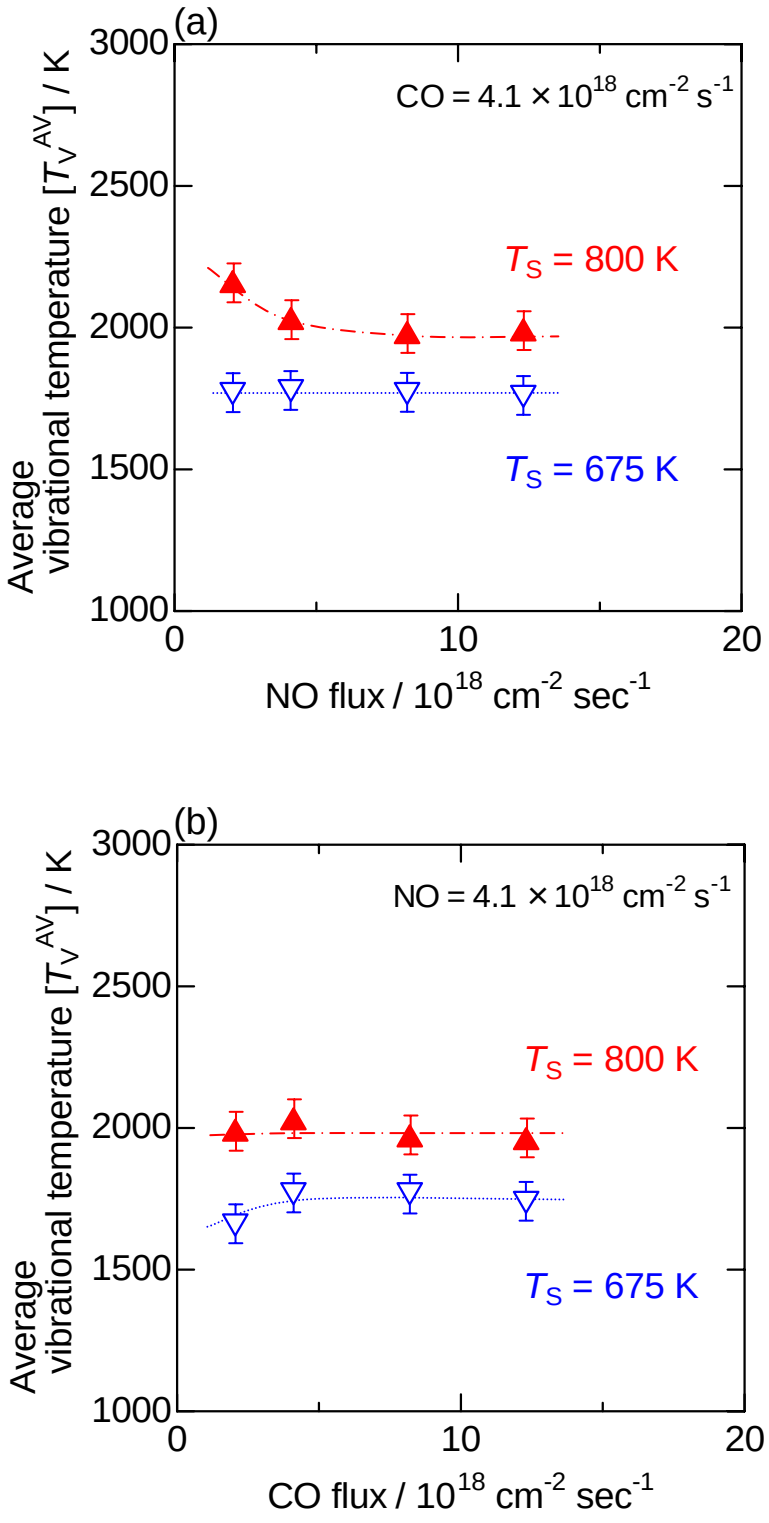

Figure 3-6 (a) NO flux and (b) CO flux dependence of average vibrational temperature (T_V^{AV}) of CO_2 formed in the CO + NO reaction on Pd(110). The surface temperature (T_S) was 675 K and 800 K. The flux conditions are as described in Figs. 3-4 and 3-5.

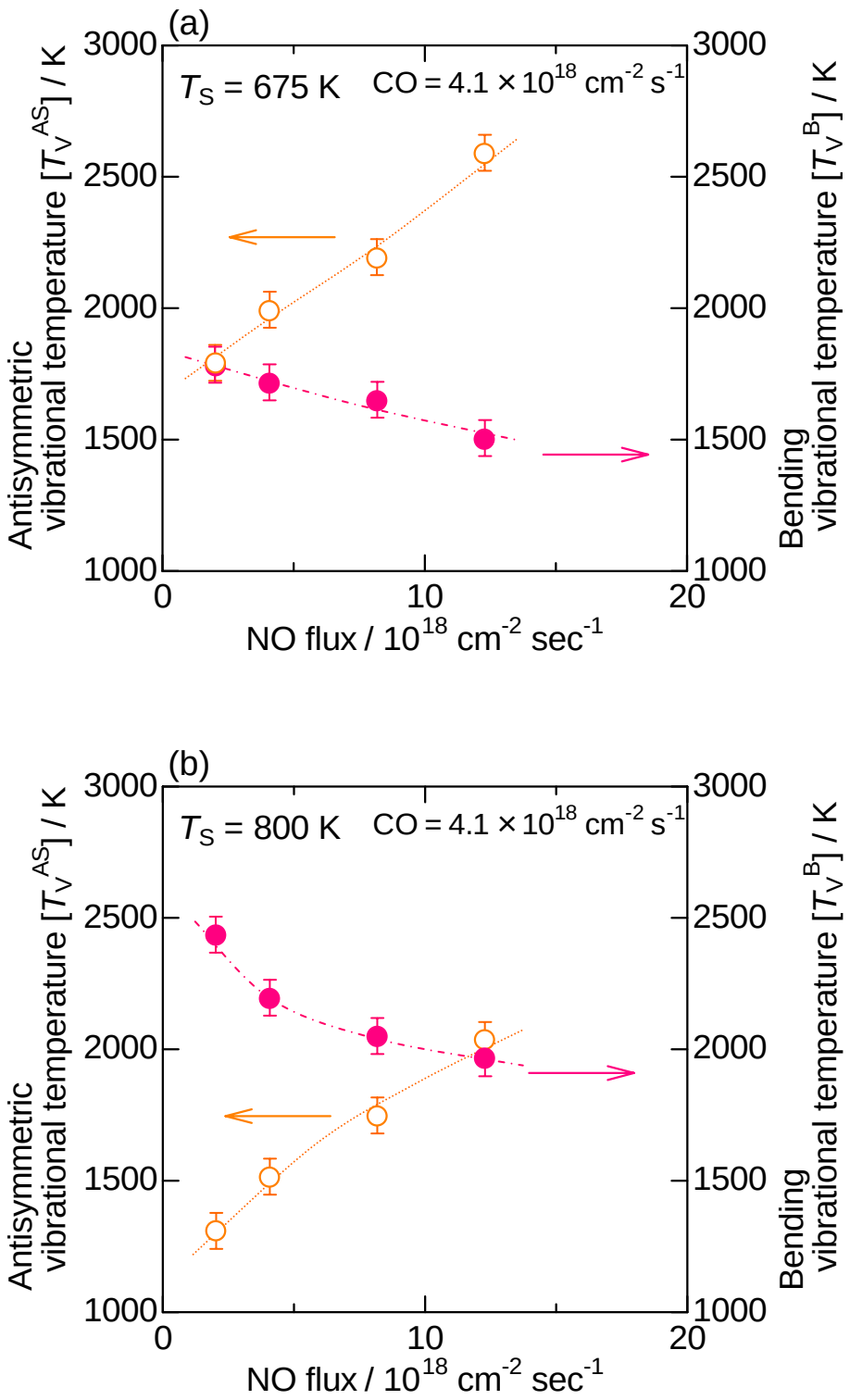

Figure 3-7 NO flux dependence of antisymmetric vibrational temperature (T_V^{AS}) and bending vibrational temperature (T_V^{B}) in CO + NO reaction on Pd(110). The surface temperature (T_S) was (a) 675 K and (b) 800 K. The flux conditions are as described in Fig. 3-4.

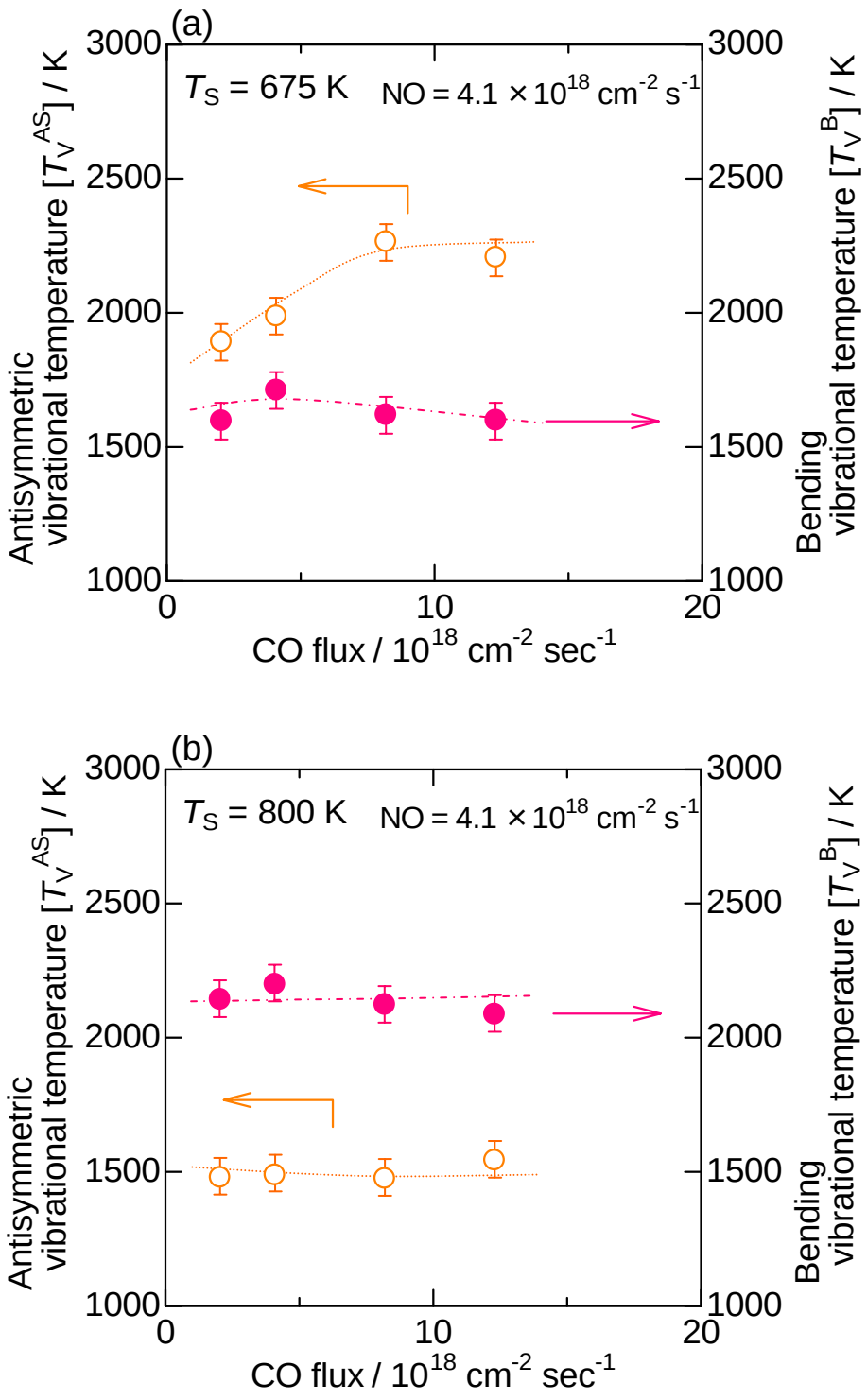

Figure 3-8 CO flux dependence of antisymmetric vibrational temperature (T_V^{AS}) and bending vibrational temperature (T_V^{B}) in CO + NO reaction on Pd(110). The surface temperature (T_S) was (a) 675 K and (b) 800 K. The flux conditions are as described in Fig. 3-5.

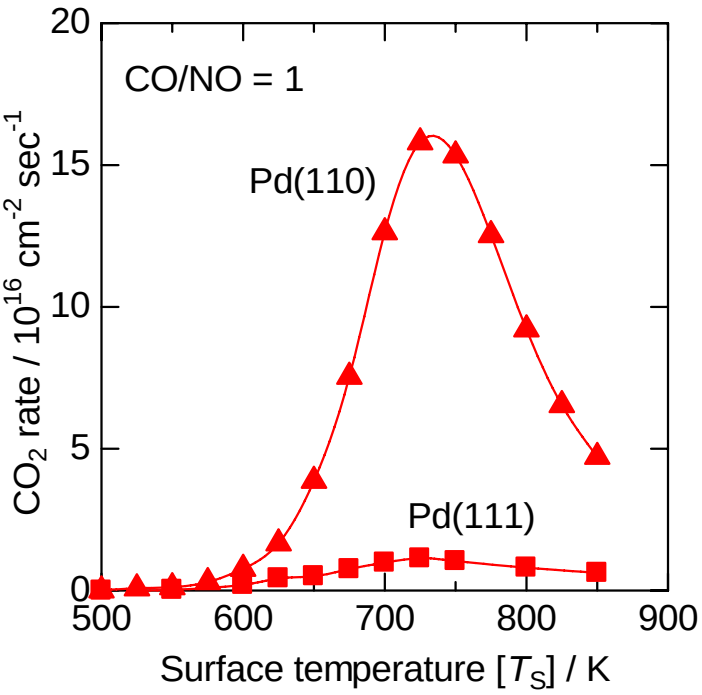

Figure 3-9 The formation rate of CO_2 during CO + NO reaction (CO/NO ratio = 1) on Pd(110) and Pd(111). The total flux of reactants (CO + NO) was 8.2×10^{18} molecules cm^{-2} s^{-1}.

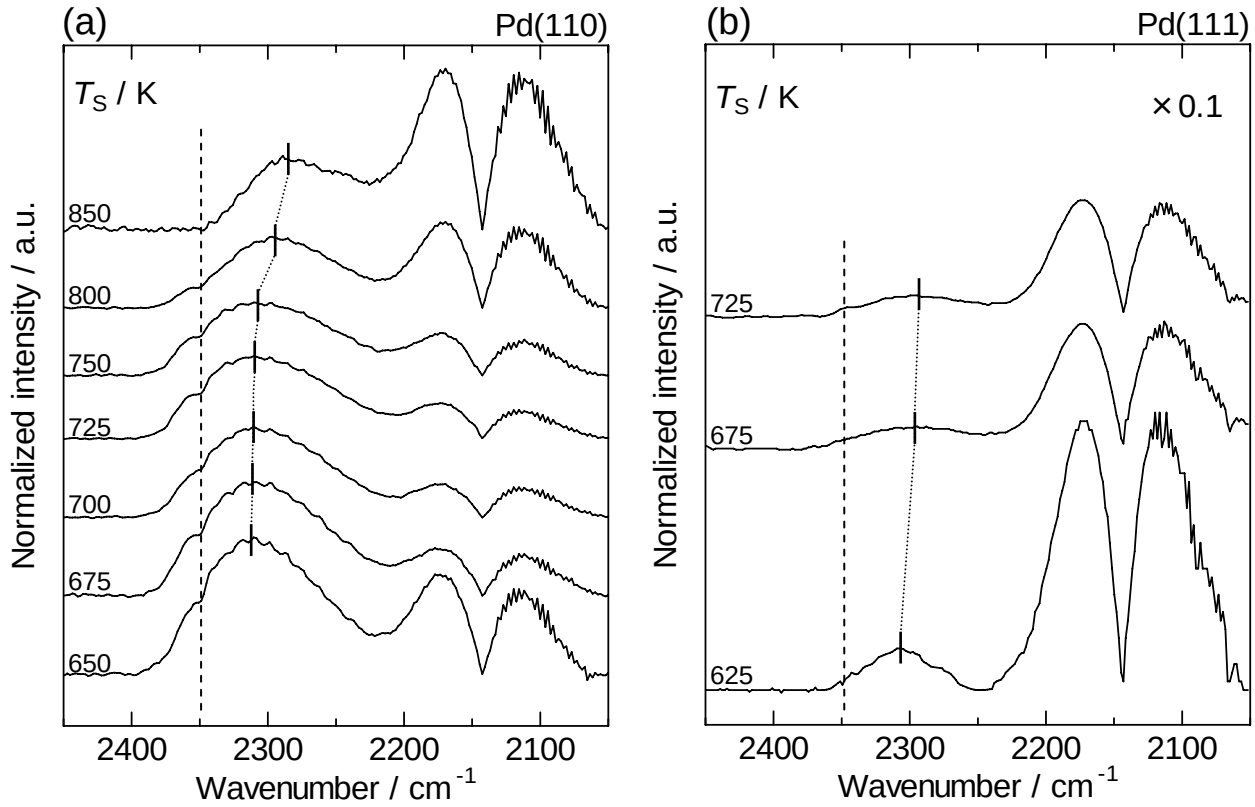

Figure 3-10 IR emission spectra of CO_2 desorbed by CO + NO reaction on (a) Pd(110) and (b) Pd(111). The surface temperature (T_S) was 625–850 K. The total flux of reactants was 8.2×10^{18} molecules cm^{-2} s^{-1} for Pd(110) and 2.1×10^{19} molecules cm^{-2} s^{-1} for Pd(111) at the CO/NO ratio = 1. The emission intensity was normalized per unit of CO_2 yield.

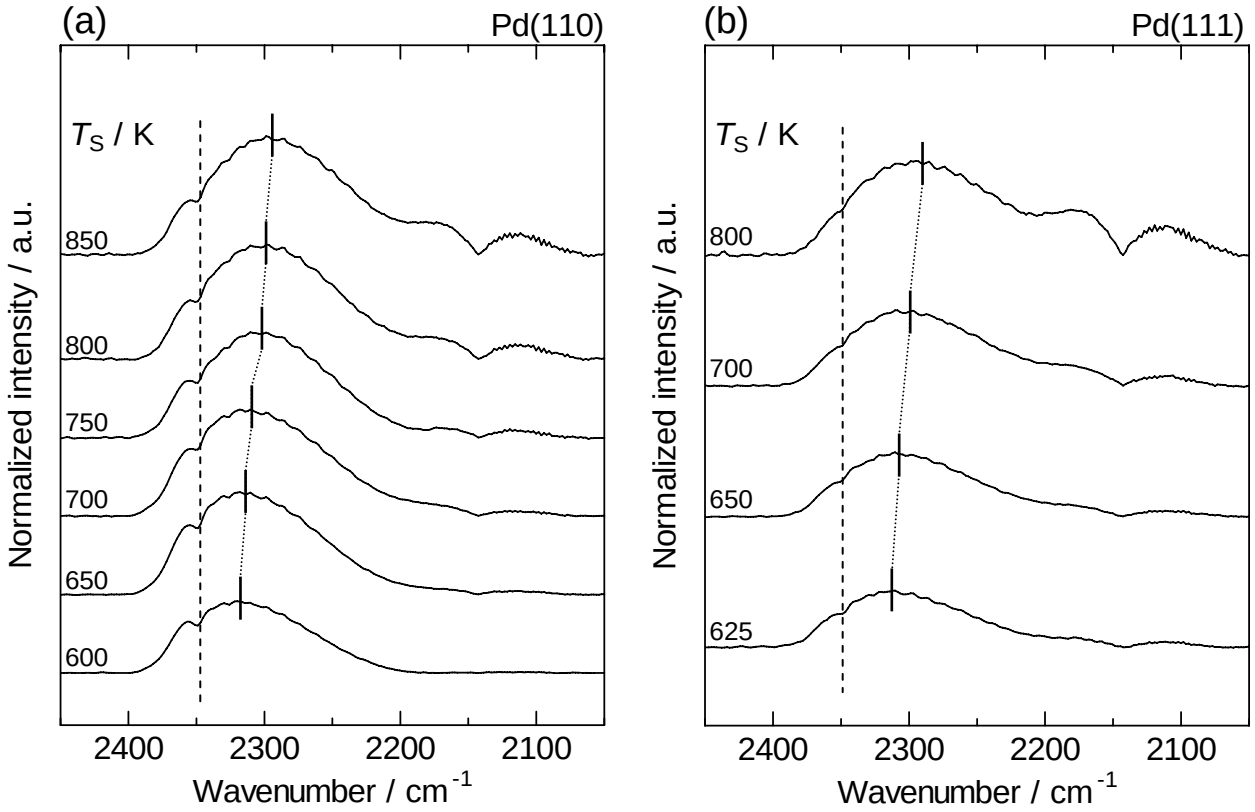

Figure 3-11 IR emission spectra of CO_2 desorbed by CO + O_2 reaction on (a) Pd(110) and (b) Pd(111). The surface temperature (T_S) was 600–850 K. The total flux of reactants was 8.2×10^{18} molecules cm^{-2} s^{-1} at the CO/O_2 ratio = 1. The emission intensity was normalized per unit of CO_2 yield.

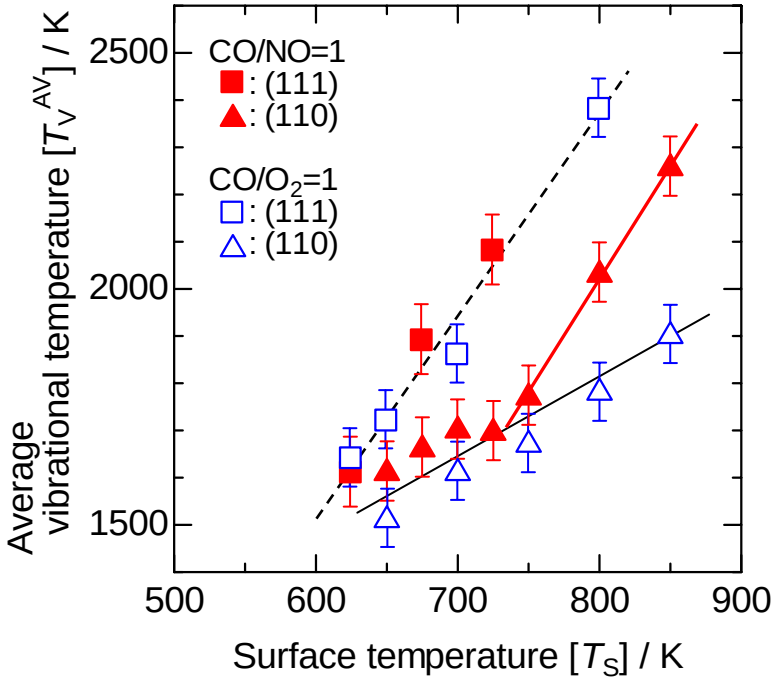

Figure 3-12 Surface temperature dependence of average vibrational temperature (T_V^{AV}) of CO_2 formed in CO + NO and CO + O_2 reactions on Pd(110) and Pd(111). The reaction conditions are as described in Figs. 3-10 and 3-11.

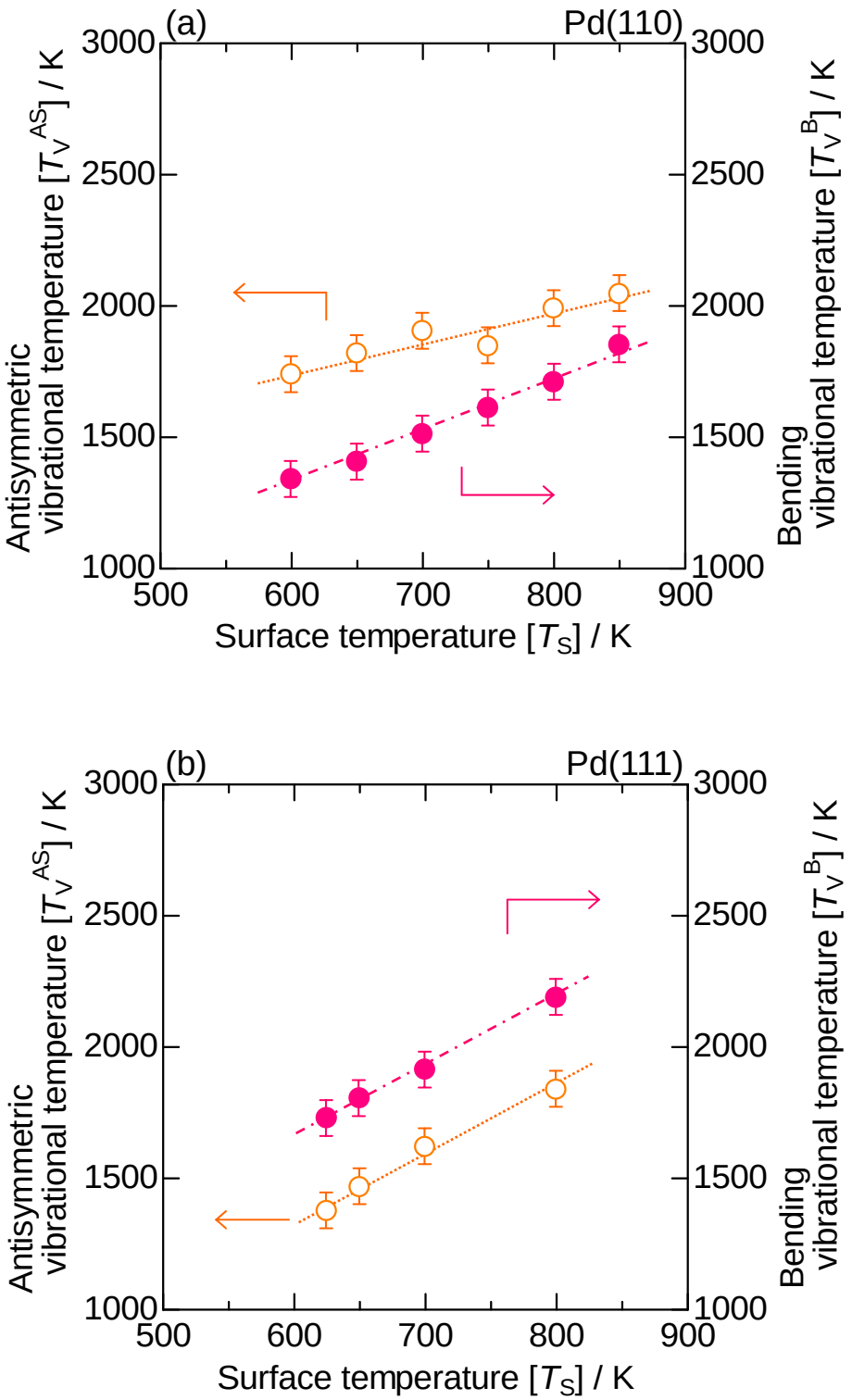

Figure 3-13 Surface temperature dependence of antisymmetric vibration al temperature (T_V^{AS}) and bending vibrational temperature (T_V^{B}) in CO + O_2 reaction on (a) Pd(110) and (b) Pd(111). The reaction conditions are as described in Fig. 3-11.

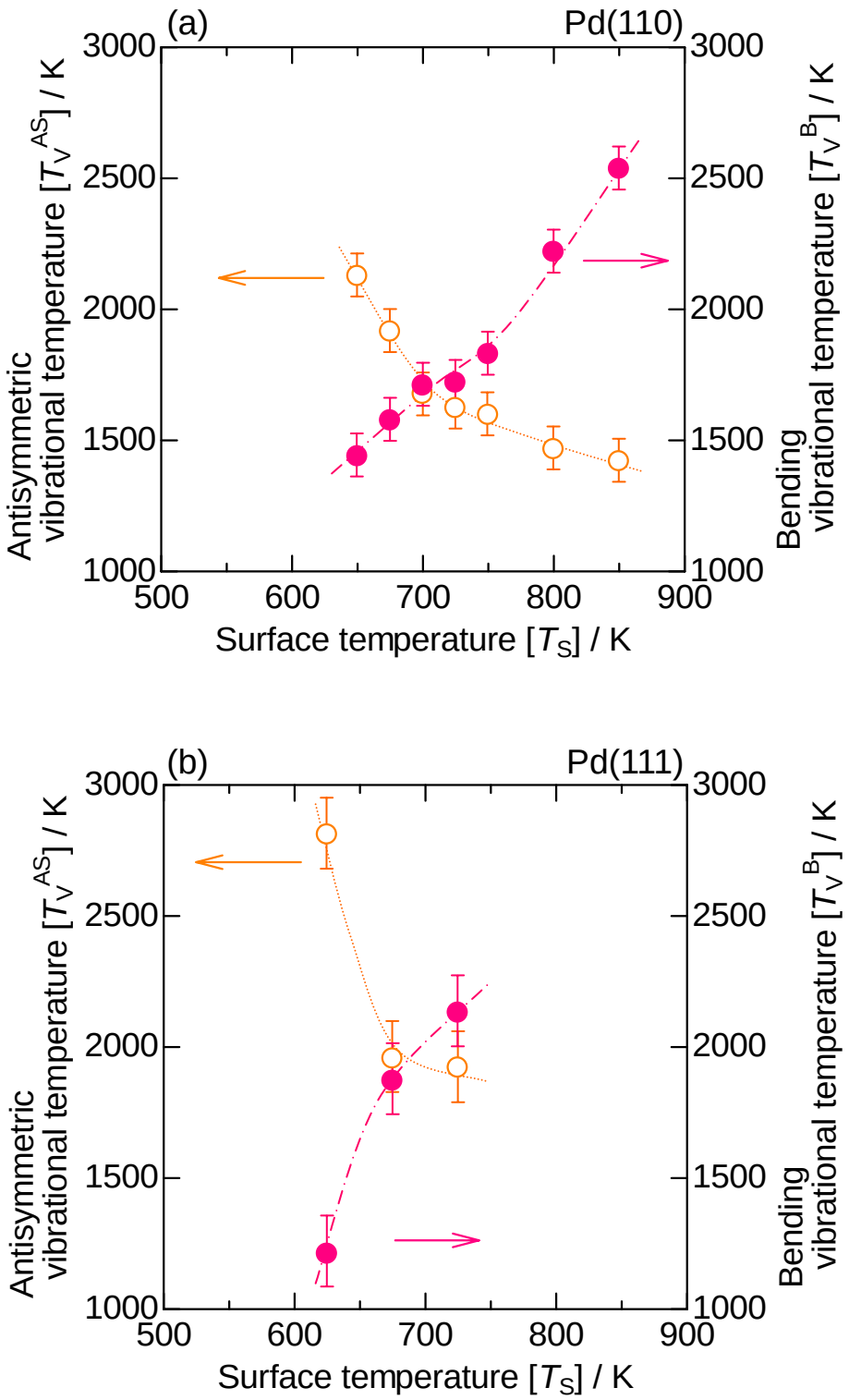

Figure 3-14 Surface temperature dependence of antisymmetric vibrational temperature (T_V^{AS}) and bending vibrational temperature (T_V^{B}) in CO + NO reaction on (a) Pd(110) and (b) Pd(111). The reaction conditions are as described in Fig. 3-10.

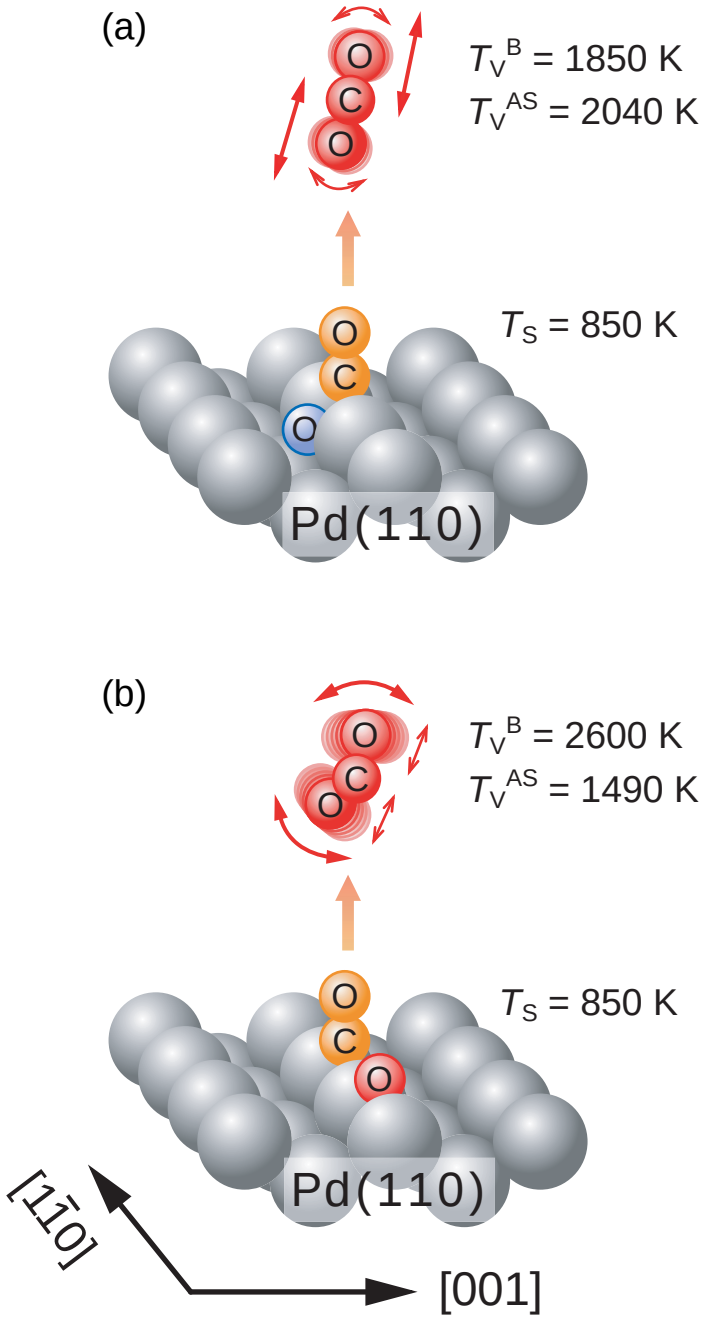

Figure 3-15 Structure of the activated complex of CO_2 formation and vibrationally excited state of desorbed CO_2 molecules during (a) CO + O_2 reaction and (b) CO + NO reaction on Pd(110) at the higher temperature region. The temperatures described in each model are based on the reaction under the total flux of reactants was 8.2×10^{18} molecules cm^{-2} s^{-1} at CO/O_2 = CO/NO = 1.

Chapter 4

Comparative study of CO_2 formation in CO oxidation by O_2, NO, and N_2O on Pd(110) surface

4.1. Introduction

In order to elucidate heterogeneous catalysis, various physicochemical methods have been attempted, and one of the conventional methods is spectroscopic observation of reaction intermediates [1–3]. Another approach is an analysis of the products desorbed from the catalyst surface in terms of translational and internal energies [4–15]. The investigation of the internal energies, i.e., vibrational and rotational states, can be useful tools [4–13]. This is because the energy states of desorbed molecules can be related to a transition state, where the surface species interacts with the surface and the activated complex is formed. When desorbed molecules are excited vibrationally, infrared chemiluminescence (IR emission) can be observed during the relaxation [4–13]. Based on the IR emission spectra, the vibrational state of the desorbed molecules can be given, and the structure of the activated complex can be discussed [7–13].

Our group has reported IR chemiluminescence of CO_2 from steady-state CO + O_2 and CO + NO reactions on single-crystal Pd surfaces combined with kinetic results [8–13]. It has been suggested that the activated complex of CO_2 formation (i.e., the transition state of CO_2 formation from CO(a) + O(a)) had a more bent structure on Pd(111) and a relatively linear structure on Pd(110), since the bending mode of CO_2 from Pd(111) was more vibrationally excited than that of CO_2 from Pd(110) [8,9,12], and this can be interpreted by the plane surface structure of Pd(111). The results also indicate that the IR chemiluminescence method can provide a direct energetic evidence of the reaction mechanism and the activated complex of CO_2 formation.

In this article, the vibrational states of CO_2 from CO + NO and CO + N_2O reactions on Pd(110) were investigated, and they are compared to those from CO + O_2 reaction. It is found that the vibrationally excited states of CO_2 from the CO + NO reaction were significantly different form those from the CO + O_2 and CO + N_2O reactions at a high surface temperature (750 K). The

detailed analysis was carried out here, and the interpretation in terms of the structure of the activated complex and the reaction mechanism is discussed.

4.2. Experimental

A molecular-beam reaction system, in combination with a FT-IR spectrometer (InSb detector Nexus670; Thermo Electron Corp.), was used to measure IR emissions of product CO_2 molecules just desorbed from metal surfaces during catalytic reactions [8–13]. A UHV chamber (base pressure $< 1.0 \times 10^{-9}$ Torr) was equipped with a CaF_2 lens, which collected IR emission, an Ar^+ ion gun for sample cleaning, and a quadrupole mass spectrometer (QMS, QME200; Pfeiffer Vacuum Technology AG) with a differential pumping system. Two free-jet molecular-beam nozzles (0.1-mm-diameter orifice) supplied the reactant gases [7]. The reactant fluxes were controlled using mass flow controllers. The CO flux was fixed at 4.1×10^{18} cm^{-2} s^{-1}, and the O_2, NO and N_2O fluxes were $0.41–12.3 \times 10^{18}$ cm^{-2} s^{-1}, $2.0–12.3 \times 10^{18}$ cm^{-2} s^{-1} and $4.1–12.3 \times 10^{18}$ cm^{-2} s^{-1}, respectively. The reactant gases (CO/O_2 = 0.3−10, CO/NO = 0.3−2, or CO/N_2O = 0.3−1) were exposed to Pd(110) surface. In the CO + N_2O reaction, the formation rate of CO_2 can't be measured by the QMS because of the overlap of mass fragments at m/e = 44 of N_2O and CO_2. Therefore, we used labeled ^{13}CO, which obtained from ISOTEC INC. Pulses of ^{13}CO gas (2.5×10^{20} molecules, 10 ml at atmospheric pressure) were introduced to ^{12}CO reactant gas under steady-state reaction conditions. The ratio of (^{13}CO + ^{12}CO)/N_2O was constant during the ^{13}CO pulse. Figure 4.1 shows an example of the mass signal profiles in the case of ^{13}CO pulse introduction to the steady-state ^{12}CO + N_2O reaction. The mass signal intensity was calibrated. When the ^{13}CO pulse was introduced at 0 sec, the signal of m/e = 29 due to ^{13}CO increased, and at the same time, the signal of m/e = 45 due to $^{13}CO_2$ increased. Assuming that the reaction rate of ^{13}CO + N_2O is the same as that of ^{12}CO + N_2O, the formation rate of CO_2 was estimated. In addition, under these reaction conditions, the signal of m/e = 32 due to O_2 was comparable to the background level, and this indicates that O_2 was not formed in the CO + N_2O reaction. Steady-state CO oxidation by O_2, NO and N_2O (pressure range at the flux conditions = $10^{-3}–10^{-2}$ Torr) was performed at temperatures of 400–850 K. Another UHV chamber (base pressure $< 2.0 \times 10^{-10}$ Torr) was used to prepare and

characterize the clean Pd(110) surface. It was equipped with a molecular-beam reaction system, an Ar^+ ion gun, low energy electron diffraction (LEED), and a QMS. Before the molecular-beam reaction, the Pd(110) surface was cleaned using a standard procedure (O_2 treatment, Ar^+ bombardment, and annealing) [8–13]. After cleaning, the sharp (1 × 1) LEED pattern was observed, and the reaction occurs on the (1 × 1) structure under steady-state condition [14].

The IR emission spectra of the CO_2 molecules desorbed from the surface were measured with 4 cm^{-1} resolution. At that low resolution (4 cm^{-1} resolution), no individual vibration-rotation lines were resolved. The IR emission spectra were analyzed based on simulation of model spectra [5,9,11]. The average vibrational Boltzmann temperature (T_V^{AV}: an average temperature of the antisymmetric stretch, symmetric stretch and bending modes), which was calculated from the degree of the red-shift from the fundamental band (2349 cm^{-1}) [5,7–13]. The emission intensity is related to the extent of excitation in the antisymmetric stretch of CO_2 [10–13]. Therefore, the antisymmetric vibrational temperature (T_V^{AS}) can be estimated from the normalized emission intensity [10–13]. Based on T_V^{AS} and T_V^{AV}, it is possible to deduce the bending vibrational temperature (T_V^{B}). The relation between T_V^{AV} and respective vibrational temperature is represented as

$$T_V^{AV} = (T_V^{AS} + T_V^{SS} + 2T_V^{B}) / 4, \qquad (1)$$

where $2T_V^{B}$ corresponds to the degeneration of the bending vibration. Assuming that T_V^{B} is equal to T_V^{SS} because of the Fermi resonance [4,6], T_V^{B} is expected to be $(4T_V^{AV} - T_V^{AS})/3$. This assumption is plausible on the basis of previous reports [4,5]. It should be added that T_V^{AV}, T_V^{AS} and T_V^{B} were used here as parameters to characterize the extent of the vibrational excitation of the product CO_2. It took about 15–90 min for the measurement of the IR emission spectra with 1000–6000 scans. The stable steady-state activity was obtained during the measurement.

4.3. Results and Discussion

Figure 4.2 shows the rate of CO_2 formation in the steady-state CO oxidation by O_2, NO and N_2O on Pd(110) as a function of surface temperature (T_S). The CO + O_2 reaction proceeded at temperatures greater than 450 K. The surface temperature dependence of the formation rate showed

a maximum on the Pd(110) surface. The behavior agrees well with the general Langmuir-Hinshelwood (LH) kinetics of CO + O_2 reaction on Pd surfaces [2,3,8,12,16]. The temperature at which the highest activity was obtained is denoted as T_S^{max}. At temperatures lower than T_S^{max}, the surface coverage of CO is known to be high. The rate-determining step is O_2 adsorption on the vacant site, which is formed by the desorption of CO(a). At temperatures higher than T_S^{max}, the formation rate of CO_2 decreased gradually with increasing surface temperature. This behavior is attributable to the decreased CO coverage. The CO + NO reaction proceeded above 550 K, and the temperature dependence of the formation rate had also a maximum. The CO + N_2O reaction also proceeded above 550 K and the temperature dependence of the formation rate also had a maximum. It is shown that the reaction rate was much dependent on the oxidizing agents, and the order is as follows: O_2 > NO > N_2O.

Figure 4.3(a) shows the rate of CO_2 formation in the steady-state CO oxidation by O_2, NO and N_2O on Pd(110) as a function of the oxidant flux under the fixed CO flux at T_S = 750 K. In the CO + O_2 reaction, the rate of CO_2 formation increased with increasing O_2 flux in the low flux range ($< 2.0 \times 10^{18}$ cm^{-2} s^{-1}), in contrast, the rate decreased with increasing O_2 flux in the high flux range ($> 2.0 \times 10^{18}$ cm^{-2} s^{-1}). This suggests that the kinetics of CO + O_2 reaction changes around O_2 flux = 2.0×10^{18} cm^{-2} s^{-1}. The rate of both CO + NO and CO + N_2O reactions increased almost proportionally with increasing the oxidant flux. In order to understand why the behavior of each reaction over Pd(110) surface is strongly dependent on the kind of oxidizing agents, we calculated the coverages of adsorbate species during the CO + O_2 and CO + NO reactions on the basis of a reaction model as shown in the reference [13].

The estimated coverages (θ_{CO} and θ_O) are plotted in Figs. 4.3(b) and (c). For the CO oxidation by O_2, the θ_O increased sharply in the low flux range, and it was almost constant in the high flux range. On the other hand, the θ_{CO} gradually decreased in all the flux range. This can explain the mountain-type dependence of CO_2 formation rate in the CO + O_2 reaction. The θ_O is low at the low O_2 flux, therefore, the rate increased with increasing the O_2 flux because of increasing θ_O. On the other hand, at the high O_2 flux, θ_O is high and approaches the saturation level ($\theta_O \sim 0.5$) [17]. Therefore, the rate decreased with increasing the O_2 flux because of decreasing θ_{CO}. The θ_O in the

CO + NO reaction was much lower than that in the CO + O_2 reaction. The θ_O increased gradually and the θ_{CO} was almost constant in all the flux range. The θ_{CO} in the CO + NO reaction was higher than that in the CO + O_2 reaction, and this is reflected by the low θ_O and the low CO_2 formation rate in the CO + NO reaction. Based on the estimated coverages in the CO + O_2 and CO + NO reactions, it is possible to estimate the rate constant (k_r) in the CO(a) and O(a) reaction by using $k_r = r_{CO_2} / \theta_{CO}$ θ_O [13]. The k_r value obtained here is $k_r = 9.5 \times 10^6$ s^{-1}.

In the CO + N_2O reaction, one of the most probable model mechanisms is as follows [18]:

$$CO(g) + V \leftrightarrow CO(a), \quad (2)$$

$$N_2O(g) + V \leftrightarrow N_2O(a), \quad (3)$$

$$N_2O(a) \rightarrow N_2(g) + O(a), \quad (4)$$

$$CO(a) + O(a) \rightarrow CO_2(g) + 2V. \quad (5)$$

In this model, it is assumed that the rate-determining step is $N_2O(a)$ dissociation (Eq.(4)), and this is based on the low sticking probability at high temperatures in the previous report [19]. Furthermore, the elementary steps (2) and (3) are considered to be more rapid than the reaction rate, and the adsorption of CO and N_2O reaches equilibrium. In order to estimate the coverages of CO and oxygen, kinetic parameters with respect to $N_2O(a)$ dissociation are necessary. However, these kinetic parameters have not been reported, and they are not available at present. Therefore, we estimated the coverages in a manner different from the case of CO + O_2 and CO + NO reactions. Since the θ_{CO} in the CO + N_2O reaction is expected to be very small based on the low CO_2 formation rate, it is supposed that the θ_{CO} in the CO + N_2O reaction is equal to that in the CO + NO reaction. In this case, the θ_O can be estimated from the equation, $r_{CO_2} = k_r \theta_{CO} \theta_O$. Here, r_{CO_2} is the CO_2 formation rate in the CO + N_2O reaction, which was obtained from the experimental results shown in Fig. 4.3(a). The k_r value for the CO(a) + O(a) reaction can also be used in the step(5). The result showed that the θ_O was much lower than those of the CO + O_2 and CO + NO reactions, and it increased gradually as shown in Fig. 3(c).

Figure 4.4 shows IR emission spectra of CO_2 molecules produced by the CO + O_2, CO + NO and CO + N_2O reactions on Pd(110) surface at T_S = 750 K for various fluxes of each oxidant at the fixed CO flux. The CO_2 emission spectra were observed in the region of 2400–2200 cm^{-1}, while

the emission spectra centered at 2143 cm^{-1} are due to the IR emission of the non-reacted CO molecules, which are scattered from the surface. In addition, the peaks centered at 2223 cm^{-1} in the CO + N_2O reaction are IR emission from the non-reacted N_2O molecules. The CO_2 emission spectra are considerably red-shifted from 2349 cm^{-1} (the fundamental band of antisymmetric stretch). The degree of the red-shift from the fundamental band, which reflects the average vibrational state of the excited CO_2 molecules, is not dependent on the oxidant fluxes, but depends on the kind of reactions. The degree of the red-shift was CO + NO > CO + O_2 > CO + N_2O. The emission intensity is almost constant under various oxidant fluxes in the CO + NO and CO + N_2O reactions, in contrast, it becomes large in the lower O_2 flux in the CO + O_2 reaction.

Figure 4.5 shows the average vibrational temperature (T_V^{AV}) derived from IR emission spectra of CO_2 as a function of the oxidant flux. The T_V^{AV} values are much greater than T_S (750 K), which indicates that the product CO_2 is vibrationally excited. It is almost constant under various oxidant fluxes in each reaction, however, the value decreased in the order corresponding to NO, O_2 and N_2O, although the difference is not so large. Figure 4.6 shows the antisymmetric vibrational temperature (T_V^{AS}) and the bending vibrational temperature (T_V^{B}) obtained from the IR emission intensity of CO_2 as a function of the oxidant flux in the three reactions. In the CO + O_2 and CO + N_2O reactions, T_V^{AS} was always higher than T_V^{B} under all the O_2 and N_2O fluxes. Especially, in the case of the CO + O_2 reaction, T_V^{AS} decreased and T_V^{B} increased gradually with increasing the O_2 flux. The difference between T_V^{AS} and T_V^{B} was much larger at the lower O_2 flux. Judging from the coverage estimation, the coverage of CO is so small that the effect of the CO coverage change can be neglected in CO + O_2 reaction. On the other hand, the dependence of θ_O on the O_2 flux is very large, as shown in Fig. 4.3(c). Therefore, it is suggested that the vibrational temperatures can be influenced by the oxygen coverage. As shown in Figs. 4.6(a) and (c), the vibrational temperatures (T_V^{AS} and T_V^{B}) in CO + N_2O are similar to those in CO + O_2 reaction under the low O_2 flux. This suggests that the structure of the activated complex in CO + N_2O reaction is similar to that in CO + O_2 reaction under the low O_2 flux.

On the other hand, in the case of the CO + NO reaction, T_V^{B} was always higher than T_V^{AS} under all the NO fluxes (Fig. 4.6(b)), which represents that the bending vibration is highly excited

and the structure of the activated complex of CO_2 formation is more bent. The oxygen coverage in the CO + NO reaction is between those in the CO + O_2 and CO + N_2O reaction. Therefore, the different structure of the activated complex in the CO + NO reaction can not be explained by the influence of the oxygen coverage. The structure of the activated complex can be strongly influenced by the adsorption sites of CO(a) and O(a). The adsorption site of CO(a) on Pd(110) at higher temperature is thought to be a bridge site of the row on the first layer [15]. On the other hand, the most stable adsorption site for atomic oxygen is a three-fold hollow site [20,21]. Judging from the high T_V^B value of the CO + NO reaction, the activated complex should have more bent structure. One possible interpretation is that the activated complex formed from the reaction of the CO(a) with O(a) located on the first layer. On the basis of the report on the adsorption energy of O(a) on the various sites over Pd(110) [21], bridged oxygen atom on the first layer has 1.1 eV higher energy than that on the three-fold hollow site. This means that the energy state of CO(a) and O(a) in the CO + NO reaction is higher than that in the CO + O_2 and CO + N_2O reactions, which can be related to the result in Fig. 4.5: T_V^{AV} of the CO + NO reaction was higher than those of the CO + O_2 and CO + N_2O reactions.

The turnover frequency (TOF) of the CO + O_2 reaction on Pd(110) and Pd(111) at 750 K under the flux of CO = O_2 = 4.1×10^{18} cm^{-2} s^{-1} was measured to be 490 and 160 s^{-1}, respectively [11]. On the other hand, the TOF of the CO + NO reaction on Pd(110) and Pd(111) at 750 K under the flux of CO = NO = 4.1×10^{18} cm^{-2} s^{-1} was determined to be 160 and 7 s^{-1}, respectively [11]. This indicates that the structure-sensitivity of the CO + NO reaction, the ratio of TOF on Pd(110) to that on Pd(111), is much higher than that of the CO + O_2 reaction. The difference can be caused by the formation mechanism of the adsorbed oxygen. The high structure-sensitivity of the CO + NO reaction suggests that the NO dissociation can proceed only on the top layer of Pd(110) surface, and not on a (111)-like part in the trough on Pd(110) surface. On the other hand, the O_2 dissociation can proceed both on the top layer and on the (111)-like part in the trough, judging from the low structure-sensitivity of the CO + O_2 reaction. The oxygen atom reacting with the adsorbed CO on the top layer may lead to more bent structure of the activated CO_2 complex in the CO + NO reaction. Furthermore, although we have not measured the CO + N_2O reaction activity on Pd(111), according

to the study of the CO + NO and CO + N_2O reactions on supported Pd catalysts with different metal particle sizes [22], the difference in the TOF of the CO + NO reaction was much higher than that of the CO + N_2O reaction. This suggests that the structure-sensitivity of the CO + NO reaction is much higher than that of CO + N_2O reaction, and the dissociation of N_2O can proceed both on the first layer and on the (111)-like part in the trough on Pd(110), which shows the tendency similar to the O_2 dissociation. The specific NO dissociation can be related to the bent activated CO_2 complex.

4.4. Conclusions

(1) Steady-state formation rate of CO_2 in the CO + O_2, CO + NO and CO + N_2O reactions on Pd(110) was investigated by using a molecular-beam reaction system, and the order of the activity was as follows: CO + O_2 > CO + NO > CO + N_2O.

(2) Dependence of the oxidant fluxes on CO_2 formation rate in the three reactions was measured at 750 K. Based on the results, we estimated the coverage of surface species, especially CO and O, using reaction models. Coverage of CO was estimated to be very small (< 10^{-3}) in all the reactions, however, coverage of oxygen was calculated to be strongly dependent on the reactions. The order of oxygen coverage was as follows: CO + O_2 > CO + NO > CO + N_2O.

(3) From the analysis of IR emission spectra of CO_2 from the three reactions, it is found that the antisymmetric vibrational mode of CO_2 was more excited in the case of the CO + O_2 and CO + N_2O reactions, in contrast, the bending vibrational mode was more excited in the case of the CO + NO reaction. These results suggest that the activated complex of CO_2 in the CO + NO reaction has more bent structure than those in the CO + O_2 and CO + N_2O reactions.

(4) Based on the previous reports, the structure-sensitivity of the CO + NO reaction was much higher than those of the CO + O_2 and CO + N_2O reactions. This suggests that NO dissociation can proceed only on the first layer of Pd(110), in contrast, the dissociation of O_2 and N_2O can proceed both on the first layer and on the (111)-like part in the trough on Pd(110). This adsorbed oxygen on the top layer from the NO dissociation make the activated CO_2 complex more bent.

References

[1] E. Ozensoy, D.W. Goodman, *Phys. Chem. Chem. Phys.* **6** (2004) 3765.

[2] M. Bowker, R.A. Bennett, I.Z. Jones, *Top. Catal.* **28** (2004) 25.

[3] J. Libuda, H.-J. Freund, *Surf. Sci. Rep.* **57** (2005) 157.

[4] D.J. Bald, S.L. Bernasek, *J. Chem. Phys.* **109** (1998) 746.

[5] D.A. Mantell, K. Kunimori, S.B. Ryali, G.L. Haller, J.B. Fenn, *Surf. Sci.* **172** (1986) 281.

[6] S.W. Coulston, G.L. Haller, *J. Chem. Phys.* **95** (1991) 6932.

[7] K. Kunimori, T. Iwade, H. Uetsuka, *J. Electron Spectrosc. Relat. Phenom.* **64/65** (1993) 451.

[8] H. Uetsuka, K. Watanabe, H. Kimpara, K, Kunimori, *Langmuir* **15** (1999) 5795.

[9] K. Nakao, H. Hayashi, H. Uetsuka, S. Ito, H. Onishi, K. Tomishige, K. Kunimori, *Catal. Lett.* **85** (2003) 213.

[10] K. Nakao, S. Ito, K. Tomishige, K. Kunimori, *Chem. Phys. Lett.* **410** (2005) 86.

[11] K. Nakao, S. Ito, K. Tomishige, K. Kunimori, *Catal. Lett.* **103** (2005) 179.

[12] K. Nakao, S. Ito, K. Tomishige, K. Kunimori, *J. Phys. Chem. B* **109** (2005) 17553.

[13] K. Nakao, S. Ito, K. Tomishige, K. Kunimori, *J. Phys. Chem. B* **109** (2005) 17579.

[14] T. Matsushima, *Surf. Sci. Rep.* **52** (2003) 1.

[15] Y. Ma, I. Kobal, T. Matsushima, *J. Phys. Chem. B* **109** (2005) 689.

[16] T. Engel, G. Ertl, *Adv. Catal.* **28** (1979) 1.

[17] J. Goschnick, M. Wolf, M. Grunze, W.N. Unertl, J.H. Block, J. Loboda-Cackovic, *Surf. Sci.* **178** (1986) 831.

[18] V.P. Zhdanov, Y. Ma, T. Matsushima, *Surf. Sci.* **583** (2004) 36.

[19] S. Haq, A. Hodgson, *Surf. Sci.* **463** (2000) 1.

[20] H. Conrad, G. Ertl, J. Küppers, E.E. Latta, *Surf. Sci.* **65** (1977) 245.

[21] Z.X. Wang, X.F. Jia, F.H. Tian, S.G. Chen, *Chinese J. Chem.* **22** (2004) 152.

[22] J.H. Holles, M.A. Switzer, R.J. Davis, *J. Catal.* **190** (2000) 247.

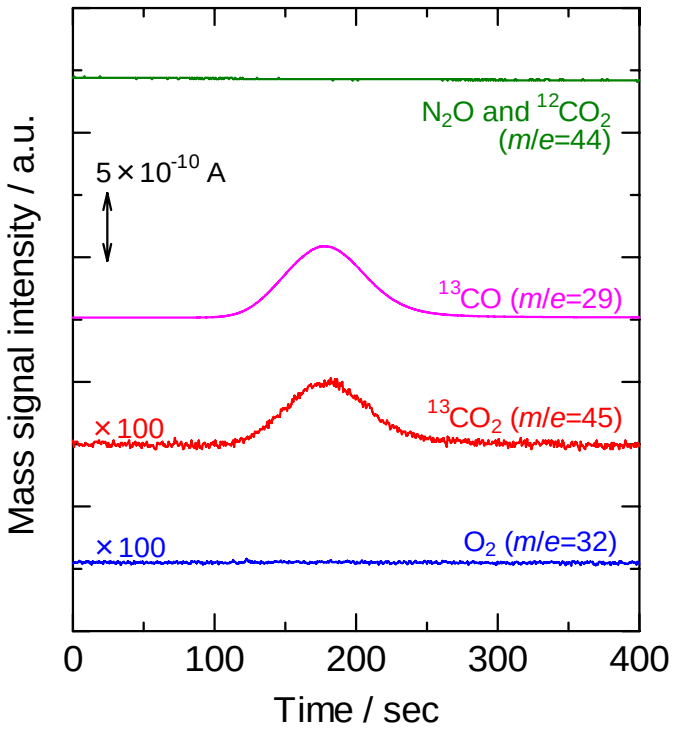

Figure 4-1 Mass signal intensity as a function of time during steady-state CO + N_2O reaction with ^{13}CO pulse. The surface temperature (T_S) was 750 K. The total flux of reactants (CO + N_2O) was 12.3×10^{18} cm^{-2} s^{-1} at the CO/N_2O = 0.5.

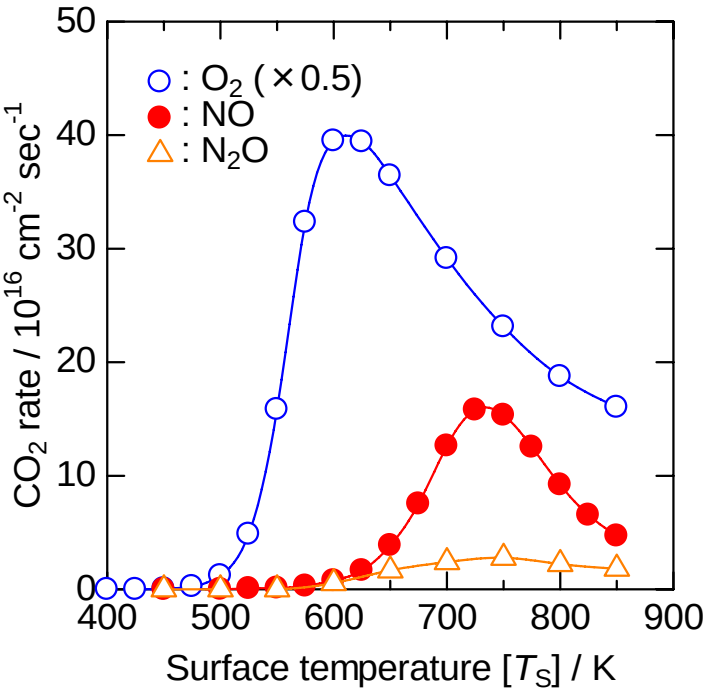

Figure 4-2 The formation rate of CO_2 during CO oxidation by O_2, NO and N_2O on Pd(110). The total flux of reactants of (CO + O_2) and (CO + NO) was 8.2×10^{18} cm^{-2} s^{-1} at the CO/O_2 and CO/NO = 1, and that of (CO + N_2O) was 12.3×10^{18} cm^{-2} s^{-1} at the CO/N_2O = 0.5.

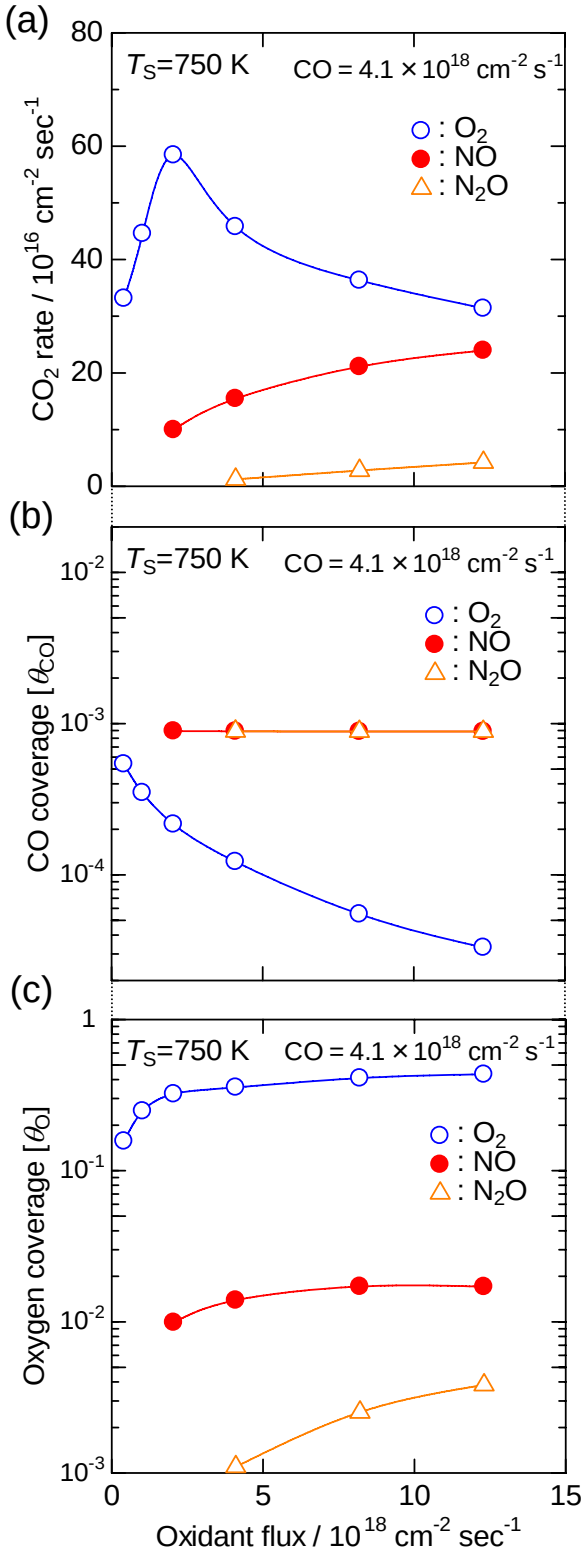

Figure 4-3 (a) The formation rate of CO_2 during CO oxidation by O_2, NO and N_2O on Pd(110) as a function of the oxidant flux under the fixed CO flux at T_S = 750 K. (b), (c) Oxidant flux dependence of (b) CO and (c) oxygen coverages.

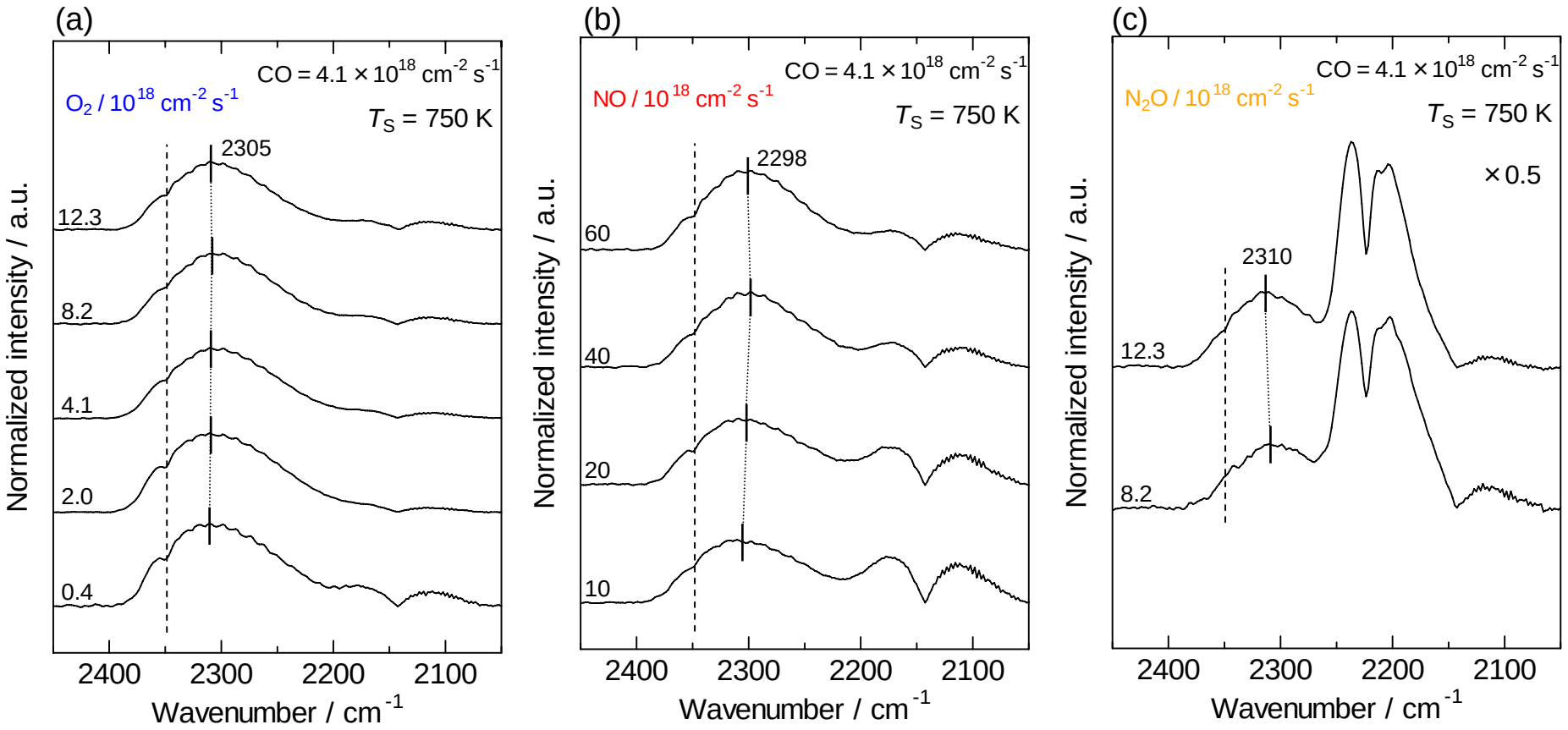

Figure 4-4 IR emission spectra of CO_2 desorbed by (a) CO + O_2, (b) CO + NO and (c) CO + N_2O reactions on Pd(110). The surface temperature (T_S) was 750 K. The oxidants flux was changed at the fixed CO flux. The emission intensity was normalized per unit of CO_2 yield.

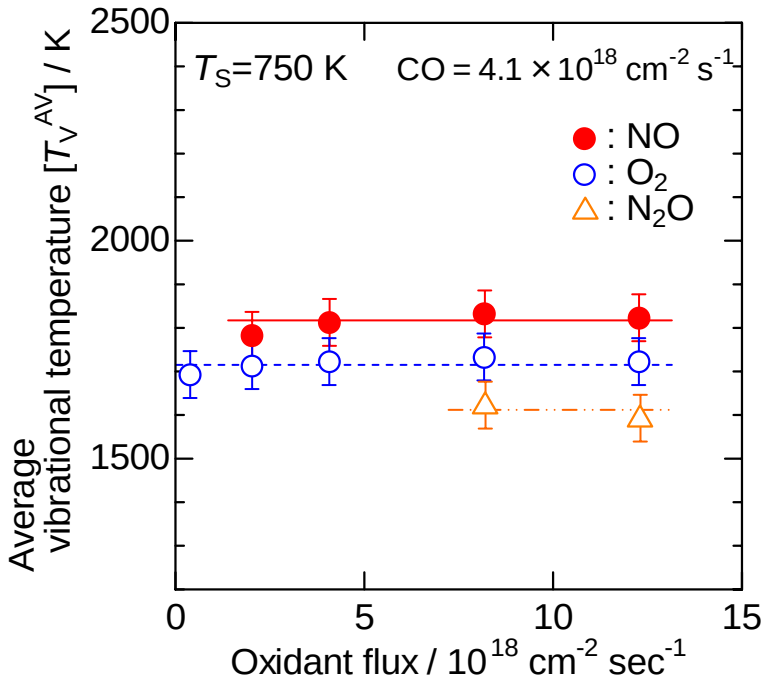

Figure 4-5 Oxidant flux dependence of the average vibrational temperature (T_V^{AV}) of CO_2 formed in CO oxidation by O_2, NO and N_2O on Pd(110). The surface temperature (T_S) was 750 K.

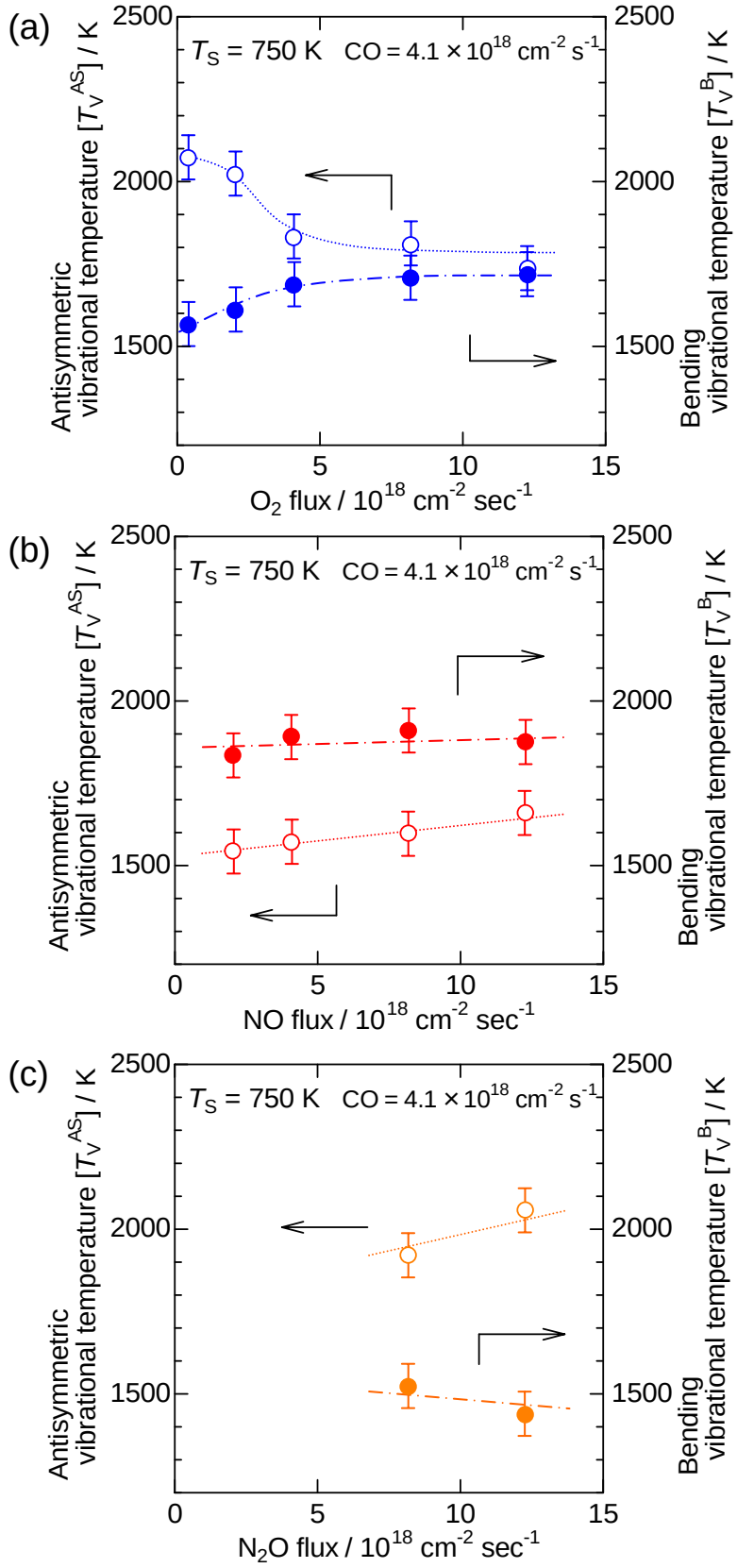

Figure 4-6 Oxidant flux dependence of the antisymmetric vibrational temperature (T_V^{AS}) and the bending vibrational temperature (T_V^{B}) in CO oxidation by (a) O_2, (b) NO and (c) N_2O on Pd(110). The surface temperature (T_S) was 750 K.

Chapter 5

Vibrational energy distribution of CO_2 formed during steady-state CO + O_2 reaction on Pt(110) and Pt(111) surfaces

5.1. Introduction

Elucidation of reaction mechanism is important for catalyst design and control of reaction routes. Single-crystal surfaces can be used to elucidate reaction mechanisms over heterogeneous catalysts [1–11]. An effective method is spectroscopic observation of reaction intermediates, which are surface species in a metastable state, to obtain information about the reaction mechanism [9–11]. Another method is investigation of internal (vibrational and rotational) energy and translational energy of desorbed molecules, which are the products of catalytic reaction, from the catalyst surface [12–29]. The energy states of desorbed molecules can reflect the catalytic reaction dynamics, which can correspond to a transition state (i.e., structure of activated complex) [12–29]. Numerous investigations of CO oxidation on Pt and Pd surfaces have revealed the elemental steps of surface-catalyzed reactions [1–29]. Furthermore, CO oxidation is a prototype reaction for the study of dynamics; measurements of internal energy states of the produced CO_2 molecules have been performed using infrared chemiluminescence (IR emission) method under steady-state catalytic reactions using molecular-beam technique [13–25]. Analyses of vibrational states can yield information about the structure of the activated CO_2 complex (i.e., the dynamics of CO oxidation) from which the gas phase molecules desorbed. Furthermore, the vibrational energy states of product CO_2 depend on its surface structure [17–25]. Consequently, information about the active sites is obtainable from the IR emission spectra of CO_2 under a steady-state catalytic reaction.

Brown and Bernasek [12] and Mantell et al. [13,14] studied the IR chemiluminescence during CO oxidation on polycrystalline Pt surfaces, and reported that the product CO_2 molecules were vibrationally excited substantially beyond thermal equilibrium with the surface. Coulston and Haller [15] studied the dynamics of CO oxidation on polycrystalline Pd, Pt, and Rh surfaces by measuring high-resolution IR emission spectra, and reported that the apparent vibrational

temperatures are in the same order as the peak reaction rates, i.e., Pd > Pt > Rh. Our group has reported IR chemiluminescence of CO_2 from the steady-state CO + O_2 reaction on single-crystal Pt and Pd surfaces combined with kinetic results [17–19,21,23,25]. The activated complex of CO_2 formation (the transition state of CO_2 formation from CO(a) + O(a)) has a more bent structure on Pd(111) and a less bent structure on Pd(110) at higher surface temperatures (T_S > 600 K), because the bending vibration was more excited for CO_2 from Pd(111) and the antisymmetric vibration was more excited for CO_2 from Pd(110) [19,23,25]. In contrast, at lower temperatures (T_S = 550–600 K) and in a high CO coverage region, the antisymmetric vibration is very highly excited on both Pd surfaces, which can be related to the activated complex of CO_2 formation in a more linear form [21,23,25]. For single-crystal Pt surfaces, Watanabe et al. [17,18] reported that the vibrational states of the product CO_2 molecules were more excited on Pt(110) than on Pt(111). At that time, however, only information on an average vibrational temperature (T_V^{AV}) was obtained [18].

A clean Pt(110) surface is reconstructed into a (1 × 2) missing-row structure above 275 K, and the reconstruction is lifted to the (1 × 1) form by CO(a). It starts at about θ_{CO} = 0.2 and is completed at θ_{CO} = 0.5 [1]. These two structures yield differently oriented oxygen adsorption sites [30,31], and the product CO_2 desorbs into different directions from the results of angle-resolved (AR) measurements [26,27]. The (1 × 2) reconstructed surface consists of three-atom-wide (111) terraces declining about 30° into the [001] direction. Desorbing product CO_2 from this surface showed well-split two-directional desorptions collimated ±25° off the surface normal into the [001] direction [26,27]. On the other hand, CO_2 from the (1 × 1) structure is desorbed along the surface normal [26,27].

In this work, we have studied the dynamics of CO_2 formation during the CO oxidation over single-crystal Pt(110) and Pt(111) surfaces. Recently, we modified the apparatus, and this has enabled the observation under severer conditions (i.e., with lower CO_2 formation rates at lower surface temperatures) [21,23,25]. Furthermore, more detailed analysis of IR emission spectra has been possible using the IR intensity [21–25]. It is the first presentation that the detailed analyses of vibrational energy states of the produced CO_2 molecules give information about the dynamics of CO_2 formation, which are changed by lifting the surface structure of Pt(110).

5.2. Experimental

A molecular-beam reaction system, in combination with a FT-IR spectrometer (InSb detector Nexus670; Thermo Electron Corp.), was used to measure IR emissions of product CO_2 molecules that desorbed on metal surface during catalytic reactions [19–25]. A UHV chamber (base pressure < 1.0×10^{-9} Torr) was equipped with a CaF_2 lens, which collected IR emission; an Ar^+ ion gun for sample cleaning; and a quadrupole mass spectrometer (QMS, QME200; Pfeiffer Vacuum Technology AG) with a differential pumping system. Two free-jet molecular-beam nozzles (0.1-mm diameter orifice) supplied the reactant gases. The reactant fluxes were controlled by mass flow controllers. The CO and O_2 gases (the total flux of 8.2×10^{18} cm^{-2} s^{-1}; $CO/O_2 = 0.33 - 3.0$) were exposed to single-crystal Pt surfaces (Pt(110) and Pt(111)). Steady-state CO + O_2 reactions were performed at temperatures of 500–900 K. Another UHV chamber (base pressure < 2.0×10^{-10} Torr) was used to prepare the samples and to characterize Pt(110) and Pt(111) surfaces. It was equipped with an identical molecular-beam reaction system, an Ar^+ ion gun, low energy electron diffraction (LEED), and a QMS. Before the molecular-beam reaction, the Pt(110) and Pt(111) surfaces were cleaned using a standard procedure (O_2 treatment, Ar^+ bombardment, and annealing) [19–25]. After cleaning, the sharp reconstructed (1 × 2) and (1 × 1) LEED patterns were observed for Pt(110) and Pt(111), respectively.

The IR emission spectra of the CO_2 molecules desorbed from the surface were measured with 4 cm^{-1} resolution. At that low resolution, no individual vibration-rotation lines were resolved. The spectra were analyzed based on simulations of model spectra [14,16]. They yielded an average vibrational Boltzmann temperature (T_V^{AV}: an average temperature of antisymmetric stretch, symmetric stretch and bending modes), which could be calculated from the degree of the red-shift from the fundamental band (2349 cm^{-1}) [14,16,23]. Although the IR emission observed here is in the antisymmetric stretch vibrational region − (n_{SS}, n_B^l, n_{AS}) → (n_{SS}, n_B^l, $n_{AS} - 1$), the vibrational excitation levels of symmetric stretch (n_{SS}) and bending (n_B) also affect this region [14,19]. Here, n_{SS}, n_B and n_{AS} are the vibrational quantum numbers of respective modes. The quantum number of vibrational angular momentum in linear molecules is denoted by l. Note that the emission intensity is normalized using the rate of CO_2 production. Consequently, the emission intensity is related to

the extent of excitation in the antisymmetric stretch of CO_2, which is given by following equation:

$$f \propto e^{-x} + e^{-2x} + e^{-3x} \cdots \fallingdotseq e^{-x}/(1-e^{-x}), \quad (1)$$

where f is the emission intensity normalized per unit of CO_2 yield, and x equals to $\Delta E_V/k_B T_V^{AS}$ (ΔE_V is the energy spacing, k_B is the Boltzmann constant and T_V^{AS} is the antisymmetric temperature). Therefore, T_V^{AS} can be estimated from the normalized emission intensity [21–25]. Based on T_V^{AS} and T_V^{AV}, it is possible to deduce the bending vibrational temperature (T_V^{B}). The relation between T_V^{AV} and respective vibrational temperatures is represented as

$$T_V^{AV} = (T_V^{AS} + T_V^{SS} + 2T_V^{B})/4, \quad (2)$$

where $2T_V^{B}$ corresponds to the degeneration of the bending vibration. Assuming that T_V^{B} is equal to T_V^{SS} because of the Fermi resonance [15,29], T_V^{B} is expected to be $(4T_V^{AV} - T_V^{AS})/3$. This assumption is plausible on the basis of previous reports [14,15,29]. It should be added that T_V^{AV}, T_V^{AS}, and T_V^{B} were used here as parameters to characterize the extent of the vibrational excitation of the product CO_2. About 30–60 min were required to measure the IR spectra with 2000–4000 scans. The activity was stable during measurement. Therefore, we infer that the results reflected the CO_2 states under steady-state conditions.

To estimate the coverages of CO (θ_{CO}) and oxygen (θ_O) under steady-state conditions, we considered the mechanism and the differential equations. As is known well, the mechanism of the CO oxidation on Pt surface is as follows [1–3]:

$$CO(g) + V \leftrightarrow CO(a), \quad (3)$$

$$O_2(g) + 2V \rightarrow 2O(a), \quad (4)$$

$$CO(a) + O(a) \rightarrow CO_2(g) + 2V, \quad (5)$$

where V is a vacant site. It is possible to make the equations regarding the coverage of each intermediate as shown below [32].

$$d\theta_{CO}/dt = f_{CO} s_{CO} [1 - (\theta_{CO}/\theta_{CO,S})^3] - k_{CO}^{des} \theta_{CO} - r_{CO_2}, \quad (6)$$

$$d\theta_O/dt = 2 f_{O_2} s_{O_2} (1 - \theta_{CO}/\theta_{CO,S} - \theta_O/\theta_{O,S})^2 - r_{CO_2}, \quad (7)$$

where f and s are the flux of reactants to the surface and the initial sticking coefficients, respectively. The k_{CO}^{des} is the rate constant for CO desorption. The rate of O_2 desorption is assumed to be small enough to be neglected [18,32]. The subscript S denotes saturation. The CO_2 formation rate, r_{CO_2},

was obtained from experimental results. The initial sticking coefficients of CO and O_2, kinetic parameters and saturation coverage used are listed in Table 5-1. More strictly, one should take into account that the activation energy of CO desorption and the (1 × 2) ↔ (1 × 1) phase transition depend on the coverages. However, we have used the above equations to estimate the surface coverages approximately.

5.3. Results and Discussion

Figure 5-1 shows the rate of CO_2 formation in the steady-state CO + O_2 reaction on Pt(110) and Pt(111) as a function of surface temperature (T_S) (CO/O_2 = 1). The CO oxidation proceeded above 550 K, and the profiles of the formation rate had a maximum on both surfaces. The behavior agrees well with the general Langmuir-Hinshelwood (LH) kinetics of CO oxidation on Pt surfaces [1,2,3,17,18]. It is known that at lower surface temperatures, the surface coverage of CO is high, and the rate-determining step is O_2 adsorption on the vacant site, which is formed by the desorption of CO(a). At higher surface temperatures, the formation rate of CO_2 decreased gradually with increasing surface temperature, and this behavior is due to the decrease of CO coverage. The temperature at which the highest activity was obtained is denoted as T_S^{max}. Obviously, the activity for CO oxidation and T_S^{max} are different between Pt(110) and Pt(111) surfaces. These results show that the CO oxidation on Pt surfaces is structure-sensitive in the kinetics under the steady-state reaction condition. The differences may depend on the difference of the coverage of oxygen and CO during the steady-state reaction. Especially, the sticking coefficient of oxygen may be different between these surfaces. For example, an initial sticking coefficient (s_0) of O_2 is 0.4 on Pt(110) [35] and 0.048 on Pt(111) [37]. It has been reported in some cases that CO oxidation on Pt(110) exhibits oscillation [3–8]. However, we did not observe the phenomenon, because the experimental conditions such as reactant pressures and temperatures differ from our conditions.

Figures 5-2(a) and 5-2(b) show IR emission spectra of CO_2 molecules produced by the CO + O_2 reaction on Pt(110) and Pt(111) surfaces (CO/O_2 = 1) for various surface temperatures. The CO_2 emission spectra observed in the region of 2400–2150 cm^{-1} are considerably red-shifted from 2349 cm^{-1} (fundamental band of antisymmetric stretch). On Pt(110) at $T_S \geq 700$ K, the higher the surface

temperature, the greater the red-shift from the antisymmetric stretch fundamental (2349 cm^{-1}) was observed in the CO_2 emission spectra, even though the emission intensity is almost constant. On the other hand, at low surface temperatures (T_S < 700 K), the lower the surface temperature, the greater the red-shift from 2349 cm^{-1} was observed, and the emission intensity increased as decreasing T_S.

Figure 5-3 shows the average vibrational temperature (T_V^{AV}) on Pt(110) and Pt(111) surfaces derived from the IR emission spectra of CO_2 as a function of T_S. The T_V^{AV} value was much greater than that of T_S, which indicates that the product CO_2 is vibrationally excited. The T_V^{AV} values on Pt(110) higher than on Pt(111) are in good agreement with the results of Watanabe et al. [17,18]. The T_V^{AV} value increases with increasing T_S at high temperatures ($T_S \geq 700$ K) on both surfaces. This is related to the exothermic reaction heat, which can be distributed to translational and internal (vibrational and rotational) energies of desorbed molecules, and it can also be distributed to the surface [27,38]. It is thought that the energy distribution to the surface can become lower at the higher surface temperatures [25]. On the other hand, the T_V^{AV} value on Pt(110) increases with decreasing T_S at low temperatures of 625–700 K, indicating that the vibrational states of the desorbed CO_2 are changed at around 700 K on Pt(110). Watanabe et al. [18] suggested that the T_V^{AV} value increased as the coverage of CO increased at the lower T_S. Figures 5-4(a) and 5-4(b) show T_V^{AS} and T_V^{B} derived from the IR emission intensity of CO_2 as a function of T_S. For surface temperatures above 700 K, the T_V^{B} value increases gradually with increasing T_S on both surfaces. Especially, the T_V^{B} values are much higher than those of T_V^{AS} at the higher T_S, meaning that the bending vibrational mode is more highly excited than the antisymmetric vibrational mode on both surfaces at the higher T_S. The structure of the activated complex of CO_2 formation can be discussed from the experimental results.

In our previous reports, the structure of the activated complex in CO + O_2 reaction on Pd(111) is more bent than that on Pd(110) based on the analysis of the vibrational excitation states of the product CO_2 [19,20,23,25]. This behavior can be explained by the flat Pd(111) surface in an atomic scale. In the case of Pt(111), the bending vibration was more excited than the antisymmetric vibration, and this can be also due to the flat surface structure. However, the bending vibrational temperature is much higher on Pd(111) (T_V^{B} = 2200 K at T_S = 800 K) [23] than on Pt(111) (T_V^{B} =

1750 K at T_S = 800 K, as shown in Fig. 5-4(b)). The higher vibrational temperatures on Pd(111), compared to Pt(111), are in good agreement with the results of Coulston and Haller [15], although polycrystalline Pd and Pt foils were used. They argued that the excess bending in the case of Pd might be due to the higher density of states at the Fermi level in the case of Pd compared to Pt [15].

In the case of Pt(110), at surface temperatures higher than 700 K, the bending vibration was also more excited than the antisymmetric vibration (Fig. 5-4(a)). This behavior does not agree with that on Pd(110) [19–21,23,25]. Both T_V^B and T_V^{AS} values are higher on Pt(110) than on Pt(111) (Fig. 5-4), while T_V^B was higher on Pd(111) than on Pd(110), and T_V^{AS} was higher on Pd(110) than on Pd(111) at higher surface temperatures [23]. As is well known, the Pt(110)(1 × 1) surface can be reconstructed to the Pt(110)(1 × 2) surface, and the reconstruction behavior is dependent on the CO coverage [1,27]. In contrast, this kind of reconstruction on Pd(110) has not been reported. These different tendencies can explain the difference in the vibrational excitation states of the product CO_2 over Pt(110) and Pd(110), and this suggests that the difference can be caused by the reconstruction of the Pt(110) surface. In the case of Pt(110), it is expected that the surface structure is reconstructed into the (1 × 2) form because of low CO coverage (θ_{CO} < 0.03 at $T_S \geq$ 700 K). On the other hand, the excited state of CO_2 was different at lower T_S. As shown in Fig. 5-4(a), the T_V^{AS} value increases drastically with decreasing T_S at temperatures below 700 K, indicating that the vibrational states of the desorbed CO_2 are changed at around 700 K on Pt(110). At lower temperatures such as 625 and 650 K, the coverage of CO can be rather high, and the high CO coverage can stabilize Pt(110)(1 × 1). Based on the coverage estimation, the coverage of CO (θ_{CO}) is calculated to be 0.25 and 0.62 at T_S = 650 and 625 K, respectively. The result suggests that the change in the vibrational states is related to the reconstruction of Pt(110)(1 × 2) to the (1 × 1) form with the higher θ_{CO}. In order to elucidate the effect of the coverage of CO and oxygen more clearly, we investigated the dependence of the CO/O_2 ratio at a fixed surface temperature.

Figure 5-5 shows the CO_2 formation rate in the steady-state CO + O_2 reaction on Pt(110) as a function of surface temperature (T_S) for various CO/O_2 ratios. The total flux of reactants was constant at 8.2×10^{18} cm^{-2} s^{-1} in all these experiments. The temperature dependence of the curves shows maxima: the observed behavior resembles that shown in Fig. 5-1. In Fig. 5-5, T_S^{max} increased

significantly with an increase in the CO/O_2 ratio. These behaviors also agree well with the general LH kinetics of CO oxidation on Pt surfaces [1,2,3,17,18]. Based on the results of CO_2 formation rate, the surface temperature was fixed to be 650 K, where the IR emission spectra were obtained.

Figure 5-6 depicts the IR emission spectra of CO_2 molecules produced by the CO + O_2 reaction on Pt(110) at T_S = 650 K for various CO/O_2 ratios. The higher CO/O_2 ratio, the larger is the red-shift from 2349 cm^{-1} observed in the CO_2 emission spectra. In addition, the emission intensity became larger as increasing the CO/O_2 ratio. Figure 5-7(a) shows T_V^{AV} obtained from the IR emission spectra of CO_2. The coverages of adsorbed CO and oxygen as a function of the CO/O_2 ratio obtained from the calculation are also shown in Fig. 5-7(a). The T_V^{AV} value increased slightly with increasing the CO/O_2 ratio. Figure 5-7(b) shows T_V^{AS} and T_V^{B} obtained from the IR emission intensity of CO_2 as a function of the CO/O_2 ratio. In the low CO/O_2 region, the T_V^{AS} value is lower than T_V^{B}, although the T_V^{B} values are almost constant with a change in the CO/O_2 ratio. In contrast, T_V^{AS} increased sharply in the higher CO/O_2 region. Therefore, the T_V^{AS} values were much higher than the T_V^{B} values in the high CO/O_2 region. These behaviors are consistent with those obtained from the results of the T_S dependence shown in Fig. 5-4. From the comparison between θ_{CO} and T_V^{AS}, T_V^{AS} drastically increased in the range of $\theta_{CO} > 0.2$. Considering that the Pt(110)(1 × 2) surface is reconstructed to the (1 × 1) form induced by the CO adsorption above θ_{CO} = 0.2, it is suggested again that the observed phenomenon is strongly related to the reconstruction.

On the basis of the excited states of vibrational modes given from the analysis of the IR emission spectra, the models of the activated complex of CO_2 formation are discussed. Figure 5-8 illustrates the models of the activated CO_2 complex formed from the adsorbed CO(a) and O(a) species. A stable adsorption site of O(a) is a three-fold hollow site and that of CO(a) is an on-top site on Pt(111) [39,40]. Based on these stable adsorption sites of CO(a) and O(a) on Pt(111), the angle of O–C–O in the activated complex of CO_2 formed from these adsorbed species was thought to be bent, and this interpretation has been applied in the CO + O_2 reaction on Pd(111) [19,20,23,25]. However, the T_V^{B} value (e.g., 1750 K) lower than that on Pd(111) (2200 K) [23,25] suggests that the activated CO_2 complex is less bent on Pt(111). Mantell et al. [13,14] estimated the angle of O–C–O to be 165° from the T_V^{B} value of 1750 K. Therefore, we used this angle to

illustrate the activated complex on Pt(111) (Fig. 5-8(a)). On the other hand, in the case of Pt(110)(1 × 1), the stable adsorption site of CO(a) is an on-top site in the first layer [31,41] and that of O(a) is a three-fold hollow site between the first and second layers [31,42,43]. The lower T_V^B value (T_V^B = 1600 K at T_S = 650 K, CO/O_2 = 3) suggests that the angle of O–C–O of the activated complex can be more linear than 165°. The characteristic point is that the very high T_V^{AS} value was observed on the Pt(110)(1 × 1) surface. Similar effects of the high CO coverage on the antisymmetric vibration were also observed on Pd(111) and Pd(110) at lower T_S [21,23,25]. The activated complex can be formed by the adsorbed CO mounting on the adsorbed oxygen atom (Fig. 5-8(b)). Besides, Zhdanov [44] has shown that the change in the energy distribution of the reaction products with increasing coverage can be related to lateral adsorbate-adsorbate interactions in the activated state for reaction. Under the condition of low CO coverage ($\theta_{CO} < 0.2$), the reconstructed Pt(110)(1 × 2) surface is stable [1]. On the Pt(110)(1 × 2) surface, the most stable adsorption site of oxygen atom is a four-fold hollow site of Pt(110)(1 × 2) missing row troughs [31,42,43], and it has been known that the oxygen atoms can also be adsorbed on a three-fold hollow site on the (111) declining terraces of Pt(110)(1 × 2) [31,42,43], although the adsorption energy of this site was a little lower than that of the four-fold hollow site. The adsorption site of CO is usually an on-top site in the first layer of Pt(110)(1 × 2). The activated CO_2 complex can be more bent on the Pt(110)(1 × 2) surface, because T_V^B was higher than that on Pt(111). The reaction sites of the CO_2 formation may be not only the terrace of the (111) structure, but also trough and/or topmost Pt atoms. According to the AR measurement, however, Matsushima et al. [26,27] have shown that CO_2 desorption splits into two inclined components collimating at ±25° in the plane along the [001] direction. These results suggest that the activated complex is formed on the inclined (111) terrace in a more bent form (Fig. 5-8(c)). Although the inclined terrace has a nominal (111) structure, the geometric environment [45] and/or the electronic states of the inclined surface may be different from those of the usual Pt(111) surface, because only the two-atom-wide (111) terraces are available for the adsorbates (Fig. 5-8(c)).

Recently, it was suggested that CO oxidation on Pt occurs via a hot-precursor mechanism [46]. On the other hand, the other recent study [47] doubts this suggestion. In the CO + O_2 reaction

on Pt and Pd surfaces, it has been considered that the adsorbed CO and oxygen are accommodated to the surface before the CO(a) + O(a) reaction [12–25]. In other words, the life time of CO(a) and O(a) is long enough to be accommodated to the surface [1] (the typical LH mechanism). On the other hand, in the CO + NO reaction on Pd(110) at high surface temperatures, we have observed more vibrationally excited CO_2 molecules [22,24]. Therefore, we have proposed that hot oxygen from NO dissociation, which reacts with CO immediately after the formation, can affect the extent of the vibrational excitation [22,24].

5.4. Conclusions

The steady-state activity of the CO + O_2 reaction over Pt(110) and Pt(111) surfaces was measured in the temperature range of 500–900 K, and the IR chemiluminescence of CO_2 formed during the reaction was studied. From the analysis of the IR emission spectra on Pt(111), T_V^B was found to be lower than that on Pd(111), indicating that the activated complex of CO_2 formation is less bent on Pt(111) than on Pd(111). Both T_V^B and T_V^{AS} values were higher on Pt(110) than on Pt(111). On the Pt(110) surface, T_V^{AS} was higher than T_V^B at the lower surface temperatures (T_S < 700 K). On the other hand, T_V^B became higher than T_V^{AS} at the higher T_S range (≥ 700 K), where the Pt(110) surface had the reconstructed (1 × 2) structure. The dependence of the CO/O_2 ratio at T_S = 650 K showed that T_V^{AS} was much higher than T_V^B at the higher CO/O_2 ratios, suggesting that the Pt(110)(1 × 2) surface was reconstructed to the (1 × 1) form with high CO coverage. At lower CO/O_2 ratios, the activated complex was formed in a more bent form on the declining (111) terrace of the Pt(110)(1 × 2) surface.

References

[1] G. Ertl, *Adv. Catal.* **37** (1990) 213.

[2] B.E. Nieuwenhuys, *Adv. Catal.* **44** (1999) 259.

[3] R. Imbihl, G. Ertl, *Chem. Rev.* **95** (1995) 697.

[4] V.P. Zhdanov, *Surf. Sci. Rep.* **45** (2002) 231.

[5] P. Thostrup, E. Kruse Vestergaard, T. An, E. Lægsgaard, F. Besenbacher, *J. Chem. Phys.* **118** (2003) 3724.

[6] B.L.M. Hendriksen, J.W.M. Frenken, *Phys. Rev. Lett.* **89** (2002) 046101.

[7] A.V. Oertzen, H.H. Rotermund, A.S. Milkhailov, G. Ertl, *J. Phys. Chem. B* **104** (2000) 3155.

[8] P.-A. Carlsson, V.P. Zhdanov, B. Kasemo, *Appl. Surf. Sci.* **239** (2005) 424.

[9] J. Xu, J.T. Yates, Jr. *J. Chem. Phys.* **99** (1993) 725.

[10] J. Yoshinobu, M. Kawai, *J. Chem. Phys.* **103** (1995) 3220.

[11] I. Nakai, H. Kondoh, K. Amemiya, M. Nagasaka, T. Shimada, R. Yokota, A. Nambu, T. Ohta, *J. Chem. Phys.* **122** (2005) 134709.

[12] L.S. Brown, S.L. Bernasek, *J. Chem. Phys.* **82** (1985) 2110.

[13] D.A. Mantell, Ph.D. Thesis, Department of Physics, Yale University, New Haven, CT, (1983)

[14] D.A. Mantell, K. Kunimori, S.B. Ryali, G.L. Haller, J.B. Fenn, *Surf. Sci.* **172** (1986) 281.

[15] S.W. Coulston, G.L. Haller, *J. Chem. Phys.* **95** (1991) 6932.

[16] K. Kunimori, G.L. Haller, *Bull. Chem. Soc. Jpn.* **65** (1992) 2450.

[17] K. Watanabe, H. Ohnuma, H. Uetsuka, K. Kunimori, *Surf. Sci.* **368** (1996) 366.

[18] K. Watanabe, H. Uetsuka, H. Ohnuma, K. Kunimori, *Catal. Lett.* **47** (1997) 17.

[19] H. Uetsuka, K. Watanabe, H. Kimpara, K. Kunimori, *Langmuir* **15** (1999) 5795.

[20] K. Nakao, H. Hayashi, H. Uetsuka, S. Ito, H. Onishi, K. Tomishige, K. Kunimori, *Catal. Lett.* **85** (2003) 213.

[21] K. Nakao, S. Ito, K. Tomishige, K. Kunimori, *Chem. Phys. Lett.* **410** (2005) 86.

[22] K. Nakao, S. Ito, K. Tomishige, K. Kunimori, *Catal. Lett.* **103** (2005) 179.

[23] K. Nakao, S. Ito, K. Tomishige, K. Kunimori, *J. Phys. Chem. B* **109** (2005) 17553.

[24] K. Nakao, S. Ito, K. Tomishige, K. Kunimori, *J. Phys. Chem. B* **109** (2005) 17579.

[25] K. Nakao, S. Ito, K. Tomishige, K. Kunimori, *Catal. Today* **111** (2006) 316.

[26] I. Rzeźnicka, Md. Golam Moula, L. Morales de la Garza, Y. Ohno, T. Matsushima, *J. Chem. Phys.* **119** (2003) 9829.

[27] T. Matsushima, *Surf. Sci. Rep.* **52** (2003) 1.

[28] D.J. Bald, R. Kunkel, S.L. Bernasek, *J. Chem. Phys.* **104** (1996) 7719.

[29] D.J. Bald, S.L. Bernasek, *J. Chem. Phys.* **109** (1998) 746.

[30] J. Schmidt, Ch. Stuhlmann, H. Ibach, *Surf. Sci.* **284** (1993) 121.

[31] W. Tappe, U. Korte, G. Meyer-Ehmsen, *Surf. Sci.* **388** (1997) 162.

[32] K. Krischer, M. Eiswirth, G. Ertl, *J. Chem. Pnys.* **96** (1992) 9161.

[33] R.W. Mccabe, L.D. Schmidt, *Surf. Sci.* **66** (1977) 101.

[34] C.E. Wartnaby, A. Stuck, Y.Y. Yeo, D.A. King, *J. Phys. Chem.* **100** (1996) 12483.

[35] R. Ducros, R.P. Merrill, *Surf. Sci.* **55** (1976) 227.

[36] C.M. Comrie, R.M. Lambert, *J. Chem. Soc. Faraday I* **72** (1976) 1659.

[37] D.R. Monroe, R.P. Merrill, *J. Catal.* **65** (1980) 461.

[38] B. Gumhalter, T. Matsushima, *Surf. Sci.* **561** (2004) 183.

[39] A. Alavi, P. Hu, T. Deutsch, P.L. Silvestrelli, J. Hutter, *Phys. Rev. Lett.* **80** (1998) 3650.

[40] N.V. Petrova, I.N. Yakovkin, *Surf. Sci.* **578** (2005) 162.

[41] R.K. Sharma, W.A. Brown, D.A. King, *Surf. Sci.* **414** (1998) 68.

[42] S. Helveg, H.T. Lorensen, S. Horch, E. Lægsgaard, I. Stensgaard, K.W. Jacobsen, J.K. Nørskov, F. Besenbacher, *Surf. Sci.* **430** (1999) L533.

[43] B.E. Hayden, A.J. Murray, R. Parsons, D.J. Pegg, *J. Electroanal. Chem.* **409** (1996) 51.

[44] V.P. Zhdanov, *Surf. Sci.* **165** (1986) L31.

[45] E.C. Sowa, M.A. Van Hove, D.L. Adams, *Surf. Sci.* **199** (1988) 174.

[46] E. Molinari, M. Tomellini, *Chem. Phys.* **277** (2002) 373.

[47] V.P. Zhdanov, *Surf. Sci.* **575** (2005) 313.

Table 5-1 Kinetic parameters for $CO + O_2$ reaction on Pt(110)

reaction equation	rate constant /s^{-1}	ν /s^{-1}	E_a /kcal mol^{-1}	Ref.
(3)	k_{CO}^{des}	2×10^{16}	36.2	[32,33]
	initial sticking coefficient			
(3)	$s_{CO} = 0.83$			[34]
(4)	$s_{O_2} = 0.4$			[35]
	saturation coverage			
(3)	$\theta_{CO,S} = 1.0$			[36]
(4)	$\theta_{O,S} = 0.35$			[35]

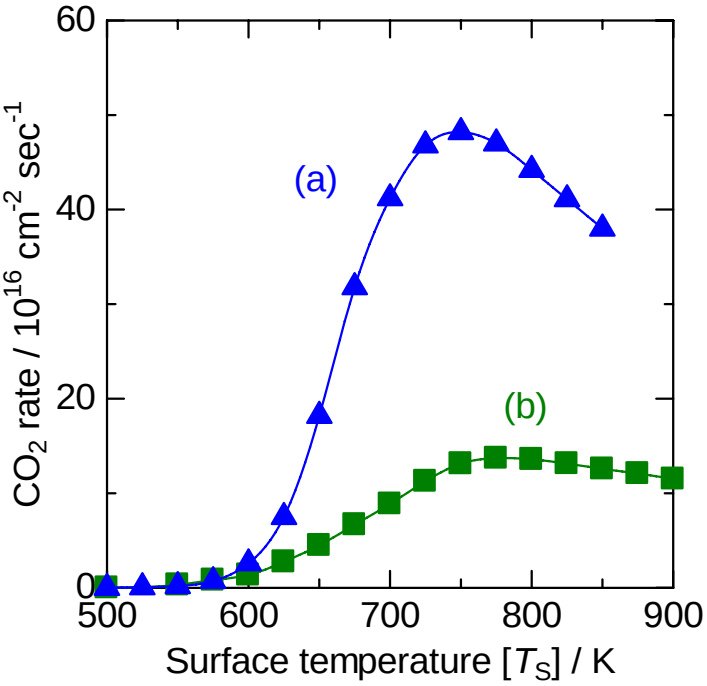

Figure 5-1 The formation rate of CO_2 during the CO + O_2 reaction (CO/O_2 = 1) on (a) Pt(110) and (b) Pt(111). The total flux of reactants (CO + O_2) was 8.2×10^{18} molecules cm^{-2} s^{-1}.

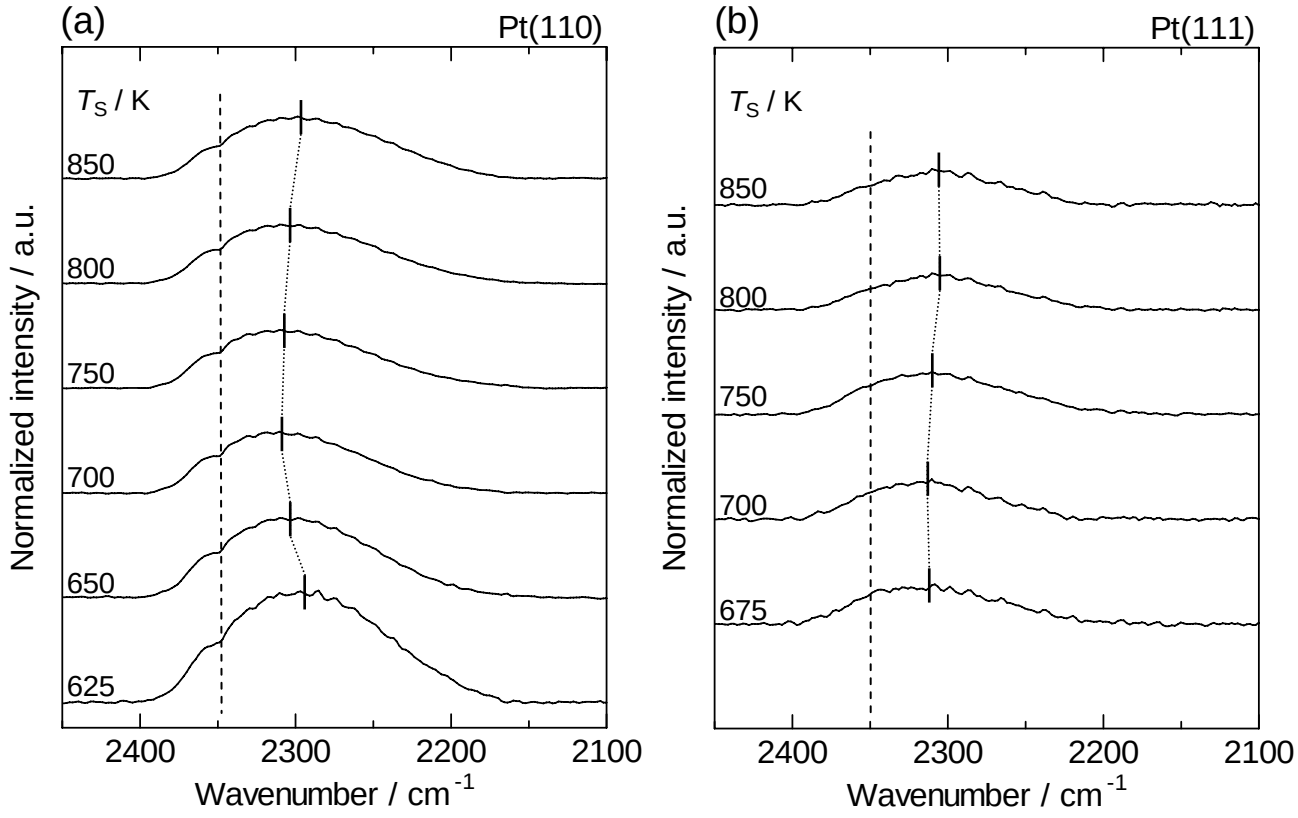

Figure 5-2 IR emission spectra of CO_2 desorbed by the CO + O_2 reaction on (a) Pt(110) and (b) Pt(111). The surface temperature (T_S) was 625–850 K. The flux conditions are as described in Fig. 5-1. The IR emission spectrum centered at 2143 cm^{-1} of the non-reacted CO was subtracted [15,16]. The emission intensity was normalized per unit of CO_2 yield.

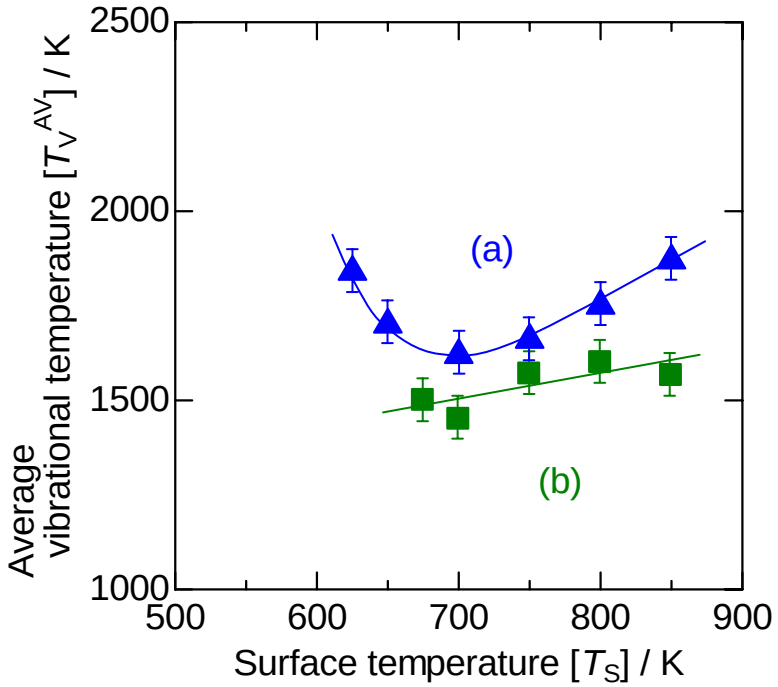

Figure 5-3 Surface temperature dependence of the average vibrational temperature (T_V^{AV}) of CO_2 formed in the CO + O_2 reaction on (a) Pt(110) and (b) Pt(111). The flux conditions are as described in Fig. 5-1.

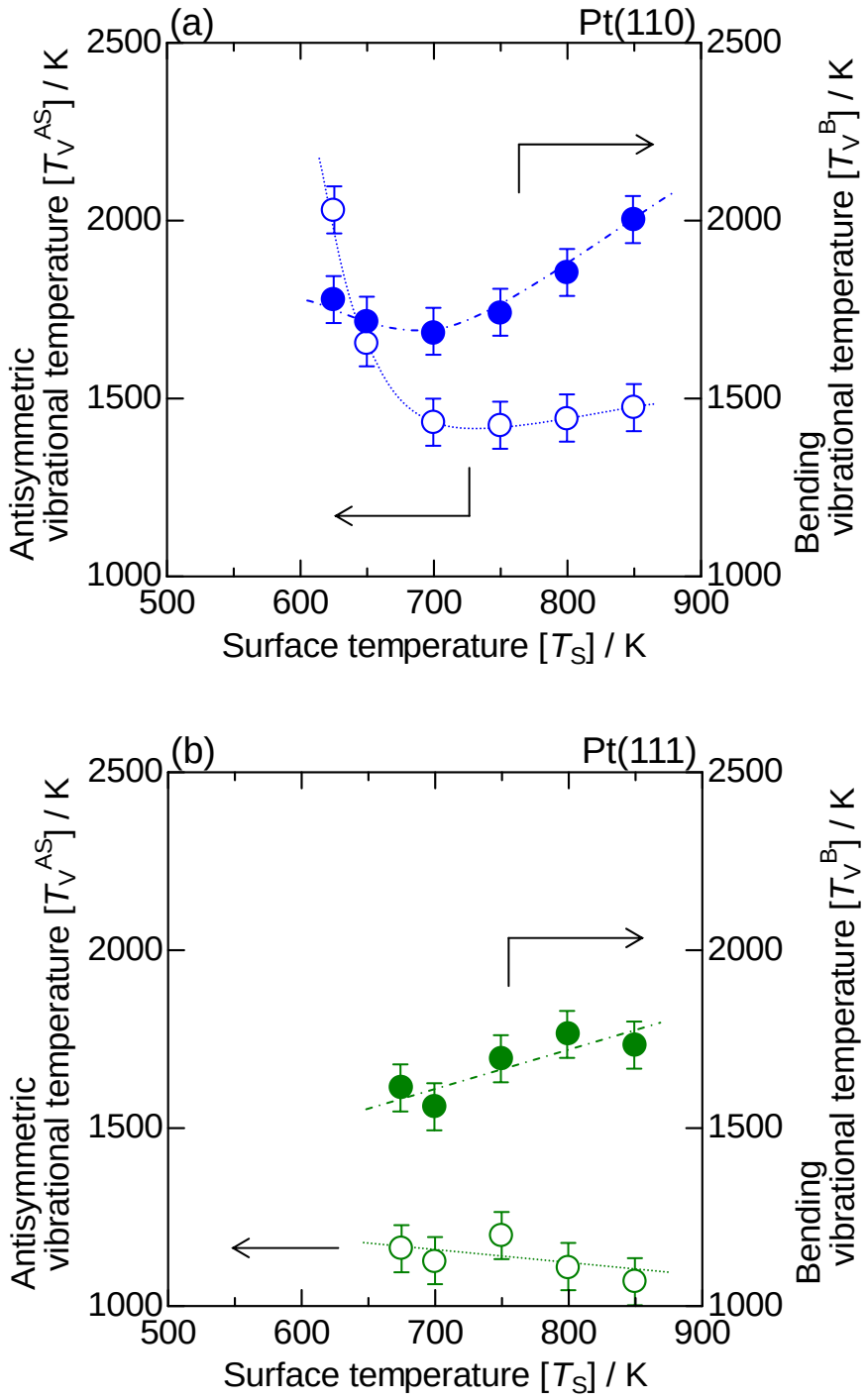

Figure 5-4 Surface temperature dependence of the antisymmetric vibrational temperature (T_V^{AS}) and the bending vibrational temperature (T_V^{B}) on (a) Pt(110) and (b) Pt(111). The flux conditions are as described in Fig. 5-1.

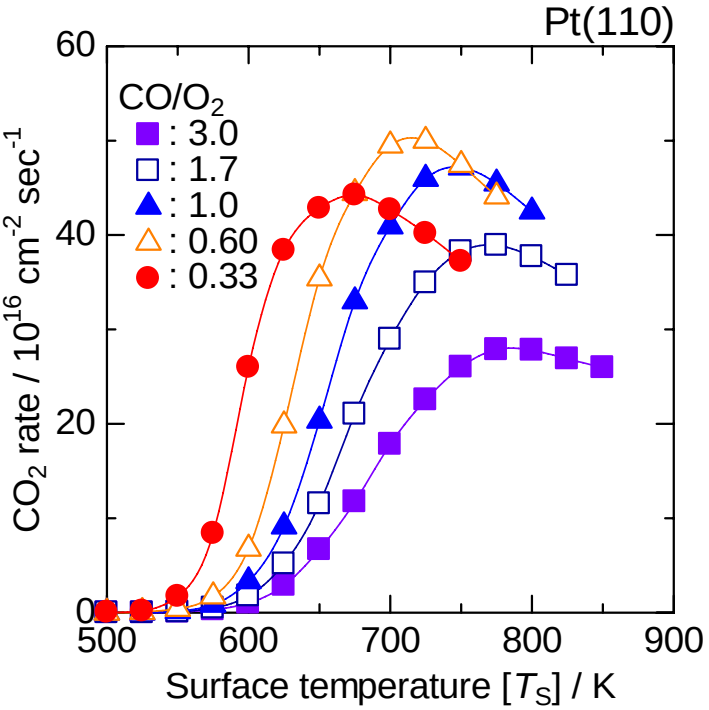

Figure 5-5 The formation rate of CO_2 during the CO + O_2 reaction (CO/O_2 = 0.33−3.0) on Pt(110). The total flux of reactants (CO + O_2) was 8.2×10^{18} molecules cm^{-2} s^{-1}.

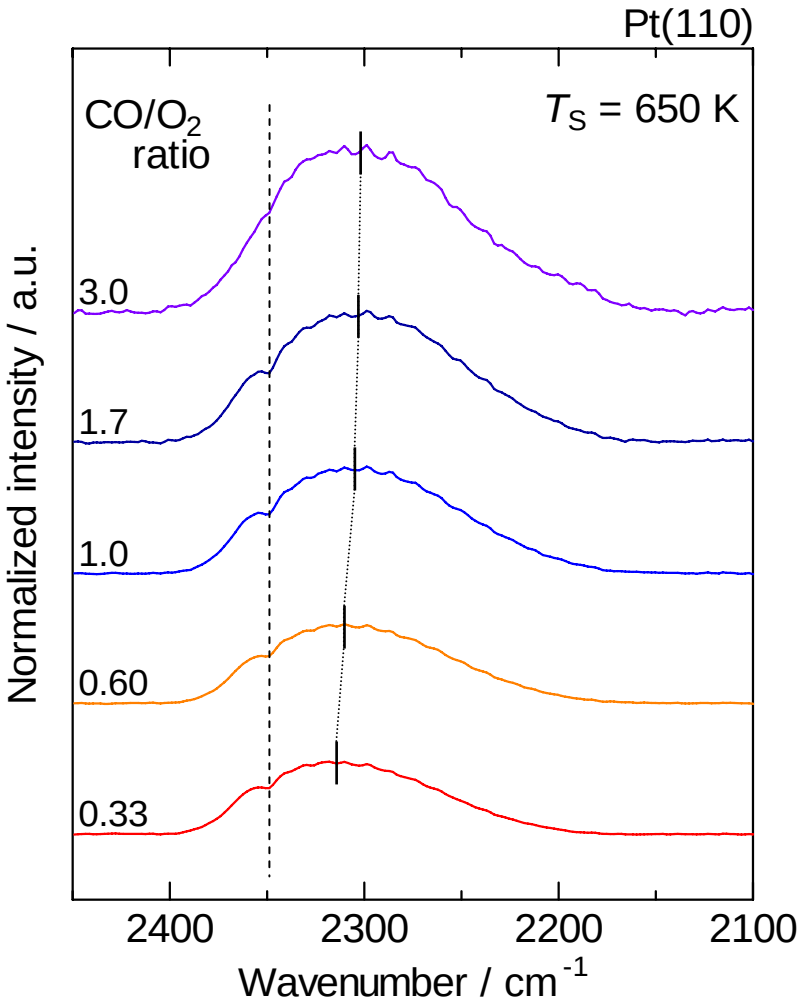

Figure 5-6 IR emission spectra of CO_2 desorbed by the CO + O_2 reaction on Pt(110). The surface temperature (T_S) was 650 K. The flux conditions are as described in Fig. 5-5. The IR emission spectrum centered at 2143 cm^{-1} of the non-reacted CO was subtracted [15,16]. The emission intensity was normalized per unit of CO_2 yield.

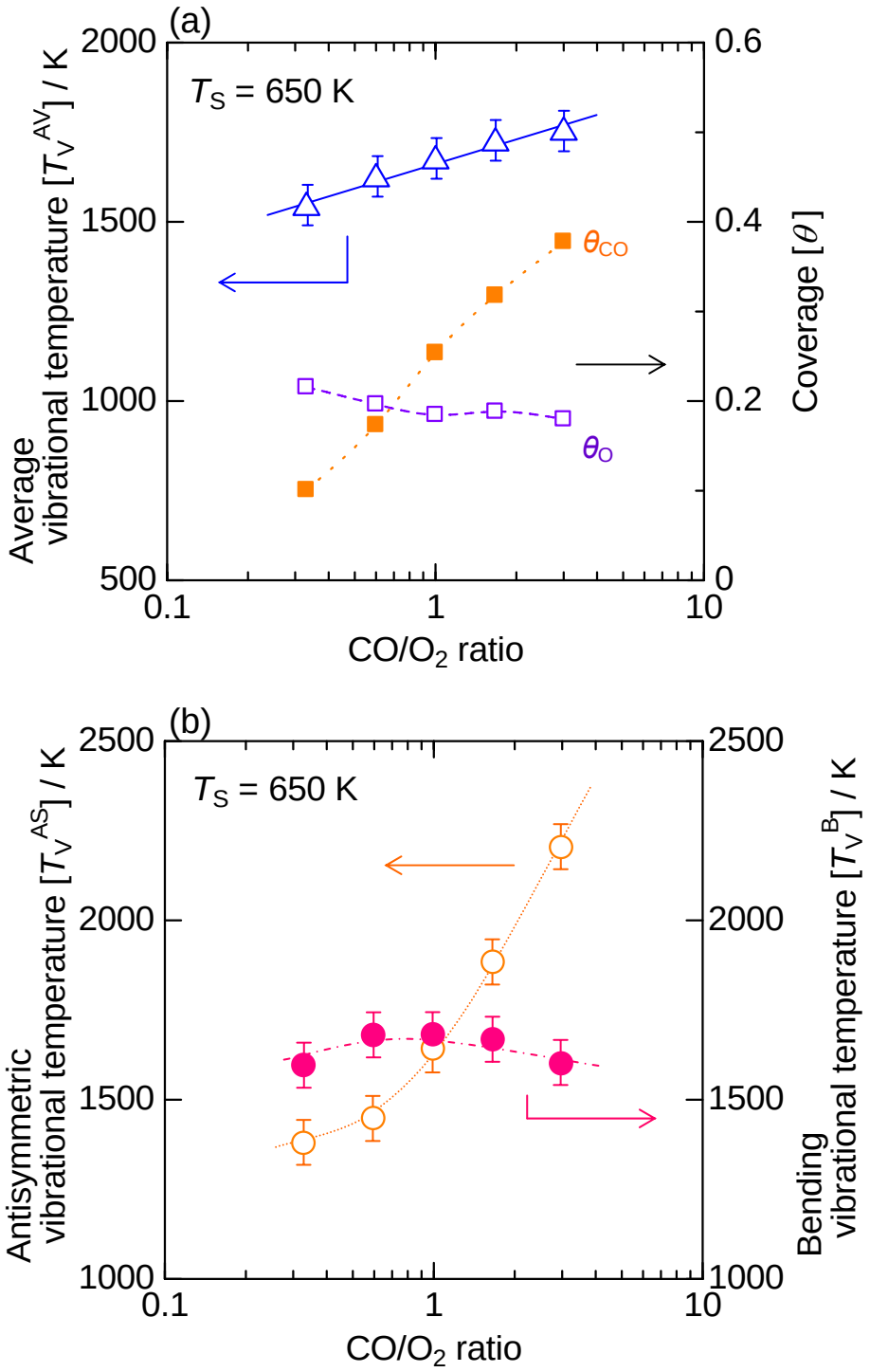

Figure 5-7 (a) CO/O_2 ratio dependence of the average vibrational temperature (T_V^{AV}) of CO_2 formed in the CO + O_2 reaction on Pt(110) and the coverages of CO and oxygen. (b) CO/O_2 ratio dependence of the antisymmetric vibrational temperature (T_V^{AS}) and the bending vibrational temperature (T_V^{B}). The flux conditions are as described in Fig. 5-5.

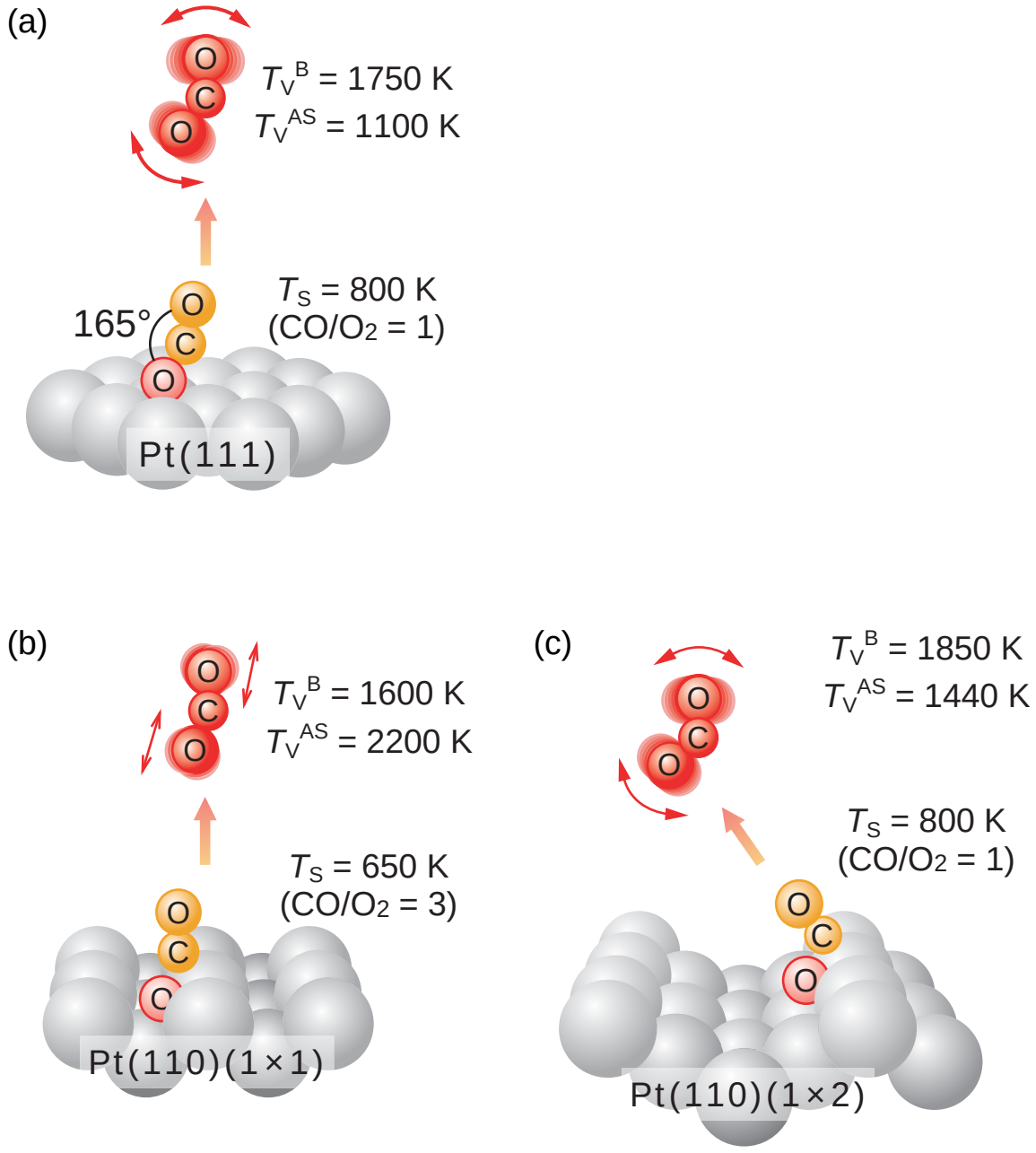

Figure 5-8 Structure of the activated complex of CO_2 formation and the vibrationally excited states of the desorbed CO_2 molecules: (a) Pt(111), (b) Pt(110)(1 × 1), and (c) Pt(110)(1 × 2).

Chapter 6

$CO + O_2$ reaction on Pd(111), Pt(111), and Rh(111) surfaces

6.1. Introduction

The catalytic oxidation of carbon monoxide (CO) on platinum group metal surfaces has been one of the most widely studied surface-catalyzed reactions [1-17]. The reaction is of practical importance for the environmental pollution control. On the other hand, the reaction is also of scientific interest because the total reaction can be divided into a few elementary steps and the theoretical approaches can be applied to the reaction to describe the kinetics of the surface-catalyzed reaction. In contrast, in order to elucidate the dynamics of the surface-catalyzed reaction, it is effective to investigate internal (vibrational and rotational) [6-14] and translational [15] energy of product molecules. Measurements of the vibrational and rotational states of the product CO_2 molecules have been performed by infrared chemiluminescence (IR emission) technique [6-14]. Analysis of the vibrational states can give the information on the structure of the activated CO_2 complex (i.e., the dynamics of CO oxidation) from which the gas-phase molecules desorbed.

Coulston and Haller [6] studied the dynamics of CO oxidation on polycrystalline Pd, Pt, and Rh surfaces by measuring high-resolution IR emission spectra and reported that the order of the apparent vibrational temperatures are as follows: Pd > Pt > Rh. Our group has reported IR emission of CO_2 from steady-state CO oxidation on single-crystal Pd and Pt surfaces combined with kinetic results [9-14]. These suggest that the activated complex of CO_2 formation (i.e., the transition state of CO_2 formation from CO(a) + O(a)) had more bent structure on Pd(111) and less bent structure on Pt(111), since the bending mode of CO_2 from Pd(111) was more vibrationally excited than that of CO_2 from Pt(111) [12,13]. Furthermore, we have confirmed that the product CO_2 molecules on Pd(111) and Pd(110) was also rotationally excited [12]. These results indicate that the IR chemiluminescence method can provide a direct energetic evidence of the reaction mechanism and the activated complex of CO_2 formation.

In this article, the dynamics of CO_2 formation during the CO oxidation over single-crystal Rh(111) surface is reported, and this corresponds to the first presentation of the IR emission studies on a single-crystal Rh surface. The obtained results were compared with those on Pd(111) and Pt(111), and the tendency was interpreted from the comparison between the experimental results and the reported theoretical studies on the transition state of CO oxidation.

6.2. Experimental

A molecular-beam reaction system, in combination with a FT-IR spectrometer (InSb detector Nexus670; Thermo Electron Corp.) was used to measure IR emissions of product CO_2 molecules just desorbed from metal surfaces during catalytic reactions [10-14]. A UHV chamber (base pressure < 1.0×10^{-9} Torr) was equipped with a CaF_2 lens, which collected IR emission, an Ar^+ ion gun for sample cleaning, and a quadrupole mass spectrometer (QMS, QME200; Pfeiffer Vacuum Technology AG) with a differential pumping system. Two free-jet molecular-beam nozzles (0.1 mm diameter orifice) supplied the reactant gases. The reactant fluxes were controlled using mass flow controllers. The CO and O_2 gases (total flux of 8.2×10^{18} cm^{-2} s^{-1}; $CO/O_2 = 1$) were exposed to single-crystal surfaces (Pd(111), Pt(111), and Rh(111)). Steady-state CO oxidation was performed at temperatures of 400–900 K. Another UHV chamber (base pressure < 2.0×10^{-10} Torr) was used to prepare and characterize the clean surfaces. It was equipped with a molecular-beam reaction system, an Ar^+ ion gun, low energy electron diffraction (LEED), and a QMS. Before the molecular-beam reaction, the single-crystal surfaces were cleaned using a standard procedure (O_2 treatment, Ar^+ bombardment and annealing) [9-14]. After cleaning, the sharp (1×1) LEED pattern was observed.

The IR emission spectra of the CO_2 molecules desorbed from the surface were measured with 4 cm^{-1} resolution. At that low resolution, no individual vibration-rotation lines were resolved. The IR emission spectra were analyzed based on simulation of model spectra [7,12,13]. The average vibrational Boltzmann temperature (T_V^{AV}: an average temperature of the antisymmetric stretching, symmetric stretching and bending modes), which was calculated from the degree of the red-shift from the fundamental band (2349 cm^{-1}) [7,9-13]. The emission intensity is related to the extent of excitation in the antisymmetric stretching of CO_2 [11-14]. Therefore, the antisymmetric

vibrational temperature (T_V^{AS}) can be estimated from the normalized emission intensity [11-14]. Based on T_V^{AV} and T_V^{AS}, it is possible to deduce the bending vibrational temperature (T_V^{B}). The relation between T_V^{AV} and respective vibrational temperature is represented as

$$T_V^{AV} = (T_V^{AS} + T_V^{SS} + 2\,T_V^{B}) / 4, \quad (1)$$

where $2T_V^{B}$ corresponds to the degeneration of the bending vibration. Assuming that T_V^{B} is equal to T_V^{SS} because of the Fermi resonance [6,8], T_V^{B} is expected to be $(4T_V^{AV} - T_V^{AS})/3$. This assumption is plausible on the basis of previous reports [6,8]. It should be added that T_V^{AV}, T_V^{AS}, and T_V^{B} were used here as parameters to characterize the extent of the vibrational excitation of the product CO_2. It took about 30–90 min for the measurement of the IR emission spectra with 2000–6000 scans. The stable steady-state activity was obtained during the measurement.

6.3. Results and Discussion

Figure 6-1(a) shows the rate of CO_2 formation in the steady-state CO oxidation on Pd(111), Pt(111), and Rh(111) as a function of surface temperature (T_S) (CO/O_2 = 1). The CO oxidation proceeded above 500 K on Pd(111) and Rh(111), and 550 K on Pt(111). The surface temperature dependence of the formation rate showed a maximum on all the surfaces. The behavior agrees well with the general Langmuir-Hinshelwood (LH) kinetics of CO oxidation on noble metal (Pd [1,4,6,12], Pt [2,6,13], and Rh [3,5,6]) surfaces. The temperature at which the highest activity was obtained is denoted as T_S^{max}. At temperatures lower than T_S^{max}, the surface coverage of CO is known to be high. The rate-determining step is O_2 adsorption on the vacant site, which is formed by the desorption of CO(a). At temperatures higher than T_S^{max}, the formation rate of CO_2 decreased gradually with increasing surface temperature. This behavior is attributable to the decreased CO coverage. The starting temperatures of reaction and T_S^{max} on Pd(111), Pt(111), and Rh(111), i.e., 650, 775 and 650 K, respectively, are similar to those on polycrystalline surfaces reported by Coulston and Haller [6]. In contrast, the order of production rate of our results (Pd(111) > Rh(111) > Pt(111)) at T_S^{max} is different from results of polycrystalline surfaces (Pd > Pt > Rh [6]). Generally, a polycrystalline surface consists of low-index planes such as (111), (100), and (110) [17]. It has been reported that the maximum production rate was strongly dependent on surface structure. In the case

of Pd and Rh, the order is Pd(100) > Pd(110) > Pd(111) [9], and Rh(100) ≈ Rh(111) [3]. Therefore, it is thought that polycrystalline Pd surface can give higher catalytic activity than Pd(111), and polycrystalline Rh surface can be comparable to Rh(111). Unfortunately, there is no report on the comparison in catalytic activity on Pt low-index surfaces, however, the different order between the polycrystalline and single-crystal surfaces presented here suggests Pt(100) > Pt(111) and Pt(110) > Pt(111). The CO_2 formation rate is plotted as a function of inverse surface temperature in the Arrhenius form as shown Figure 6-1(b). From the low temperature range T_S = 475–600 K of this plot, the apparent activation energy (E_{app}) of Pd(111) is estimated as 27.8 kcal/mol, from T_S = 550–625 K, that of Pt(111) is estimated as 19.0 kcal/mol, and from T_S = 550–575 K, that of Rh(111) is estimated as 22.2 kcal/mol. These values agree with the value of 28.1 kcal/mol on Pd(111) [4], which was obtained by Goodman et al., that of 24.1 kcal/mol on Pt(111) [2], which was obtained by Ertl et al., and that of 19.9 kcal/mol on Rh(111) [5], which was obtained by Schmidt et al..

Figure 6-2 shows IR emission spectra of CO_2 molecules produced by the CO oxidation on Rh(111) surface at various surface temperatures. The CO_2 emission spectra were observed in the region of 2400–2220 cm^{-1}, while the emission spectra centered at 2143 cm^{-1} are due to the IR emission of the non-reacted CO molecules, which are scattered from the surface. The CO_2 emission spectra are considerably red-shifted from 2349 cm^{-1} (the fundamental band of antisymmetric stretch). The degree of the red-shift from the fundamental band, which reflects the average vibrational state of the excited CO_2 molecules, is not strongly influenced by the surface temperatures. The emission intensity is also almost constant under various surface temperatures.

Figure 6-3 shows the average vibrational temperature (T_V^{AV}) derived from IR emission spectra of CO_2 on Pd(111), Pt(111), and Rh(111) surfaces as a function of surface temperature. The T_V^{AV} values are much greater than T_S, which indicates that the product CO_2 is vibrationally excited. It is shown that the order of T_V^{AV} is as follows: Pd(111) > Pt(111) > Rh(111). This tendency agrees well with the results of polycrystalline Pd, Pt, and Rh surfaces studied by Coulston and Haller [6]. In addition, the T_V^{AV} values on Pd(111) is much more dependent on the T_S than those on Pt(111) and Rh(111). The reason for different surface temperature dependence on these surfaces is not clear at present.

Eichler [16] has studied CO oxidation on transition metal surfaces using density functional theory (DFT) calculations. He reported that the potential energies of transition state (E_{TS}) and the activation energies (E_a) in CO oxidation on Pd(111), Pt(111) and Rh(111) as listed in Table 6-1, and the potential energy diagram is illustrated in Figure 6-4. He exhibited that the E_{TS} values in CO oxidation on Pd(111), Pt(111), and Rh(111) were –0.98, –1.38 and –1.88 eV, respectively [16], that is, the transition state on Pd(111) has the highest potential energy and that on Rh(111) is the lowest one. IR emission measurements are reflected by the excited energy ($E_{excited}$) of the product CO_2, which can be distributed to internal (vibrational and rotational) and translational energies of desorbed CO_2 molecules. Therefore, it is suggested that the excitation level of desorbed CO_2 can be originated from the height of potential energy of the transition state as shown in Figure 6-4.

Figure 6-5 shows the bending vibrational temperature (T_V^B) and the antisymmetric vibrational temperature (T_V^{AS}) obtained from the IR emission intensity of CO_2 as a function of surface temperature. The T_V^B values are higher than those of T_V^{AS} on each surface, which means that the bending vibrational mode is more excited than the antisymmetric vibrational mode on each surface. However, the bending vibrational temperature at T_S = 800 K is much higher on Pd(111) (T_V^B = 2200 K) than on Pt(111) (T_V^B = 1750 K) and Rh(111) (T_V^B = 1400 K) as shown in Fig. 6-5(a). The higher vibrational temperatures on Pd(111), compared to Pt(111) or Rh(111), are in good agreement with the polycrystalline results of Coulston and Haller [6]. They argued that the excess bending excitation in the case of Pd might be due to the higher density of states at Fermi level compared to Pt or Rh. In fact, the antisymmetric vibrational temperature on Pd(111) was also rather high, and this can be corresponded to higher potential energy of the transition state (Table 6-1). Regarding Pt(111) and Rh(111), the bending vibrational temperature of Pt(111) was higher than that of Rh(111) and this can be related to the angle of O–C–O ($\angle_{OCO}$) in the transition state. Eichler [16] has also reported that the $\angle_{OCO}$ in the transition states on Pt(111) and Rh(111) were 109° and 112°, respectively, as shown in Table 6-1. In addition, the smaller the $\angle_{OCO}$ at the transition state, the larger the energy amount in the bending vibrational mode of desorbed CO_2 molecules. This can be explain the difference in the bending vibrational temperature on Pt(111) and Rh(111). On the other hand, in the case of Pd(111), the angle is relatively large like Rh(111). However, the product CO_2

molecules on Pd(111) are much more excited in both bending and antisymmetric vibrations than those on Pt(111) and Rh(111). At present, it is interpreted that the vibrational excited states on Pd(111) can be controlled mainly by the large excited energy ($E_{excited}$) than by the angle of activated complex in the transition state.

6.4. Conclusions

We measured the steady-state activity of CO oxidation over Pd(111), Pt(111), and Rh(111) surfaces in the temperature range of 400–900 K. Measurements and analyses of IR chemiluminescence of CO_2 formed during the steady-state CO oxidation supplied the vibrational energy states of CO_2, as the average vibrational temperature (T_V^{AV}), antisymmetric vibrational temperature (T_V^{AS}), and bending vibrational temperature (T_V^{B}). The order of the T_V^{AV} values of CO_2 formed during CO oxidation was as follows: Pd(111) > Pt(111) > Rh(111). It is suggested that the order corresponds to the potential energy of the transition state expected from the theoretical studies. The T_V^{B} values are higher than those of T_V^{AS} on each surface, which means that the bending vibrational mode is more excited than the antisymmetric vibrational mode. The order of the T_V^{B} was as follows: Pd(111) > Pt(111) > Rh(111), and this can be influenced by both the angle of the activated complex ($\angle_{OCO}$) and $E_{excited}$.

References

[1] T. Engel, G. Ertl, *Adv. Catal.* **28** (1979) 1.

[2] C.T. Campbell, G. Ertl, H. Kuipers, J. Segner, *J. Chem. Phys.* **73** (1980) 5862.

[3] C.H.F. Peden, D.W. Goodman, D.S. Blair, P.J. Berlowitz, G.B. Fisher, S.H. Oh, *J. Phys. Chem.* **92** (1988) 1563.

[4] J. Szanyi, W.N. Kuhn, D.W. Goodman, *J. Phys. Chem.* **98** (1994) 2978.

[5] S.B. Schwartz, L.D. Schmidt, G.B. Fisher, *J. Phys. Chem.* **90** (1986) 6194.

[6] S.W. Coulston, G.L. Haller, *J. Chem. Phys.* **95** (1991) 6932.

[7] D.A. Mantell, K. Kunimori, S.B. Ryali, G.L. Haller, J.B. Fenn, *Surf. Sci.* **172** (1986) 281.

[8] D.J. Bald, S.L. Bernasek, *J. Chem. Phys.* **109** (1998) 746.

[9] H. Uetsuka, K. Watanabe, H. Ohnuma, K. Kunimori, *Surf. Rev. Lett.* **4** (1997) 1359.

[10] H. Uetsuka, K. Watanabe, H. Kimpara, K, Kunimori, *Langmuir* **15** (1999) 5795.

[11] K. Nakao, S. Ito, K. Tomishige, K. Kunimori, *Chem. Phys. Lett.* **410** (2005) 86.

[12] K. Nakao, S. Ito, K. Tomishige, K. Kunimori, *J. Phys. Chem. B* **109** (2005) 17553.

[13] K. Nakao, S. Ito, K. Tomishige, K. Kunimori, *J. Phys. Chem. B* **109** (2005) 24002.

[14] K. Nakao, S. Ito, K. Tomishige, K. Kunimori, *Catal. Today* **111** (2006) 316.

[15] T. Matsushima, *Surf. Sci. Rep.* **52** (2003) 1.

[16] A. Eichler, *Surf. Sci.* **498** (2002) 314.

[17] J. Lauterbach, G. Haas, H.H. Rotermund, G. Ertl, *Surf. Sci.* **294** (1993) 116.

Table 6-1 Potential energies in the initial (E_{ini}) and the transition (E_{TS}) states, the activation energies (E_a) and O–C–O angle ($\angle_{OCO}$) at the transition states for the CO + O_2 reaction over Pd(111), Pt(111), and Rh(111) surfaces taken from Ref. [16] [a].

	Pd(111)	Pt(111)	Rh(111)
E_{ini} [b] / kcal mol^{-1}	–54.8	–48.8	–67.0
E_{TS} / kcal mol^{-1}	–22.6	–31.8	–43.3
E_a [c] / kcal mol^{-1}	32.2	17.0	23.7
$\angle_{OCO}$	112°	109°	112°

[a] The zero of potential energies based on the free molecules (CO + 1/2O_2).

[b] The initial states means the states of CO and O adsorbed on surfaces.

[c] $E_a = E_{TS} - E_{ini}$

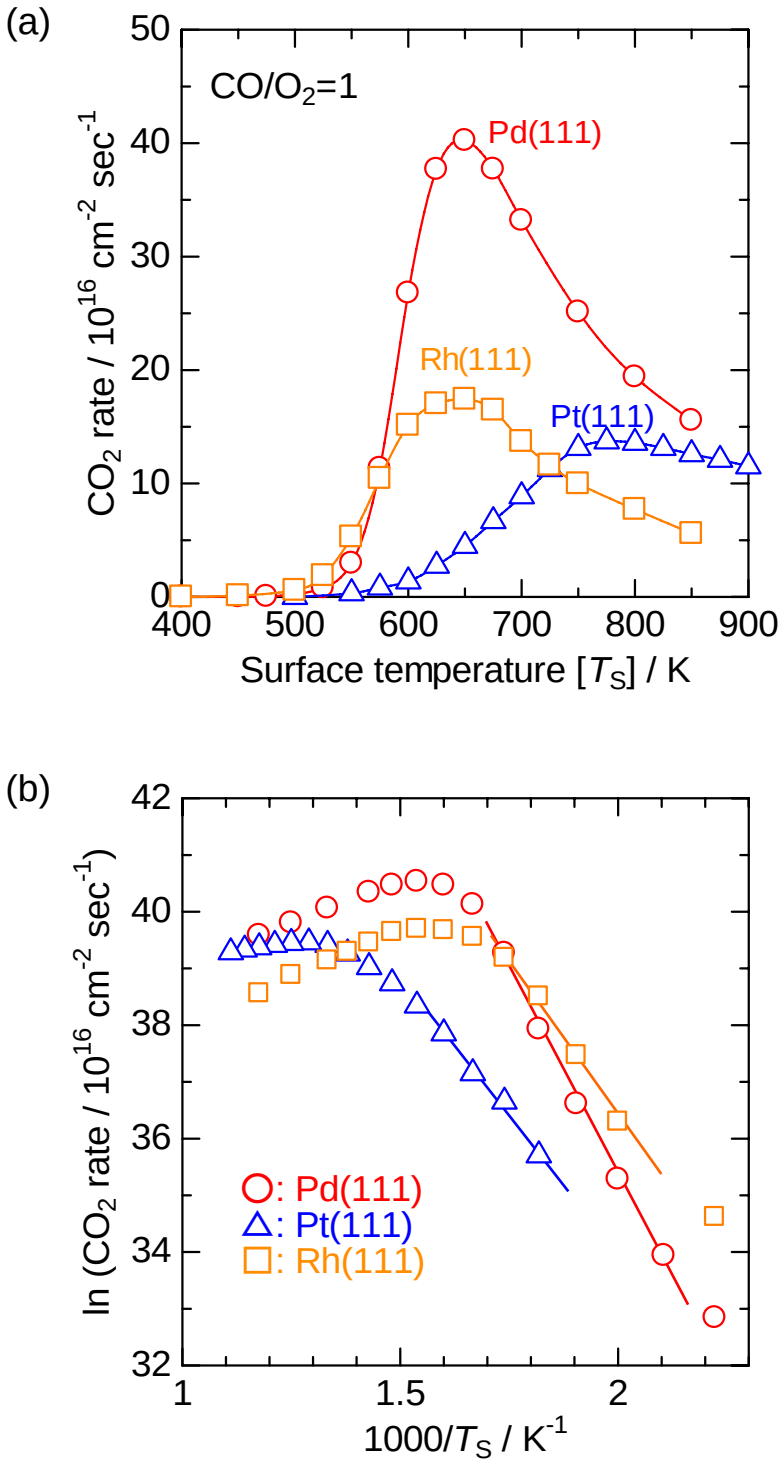

Figure 6-1 (a) The formation rate of CO_2 during CO + O_2 reaction on Pd(111), Pt(111), and Rh(111), and (b) the Arrhenius plot obtained from Fig. 6-1(a). The total flux of reactants of (CO + O_2) was 8.2×10^{18} cm^{-2} s^{-1} at the CO/O_2 = 1. The values of Pd(111) and Pt(111) are taken from Ref. [12,13].

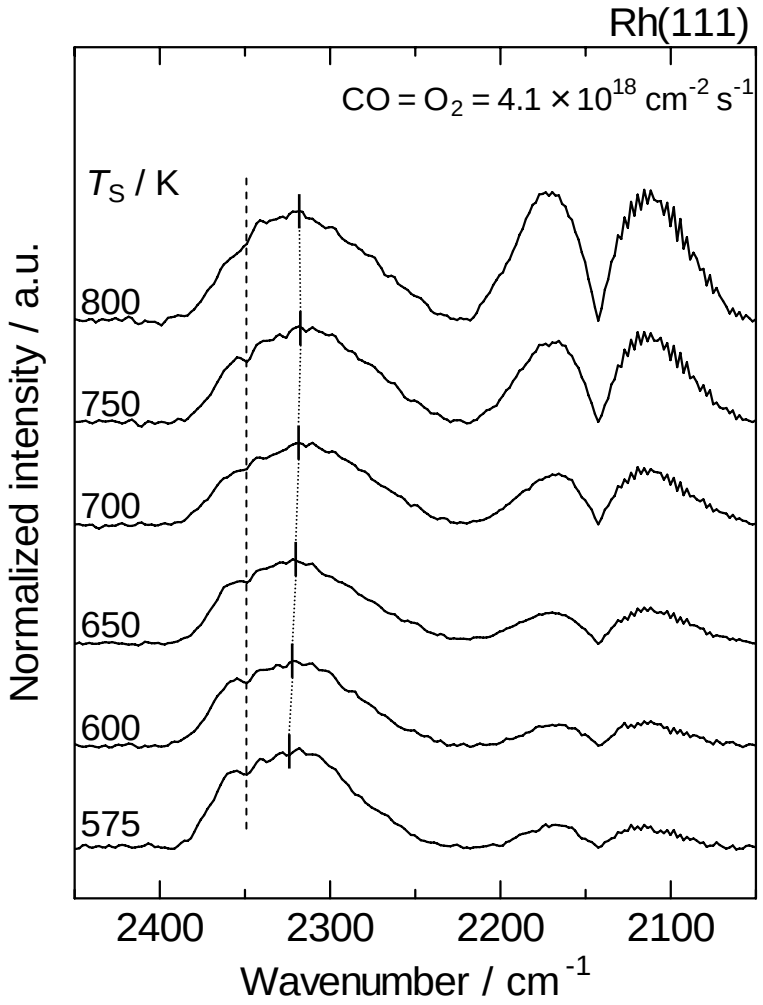

Figure 6-2 IR emission spectra of CO_2 desorbed by CO + O_2 reaction on Rh(111). The surface temperature (T_S) was 575–800 K. The flux conditions are as described in Fig. 6-1. The emission intensity was normalized per unit of CO_2 yield.

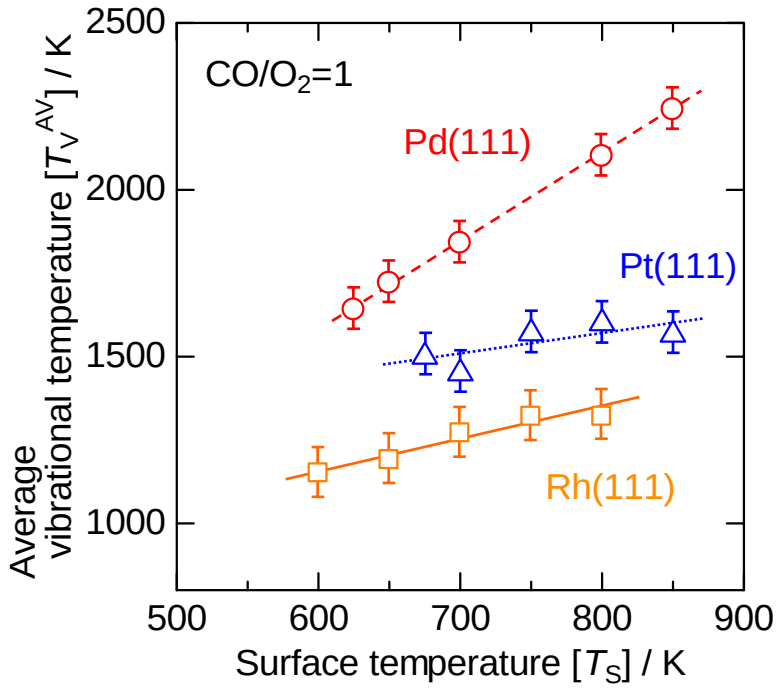

Figure 6-3 Surface temperature dependence of average vibrational temperature (T_V^{AV}) of CO_2 formed in CO + O_2 reaction on Pd(111), Pt(111), and Rh(111). The flux conditions are as described in Fig. 6-1. The values of Pd(111) and Pt(111) are taken from Ref. [12,13].

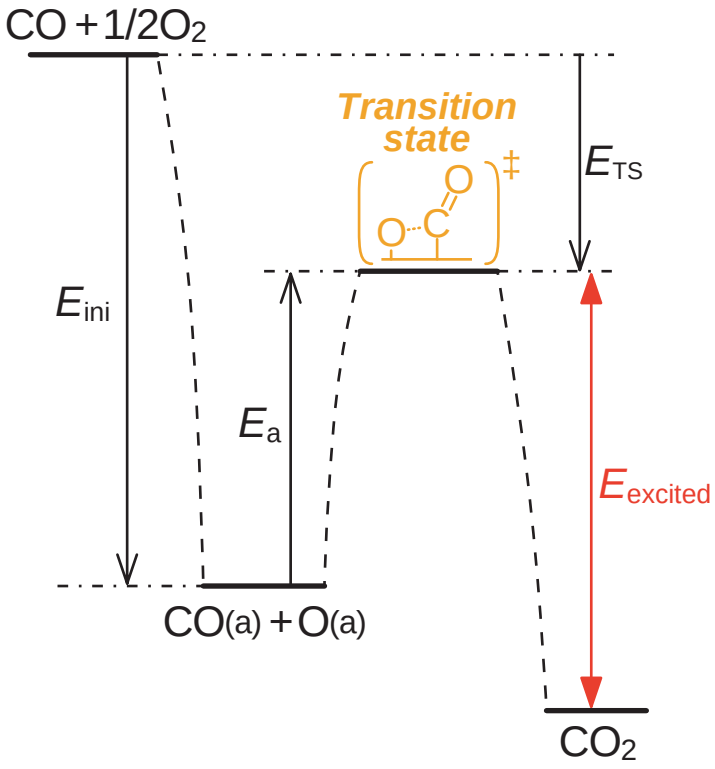

Figure 6-4 Potential energy diagram for the CO + O_2 reaction on noble metal surfaces (Pd, Pt, Rh). The E_{ini} and E_{TS} are the potential energies in the initial and transition states, respectively. The E_a and $E_{excited}$ are the activation energy in CO + O_2 reaction and the excited energy of the product CO_2, respectively (see Table 6-1).

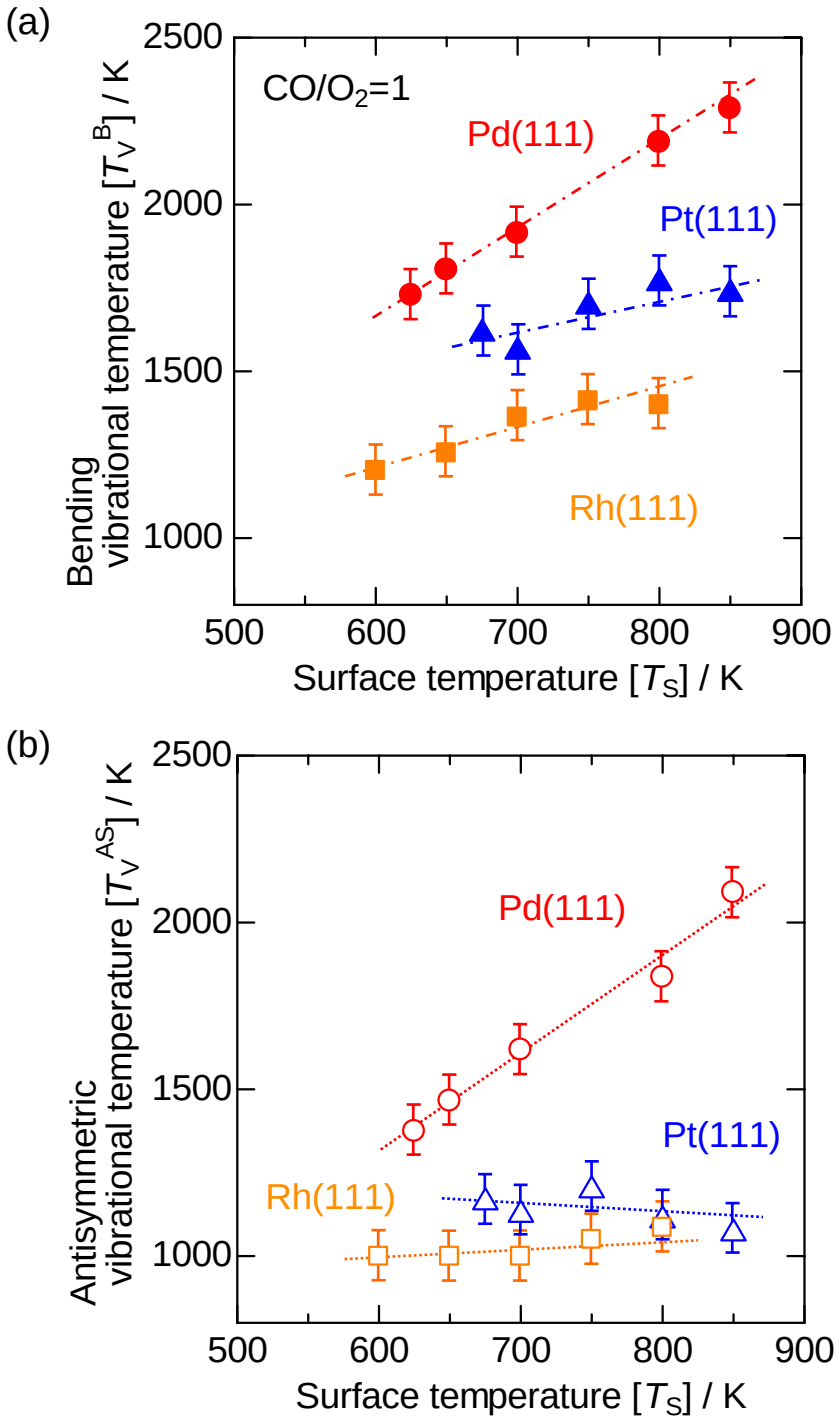

Figure 6-5 Surface temperature dependence of (a) bending vibrational temperature (T_V^B) and (b) antisymmetric vibrational temperature (T_V^{AS}) of CO_2 formed in CO + O_2 reaction on Pd(111) (●,○), Pt(111) (▲,△), and Rh(111) (■,□). The flux conditions are as described in Fig. 6-1. The values of Pd(111) and Pt(111) are taken from Ref. [12,13].

Chapter 7

Summary

For this thesis, the author investigated the kinetics and dynamics of CO_2 formation during CO oxidation by O_2, NO, and N_2O over noble metal (Pd, Pt, and Rh) single-crystal surfaces using a free-jet molecular beam technique and infrared chemiluminescence (IR emission) measurements.

The steady-state activities of CO + O_2 over Pd(110), Pd(111), Pt(110), Pt(111), and Rh(111) surfaces were measured at surface temperatures (T_S) of 400–900 K for reactant pressures between 10^{-3} and 10^{-2} Torr. The CO_2 formation rate profile with regard to the surface temperature was maximal. These behaviors agree well with the general Langmuir-Hinshelwood (LH) kinetics of CO + O_2 reaction on noble metal surfaces. The reaction rate was sensitive to metal species (Pd(111) > Rh(111) > Pt(111)) and surface structure (Pd(110) > Pd(111) and Pt(110) > Pt(111)) (Chapters 2, 5, and 6). Measurements and analyses of IR emission of CO_2 formed during the reaction obtained vibrational and rotational energy states of CO_2 as the average vibrational temperature (T_V^{AV}), antisymmetric vibrational temperature (T_V^{AS}), bending vibrational temperature (T_V^{B}), and rotational temperature (T_R). Results showed that these vibrational and rotational temperatures were much higher than surface temperature under all conditions, indicating that the product CO_2 molecules was excited both vibrationally and rotationally.

At higher surface temperatures, T_V^{B} was higher than T_V^{AS} on Pd(111) and T_V^{AS} was higher than T_V^{B} on Pd(110). This fact suggests that the activated CO_2 complex is more bent on Pd(111), and less bent on Pd(110) at the higher surface temperature, where the CO coverage was rather low. In contrast, the T_V^{AV} values of CO_2 were similar on Pd(110) and Pd(111) surfaces when the surface temperature was low. Furthermore, the T_V^{AS} value of CO_2 increased drastically with decreasing T_S, thereby indicating that antisymmetric vibration is much more highly excited than other vibrational modes. In turn, that high excitation suggests that the structure of the activated complex of CO_2 formation is straighter (Chapter 2).

Both T_V^{B} and T_V^{AS} values were higher on Pt(110) than on Pt(111). On the Pt(110) surface, T_V^{AS} was higher than T_V^{B} at lower surface temperatures (T_S < 700 K). On the other hand, T_V^{B}

became higher than T_V^{AS} at the higher T_S range (≥ 700 K), where the Pt(110) surface had a reconstructed (1 × 2) structure. Dependence of the CO/O_2 ratio at T_S = 650 K showed that T_V^{AS} was much higher than T_V^{B} at higher CO/O_2 ratios, suggesting that the Pt(110)(1 × 2) surface was reconstructed to the (1 × 1) form with high CO coverage. At lower CO/O_2 ratios, the activated complex was formed in a more bent form on the declining (111) terrace of the Pt(110)(1 × 2) surface (Chapter 5).

The order of the T_V^{AV} values of CO_2 formed during CO oxidation over Pd(111), Pt(111), and Rh(111) surfaces was as follows: Pd(111) > Pt(111) > Rh(111). It is suggested that the order corresponds to the potential energy of the transition state expected from the theoretical studies. The T_V^{B} values were higher than those of T_V^{AS} on each surface, which means that the bending vibrational mode is more excited than the antisymmetric vibrational mode. The order of the T_V^{B} was as follows: Pd(111) > Pt(111) > Rh(111), which can be influenced by the angle of the activated complex ($\angle_{OCO}$) (Chapter 6).

Rates of CO_2 formation during the steady-state CO + NO reaction were measured over Pd(110) and Pd(111) at pressures of 10^{-2}–10^{-1} Torr and the T_S range of 400–900 K. The activity of Pd(110) was much higher than that of Pd(111) in our condition, which means that the rate-determining step is NO dissociation on step sites and the CO + NO reaction on Pd surfaces is extremely structure-sensitive. The IR emission spectra of CO_2 during the CO + NO reaction over both Pd surfaces showed that T_V^{B} was higher than T_V^{AS} at temperatures higher than 700 K. The T_V^{B} in the CO + NO reaction on Pd(110) at 800 and 850 K was much higher than that in the CO + O_2 reaction, meaning that the structure of the activated complex of CO_2 formation in the CO + NO reaction has a bent form unlike in the case the CO + O_2 reaction, as above mentioned, and suggests a difference in the dynamics of both reactions (Chapter 3).

The steady-state CO_2 formation rate in the CO + N_2O reaction on Pd(110) was investigated; the activity was very low. The order of the activity of CO oxidations on Pd(110) was CO + O_2 > CO + NO > CO + N_2O. Results also showed that the antisymmetric vibrational mode of CO_2 was more excited in the CO + N_2O reaction, as in the case of the CO + O_2 reaction. These results suggest that the activated complex of CO_2 in the CO + N_2O reaction has a less bent structure, as in the case of the CO + O_2 reaction, and unlike the case of the CO + NO reaction.

Acknowledgements

The author is most grateful to Prof. Kimio Kunimori (Institute of Materials Science, University of Tsukuba) for guidance to this interesting and important research field of catalytic surface reactions. Invaluable instruction, many fruitful comments, advice, and suggestions encouraged the author throughout this work.

Deeply appreciation is extended to Prof. Keiichi Tomishige (Institute of Materials Science, University of Tsukuba) for helpful discussions, which have led to the author's study in the Ph.D. course. His helpful discussions, suggestions and continued support were extremely helpful. The author also expresses his gratitude to Prof. Hidemi Shigekawa (Institute of Applied Physics, University of Tsukuba), Prof. Junji Nakamura (Institute of Materials Science, University of Tsukuba) and Prof. Masahiro Sasaki (Institute of Applied Physics, University of Tsukuba) for their kind participation in the degree committee.

Earnest thanks are offered to Dr. Hiroshi Uetsuka (National Institute of Advanced Industrial Science and Technology (AIST)) for many helpful suggestions, and kind instruction and assistance at the early stage of this work, and to Dr. Shin-ichi Ito (Technical staff of University of Tsukuba) for his technical help and support, fruitful discussions and comments, and to Mr. Hidetaka Hayashi (Toyota Industries Corp.) for instruction and assistance at the early stage of this work.

Special thanks are owed to Mr. Toshiaki Sasaki (graduate student, University of Tsukuba) and Mr. Osamu Watanabe (undergraduate student, University of Tsukuba) for their great support. This thesis could not have been completed without their kind cooperation. The author also thanks Dr. Shigeru Kado (Chiyoda Corporation), Dr. Takeshi Nobukawa (Toyota Motor Company), and all other members of the Kunimori & Tomishige Laboratory at the University of Tsukuba for lendng valuable advice, discussion, encouragement, and pleasurable experience in my research and laboratory life.

The author also thanks Prof. V.P. Zhdanov (Boreskov Institute of Catalysis, Russian Academy of Sciences), Prof. Tatsuo Matsushima and Dr. Toshiro Yamanaka (Catalysis Research Center, Hokkaido University) for their valuable comments, advice and fruitful suggestions. Hearty

thanks are also extended to Dr. Takahiro Kondo (Surface Chemistry Laboratory, RIKEN) for his valuable discussion, encouragement, and warm moral support.

A part of this research was supported by the 21st Century Center of Excellence (COE) Program, *"Promotion of Creative Interdisciplinary Materials Science for Novel Functions"* under the Ministry of Education, Culture, Sports, Science and Technology (MEXT), Japan. I am grateful for my research fellowship of the Japan Society for the Promotion of Science (JSPS) for Young Scientists. I was supported financially by the Japan Student Services Organization and by the Teaching Assistantship of the Graduate School of Pure and Applied Sciences, University of Tsukuba.

Finally, I wish to express my deepest gratitude to my parents, my brother, my sister, my uncles, my aunts, and my love for their heartfelt encouragement and support. I dedicate this thesis to them.

February 2007

Institute of Materials Science

University of Tsukuba

List of Publications

1. **Kenji Nakao**, Hidetaka Hayashi, Hiroshi Uetsuka, Shin-ichi Ito, Hiroshi Onishi, Keiichi Tomishige, Kimio Kunimori
   "Elucidation of CO_2 formation mechanism in CO + NO reaction on Pd(111) and Pd(110) surfaces using IR chemiluminescence method"
   Catalysis Letters, **85** (2003) 213-216.

2. **Kenji Nakao**, Hidetaka Hayashi, Hiroshi Uetsuka, Shin-ichi Ito, Hiroshi Onishi, Keiichi Tomishige, Kimio Kunimori
   "Molecular-beam infrared chemiluminescence study of the mechanism of CO_2 formation in steady-state CO + NO reaction on single crystal Pd surfaces."
   Hyomenkagaku (Journal of the Surface Science Society of Japan), **24** (2003) 461-467.

3. **Kenji Nakao**, Shin-ichi Ito, Keiichi Tomishige, Kimio Kunimori
   "Infrared chemiluminescence study of CO + O_2 reaction on Pd(110): Activated complex of CO_2 formation at high CO coverage"
   Chemical Physical Letters, **410** (2005) 86-89.

4. **Kenji Nakao**, Shin-ichi Ito, Keiichi Tomishige, Kimio Kunimori
   "Vibrationally excited CO_2 formed in CO + NO reaction on Pd(110) surface in high surface temperature range"
   Catalysis Letters, **103** (2005) 179-184.

5. **Kenji Nakao**, Shin-ichi Ito, Keiichi Tomishige, Kimio Kunimori
   "Structure of activated complex of CO_2 formation in CO + O_2 reaction on Pd(110) and Pd(111)"
   Journal of Physical Chemistry B, **109** (2005) 17553-17559.

6. **Kenji Nakao**, Shin-ichi Ito, Keiichi Tomishige, Kimio Kunimori
   "Infrared chemiluminescence study of CO_2 formation in CO + NO reaction on Pd(110) and Pd(111) surfaces"
   Journal of Physical Chemistry B, **109** (2005) 17579-17586.

7. **Kenji Nakao**, Shin-ichi Ito, Keiichi Tomishige, Kimio Kunimori
   "IR chemiluminescence probe of the vibrational energy distribution of CO_2 formed during steady-state CO oxidation on Pt(111) and Pt(110) surfaces"
   Journal of Physical Chemistry B, **109** (2005) 24002-24007.

8. **Kenji Nakao**, Shin-ichi Ito, Keiichi Tomishige, Kimio Kunimori
   "Reaction mechanism and structure of activated complex of CO_2 formation in CO + O_2 reaction on Pd(110) and Pd(111) surfaces by means of infrared chemiluminescence method"
   Catalysis Today, **111** (2006) 316-321.

9. **Kenji Nakao**, Toshiaki Sasaki, Shin-ichi Ito, Keiichi Tomishige, Kimio Kunimori
   "IR chemiluminescence study of CO_2 formed during steady-state CO oxidation on Pt(110) and Pt(111) surfaces"
   Hyomenkagaku (Journal of the Surface Science Society of Japan), **24** (2006) 461-467.

10. Toshiaki Sasaki, **Kenji Nakao**, Shin-ichi Ito, Keiichi Tomishige, Kimio Kunimori
    "Promoting effect of energetic activation of methane molecular-beam in direct catalytic partial oxidation of methane"
    Chemical Communications, (2006) 3821-3823.

11. **Kenji Nakao**, Shin-ichi Ito, Keiichi Tomishige, Kimio Kunimori
    "Comparative study of CO_2 formation in CO oxidation by O_2, NO and N_2O on Pd(110) surface using infrared chemiluminescence"
    Surface Science, **600** (2006) 4221-4227.

12. **Kenji Nakao**, Osamu Watanabe, Toshiaki Sasaki, Shin-ichi Ito, Keiichi Tomishige, Kimio Kunimori
    "CO oxidation on Pd(111), Pt(111), and Rh(111) surfaces studied by infrared chemiluminescence spectroscopy"
    Surface Science, in press.

13. Shigeru Kado, Mohammad Nurunnabi, Yuya Mukainakano, Tomohisa Miyazawa, **Kenji Nakao**, Kazu Okumura, Toshihiro Miyao, Shuichi Naito, Kimihito Suzuki, Ken-ichiro Fujimoto, Kimio Kunimori, Keiichi Tomishige
    "Performance and characterization of NiO-MgO solid solution modified with noble metals in oxidative steam reforming of methane under pressurized conditions"
    ACS Symposium Series, in press.

Miscellaneous

1. **Kenji Nakao**, Shin-ichi Ito, Keiichi Tomishige, Kimio Kunimori
   "Structure of activated complex of CO_2 formation in CO + O_2 reaction on Pd single crystal surfaces: Effect of CO coverage"

Shokubai (Catalysts & Catalysis), **47** (2005) 146-148.

2. **Kenji Nakao**, Osamu Watanabe, Toshiaki Sasaki, Shin-ichi Ito, Keiichi Tomishige, Kimio Kunimori
   "Structure of activated complex of CO_2 formation in CO Oxidation on Pt single crystal surfaces: Effect of surface reconstruction"
   Shokubai (Catalysts & Catalysis), **48** (2006) 433-435.